The Pennsylvania State University

The Graduate School

Department or Civil and Environmental Engineering

DISSOLUTION OF CLAY MINERALS AND REDOX REACTIONS BETWEEN CLAY MINERALS AND URANIUM UNDER HIGH PRESSURE CO_2 CONDITIONS

A Thesis in

Environmental Engineering

by

Yan Liu

Submitted in Partial Fulfillment
of the Requirements
for the Degree of

Master of Science

May 2013

The thesis of Yan Liu was reviewed and approved* by the following:

William D. Burgos
Professor of Environmental Engineering
Thesis Advisor

Fred Cannon
Professor of Environmental Engineering

Christopher Gorski
Assistant Professor of Civil Engineering

Peggy A. Johnson
Professor of Civil Engineering
Head of the Department of Civil and Environmental Engineering

*Signatures are on file in the Graduate School

ABSTRACT

Geological carbon sequestration is a promising technology to mitigate global warming. However, there are concerns that the acidic nature of the injected supercritical CO_2 may dissolve minerals in the injection well seals or in other regions of the storage reservoir. Mineral dissolution could create pathways for CO_2 to migrate to other geologic units. If mineral dissolution also mobilized contaminants (e.g., U, Pb, As), leakage of CO_2 could pose risks to overlying drinking water reservoirs. In this study we examined the dissolution of specimen clay minerals in synthetic brine solutions under high pressure CO_2 conditions (P_T = 9.66 bar, $P_{CO2} \geq$ 8.66 bar CO_2). Specimen clay minerals included nontronite NAu-2, montmorillonite SWy-2, and chlroite CCa-2. Unaltered and partially reduced NAu-2 (R-NAu-2) were used to measure the effect of clay-Fe(III) reduction on acid-promoted dissolution. Synthetic brines included 1.0 M NaCl, 0.33 M $CaCl_2$, and 0.33 M Na_2SO_4. Uranium was used as a redox-active inorganic contaminant and was added either as soluble uranyl(VI) or sparingly soluble biogenic uraninite(IV). High pressure CO_2 conditions were established by adding a measured mass of dry ice to a pressure tube containing clay mineral, brine, and U. Reaction kinetics were measured over a 15 day period by sacrificing pressure tubes, analyzing the supernatant for dissolved mineral components and U, and analyzing the speciation of Fe(II/III) in solution and in the clay mineral pellet. H_3PO_4-H_2SO_4 (1.40 M-0.50 M) was used to measure acid-promoted clay mineral dissolution in a stronger acid. Control reactors were maintained under ambient pressure conditions (P_T = 1.0 bar, N_2:H_2 = 95:5%).

For three types of unaltered clay minerals in three different brines, very little dissolution occurred, showing these clay minerals are stable under high pressure CO_2 conditions. In 1.40 M H_3PO_4-0.50 M H_2SO_4 solution, increased acidity enhanced dissolution of unaltered NAu-2 and partially reduced NAu-2. R-NAu-2 was easier to be dissolved than unaltered NAu-2 under high pressure CO_2 conditions and in 1.40 M H_3PO_4-0.50 M H_2SO_4. Fe(II) was less stable in clay

mineral and acid dissolved Fe had higher Fe(II)/Fe ratios than clay mineral itself. No redox reactions between unaltered or partially reduced NAu-2 with U(VI) was observed. UO_2 was oxidized by unaltered NAu-2, and reaction had a faster rate and greater extent under high pressure CO_2 conditions than under ambient pressure conditions ((P_T = 1.0 bar, N_2:H_2 = 95:5%)). Also, the redox reaction enhanced dissolution of unaltered NAu-2. Such CO_2 enhanced dissolution of clay mineral and enhanced oxidation of UO_2 to U(VI) (aq) indicates possible environmental risks related with carbon sequestration process.

TABLE OF CONTENTS

LIST OF FIGURES

LIST OF TABLES

ACKNOWLEDGEMENTS

I acknowledge Dr. William Burgos for his guidance on this project. I thank Dr. Fubo Luan for helpful discussions on experiment operations and data analysis, Henry Gong for performing ICP-AES measurements, Nichole Wonderling and Mark Angelone for their help in XRD analysis, Maria Klimkiewicz for her help with SEM and SEM-EDS. This research was supported by the National Energy Technology Laboratory (NETL).

Chapter 1

Background

Global warming will be a big challenge for human beings' development. According to the Intergovernmental Panel on Climate Change (IPCC) report, the global surface temperature had increased by 0.74 ± 0.18 ℃ during the 20th century (IPCC, 2007), which was mainly induced by increasing emission of greenhouse gases: CO_2, CH_4, etc. Combustion of fossil fuels is still the fundamental energy source for society. Reducing CO_2 emission is an urgent mission for mankind. Geological sequestration of carbon dioxide technology provides a potential solution.

1.1 Introduction to geological carbon sequestration

Geological carbon sequestration is a process where CO_2 is captured from flue gases, purified and compressed, and then injected into and stored within underground reservoirs. Power plants are major CO_2 sources, with high CO_2 purity and emission amounts in their flue gases. Deep saline aquifers, depleted oil and gas reservoirs, and unmineable coal areas are considered as candidate geologic formations for CO_2 storage (Shukla et al., 2010). CO_2 storage is generally expected to take place at depths below 800 m. Under such temperature (57–127 ℃) and pressure (100–300 bar) conditions, CO_2 will be in supercritical state (Figure 1.1), and the density of CO_2 will range from 50 to 80% of the density of water, resulting in buoyant forces that tend to drive CO_2 upwards (IPCC, 2005).

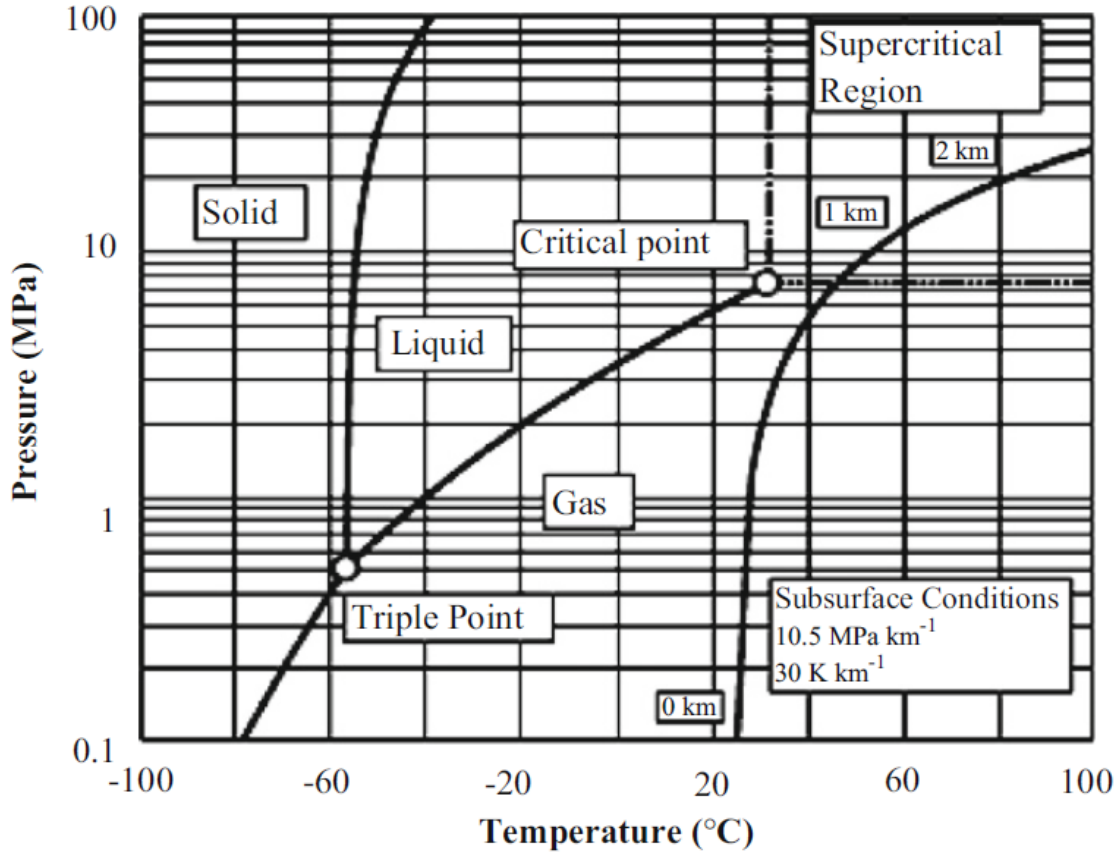

Figure 1.1. Phase diagram of CO_2 (Aydin et al., 2010).

Physical and geochemical processes are major mechanisms for trapping CO_2. Physically, impermeable cap-rock prevents upflow of CO_2 and pore spaces are able to retain CO_2 by capillary forces. Geochemically, after dissolving into brine (time scale of hundreds to thousands of years), CO_2-laden water will sink due to its higher density, dissolved CO_2 will react with rock to form carbonate minerals and carbonic ions (over millions of years) (IPCC, 2005).

Currently, approximately 30 to 50 million metric tons of CO_2 are injected annually in the United States into declining oil fields (IPCC, 2005). This option is attractive because the geology of hydrocarbon reservoirs is generally well understood, such as porosity, permeability, pressure, temperature and storage capacity. The reservoirs have a seal capable of retaining liquids or gases

for thousands to millions of years (IPCC, 2005). Also storage costs can be partly offset by the sale of recovered residual oil. However, their storage capacity and availability are restricted.

Saline formations are layers of porous rock saturated with brine and capped by non-porous rock. Saline aquifers have been used for storage of chemical waste. The main advantage of saline aquifers is its wide distribution and large capacity (Bachu and Adams 2003). The storage capacity of saline aquifers in North America was estimated as low as 3300 Gt, as high as 12600 Gt (NETL, 2008). The United States can inject approximately 65 percent of CO_2 produced by power plants directly into deep-saline aquifers below the plants (White et al., 2005).The major disadvantage is that relatively little is known about saline formations, especially compared to oil fields.

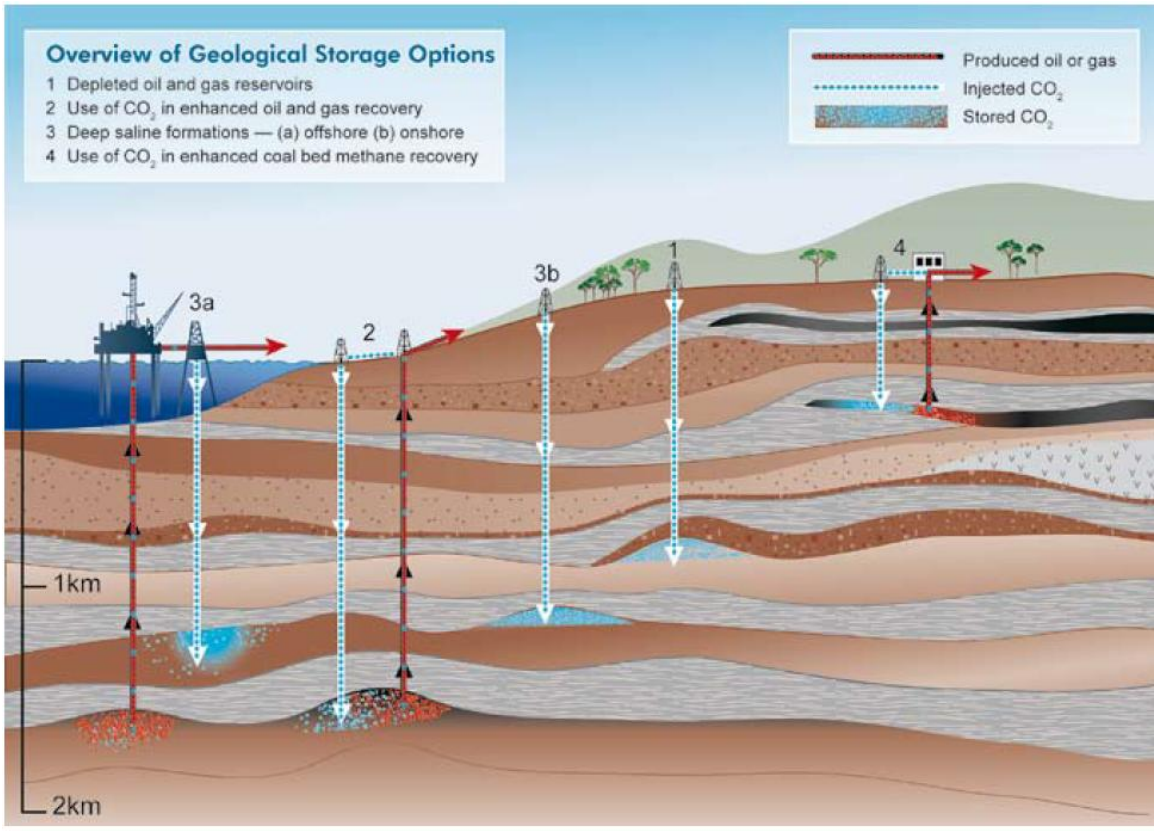

Figure 1.2. Carbon storage sites (IPCC, 2005).

1.2 Solubility of CO_2 in brine

The solubility of CO_2 in brine is crucial to assess aquifer storage capacity and reactivity of acidified brine with rocks. Under subsurface conditions, 5–6 g CO_2 can be dissolved in100g freshwater (Aydin et al., 2010). However, solubility decreases with increasing salinity or temperature. Spycher & Pruess (2010) used a phase-partitioning model that relied on activity coefficients for the H_2O-rich phase and fugacity coefficients for the CO_2-rich phase to model solubility of CO_2 in brine. Their modeled results correlated very well with previously published experiment data (Koschel et al., 2006, Takenouchi & Kennedy, 1965, Rumpf et al,. 1994, Prutton & Savage, 1945). (Figure 1.3)

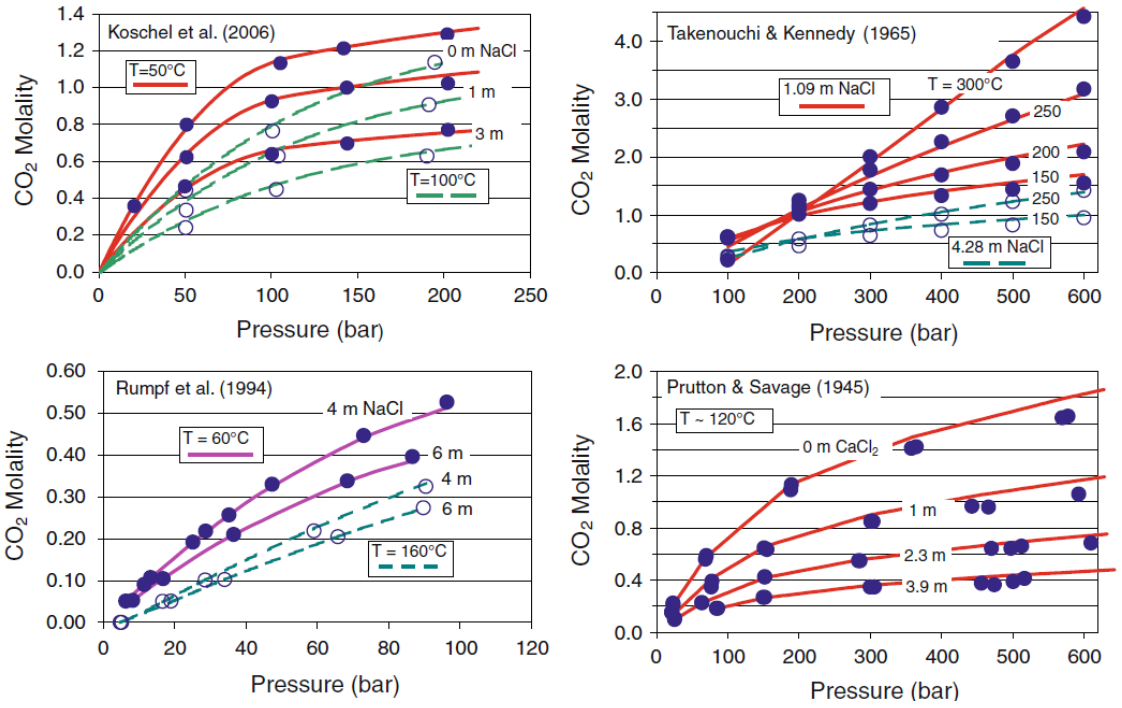

Figure 1.3. Solubility of CO_2 in saline solutions: comparison of model results (lines) with experimental data (symbols) at various temperatures and pressures (Spycher & Pruess, 2010).

1.3 Impurities with CO_2 injection

Sequestrated CO_2 originates from fossil fuel combustion, and there are impurities produced from the fuel itself or during the whole combustion and transportation process. Table 1.1 summarized possible impurities and their concentrations for different CO_2 capture techniques (Wang et al., 2011). Except for Pre-combustion, the other two processes will lead to acid gases such as NO_x SO_2 and SO_3 (for Oxyfuel) collected with CO_2.

Table 1.1 Concentrations of CO_2 and impurity gases resulted from different CO_2 capture techniques (Wang et al., 2011).

Component	Pre-combustion		Post-combustion			Oxyfuel		
	Selexol	Rectisol	Comp.1	Comp.2	Comp.3	Comp.1	Comp.2	Comp.3
CO_2 (vol %)	97.95	99.7	99.93	99.92	99.81	85.0	98.0	99.94
O_2 (vol %)	-	-	0.015	0.015	0.03	4.70	0.67	0.01
N_2 (vol %)	0.9	0.21	0.045*	0.045*	0.09*	5.80	0.71	0.01
Ar (vol %)	0.03	0.15				4.47	0.59	0.01
H_2O (ppm)	600	10	100	100	600	100	100	100
NO_x (ppm)	-	-	20	20	20	100	100	100
SO_2 (ppm)	-	-	10†	10†	20†	50	50	50
SO_3 (ppm)	-	-				20	20	20
CO (ppm)	400	400	10	10	20	50	50	50
H_2S+COS (ppm)	100	100	-	-	-	-	-	-
H_2	1 vol%	20 ppm	-	-	-	-	-	-
CH_4 (ppm)	100	100	-	-	-	-	-	-
NH_3 (ppm)	-	-	-	50	-	-	-	-
CH_3OH (ppm)	-	200	-	-	-	-	-	-

*Total concentration of N_2 + Ar
†Total concentration of SO_2 + SO_3

Data provided by IEA GHG, based on CO_2 quality recommended by COORETEC study for fossil-fueled power plants.
Selexol/rectisol are two acid gas removal processes.
Comp.1, 2, 3 are three scenarios with different CO_2 purities.

Post-combustion CO_2 capture process is analogous to flue gas desulphurization, only CO_2 is collected from the flue gas. The oxyfuel method uses pure oxygen instead of air for combustion which will increase CO_2 concentration to above 80% in the flue gas. In pre-combustion CO_2 capture, fuel is gasified (partially oxidized) to CO_2 and H_2. CO_2 is collected at this step. H_2 can be used to produce energy for equipments. Following are major reactions involved in pre-combustion (Olajire, 2010):

$$2C + O_2 + H_2O = H_2 + CO + CO_2$$

$$C + H_2O = CO + H_2$$

$$CO + H_2O = CO_2 + H_2$$

$$CH_4 + H_2O = CO + 3H_2$$

$$2CH_4 + O_2 = 2CO + 4H_2$$

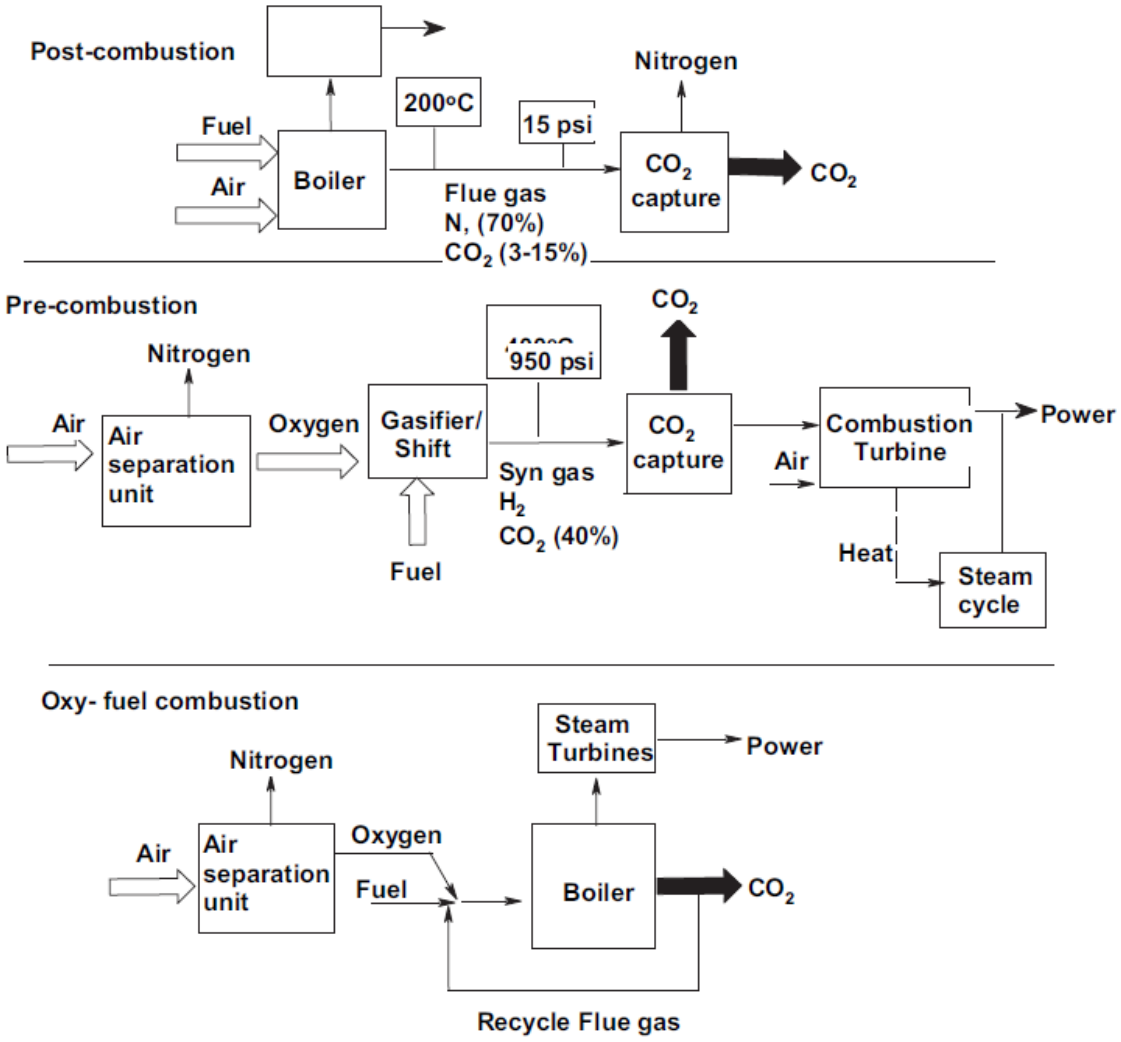

Figure 1.4. Block diagrams illustrating post-combustion, pre-combustion and oxyfuel combustion techniques (Olajire, 2010)

NO_x, SO_2, SO_3 will decrease the pH after dissolving into brine (Wang et al., 2011):

$2NO_2 + H_2O = HNO_2 + HNO_3$

$4SO_2 + 4H_2O = 3H_2SO_3 + H_2S$

$SO_3 + H_2O = H_2SO_4$

$SO_2(\text{dissolved}) + HNO_3 = NOHSO_4$

$NOHSO_4 + HNO_2 = H_2SO_4 + NO_2 + NO$

$SO_2(dissolved) + 2HNO_2 = H_2SO_4 + 2NO$

$2NO + O_2 = 2NO_2$

Knauss et al. (2005) developed a reactive transport model, using fluid and rock data of the Frio Formation Texas (proposed site for CO_2 sequestration pilot project) and found after adding 10^{-6} bar of SO_2 along with 84.3 bar CO_2, the incoming fluid had pH of 1 by the end of injection and resulted in significant mineral dissolution. Xu et al. (2007) used a non-isothermal reactive geochemical transport model and studied co-injection of 0.0364 kg/s SO_2 with 1 kg/s CO_2 and 0.4636 kg/s water (fluid mass injection rates over 10 m thick sandstone aquifer layer). They demonstrated the acidified zone resulting from injection of CO_2 together with SO_2 extended to a radial distance of 200 m from the well bore, compared with that resulting from injection of CO_2 alone, which extends to 50 m, and the pH was as low as 0 within 100m radial distance from well bore in 100 years. In the acidified zone, with co-injection of SO_2, porosity of the sandstone formation increased from 0.3 to 0.43 after 100 years compared with 0.33 when only CO_2 was injected. Wang et al. (2011) evaluated long-term dissolution reactions of caprock minerals by thermochemical calculations. They found that dissolution of K-feldspar increases slightly in the presence of SO_x and NO_x and dissolution of limestone increases by 50% in the presence of 1.5% (vol) total concentration of SO_x and NO_x compared with CO_2 only condition. As a result, NO_x, SO_2 and SO_3 has the potential to greatly decrease brine pH and enhance dissolution of rock, thus the effect of strong acid on geochemical reactions of minerals should be studied.

1.4 Porosity and permeability changes of cap rock

Before carbon sequestration technology is widely utilized, it is crucial to assess potential risks and storage effectiveness. As supercritical CO_2 dissolves into brine, the increase of acidity and bicarbonate concentration will induce dissolution and precipitation of rock materials, affecting permeability. Thus leaking possibilities and seal efficiency of the cap rock will be affected.

Previous experiments and modeling work showed controversial results about the impact of CO_2 on porosity or permeability of rocks. G. Rimmel é et al. (2010) set up reactions of Lavoux limestone and Adamswiller sandstone, collected from a basin in France, with wet supercritical CO_2 or CO_2-saturated water under simulated reservoir conditions (90 ℃ and 28 MPa). They found that the porosity and permeability increased after reaction. Tianfu Xu et al. (2004) developed a non-isothermal reactive geochemical transport model and demonstrated that the porosity for all three samples: Glauconitic sandstone, Gulf Coast sediments, Dunite decreased after CO_2 injection. Factors such as concentration of sulfate, NaCl in brine and initial rock porosity significantly affect porosity and permeability change after CO_2-water-rock reaction. To fully understand this issue, dissolution reactions of specimen minerals such as clay minerals should be performed, and geochemical properties of storage site should be assessed.

1.5 Possible contaminants during carbon sequestration process

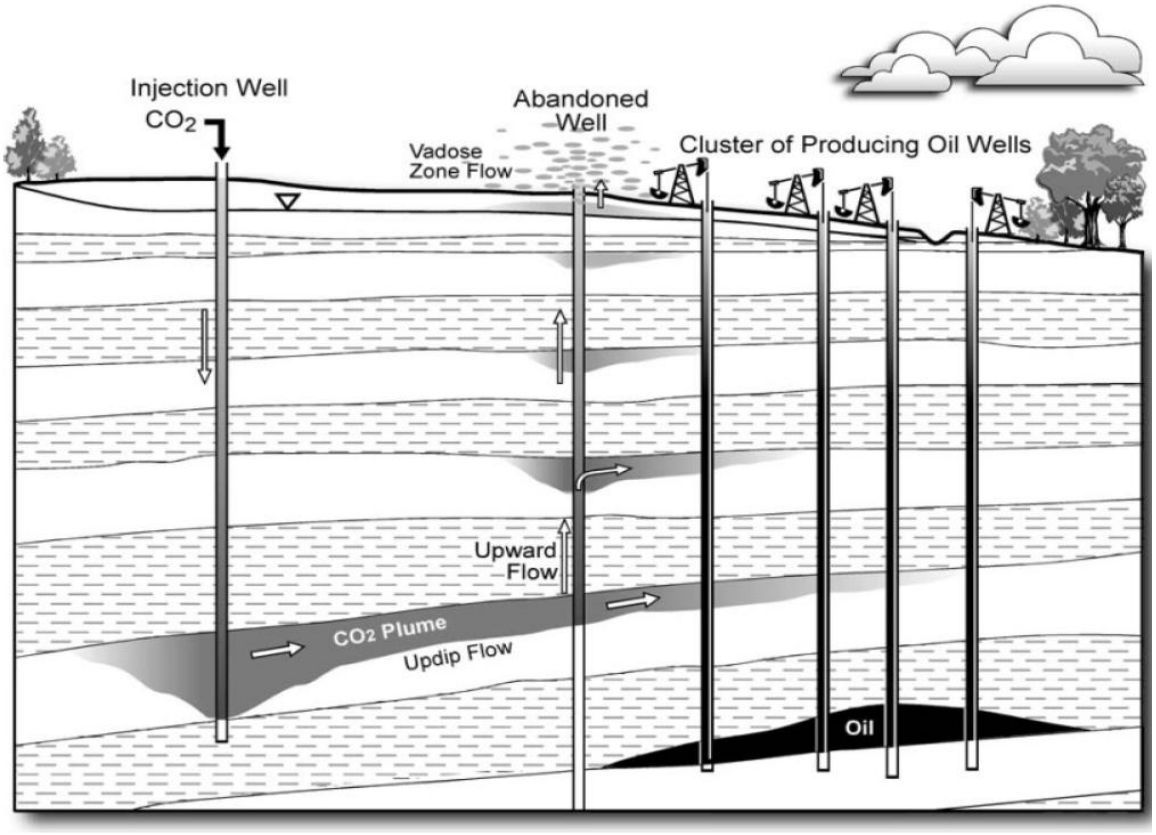

Figure 1.5. Potential leakage pathways of carbon sequestration (Gasda et al., 2004)

Once leakage happens, increased acidity in groundwater could possibly cause dissolution and desorption of contaminants, posing health risks to human beings and other creatures. Model simulation (Wang et al., 2004; Zheng et al., 2009), lab batch reaction (Little & Jackson, 2010; Lu et al., 2010), and field site monitoring (ZERT field site, Bozeman, Montana (Kharaka et al., 2010); Chimayo site, New Mexico (Keating et al., 2010)) have all shown decrease of pH and potential increase in concentration of contaminants such as Pb, U, and As after injection of CO_2. Zheng et al. (2009) set up a reactive transport model and found CO_2 leakage into shallow aquifer can mobilize significant amount of lead and arsenic. Lu et al. (2010) collected aquifer rock samples

from current and potential Department of Energy (DOE) pilot sites, including Dockum, Trinity, and Ogallala formations near the SACROC site in Texas, and the Cranfield formation near the Gulf Coast Stacked Storage Project in Mississippi. They submerged rocks into 40 ppm Cl^- solution and kept bubbling CO_2 gas into the brine. Sr, Mn, Ba, Co, B and Zn were mobilized. Concentrations of Fe, Mn, Pb, As, Zn and BTEX were found increasing during monitoring of pilot study at ZERT field site, Bozeman, Montana (Kharaka et al., 2010). In the study of Chimayo site, New Mexico (Keating et al., 2010), elevated As, U, and Pb concentrations were detected, and was attributed to brine leakage through CO_2 leakage pathways.

In the batch experiments listed above, Little & Jackson (2010) bubbled CO_2 gas into nanopure water (18.6MΩ/cm) with pre-dried aquifer sediment inside at room temperature, then measured dissolved ions; Lu et al. (2010) also ran reaction by bubbling CO_2 gas into 40ppm Cl^- solution with aquifer sediment samples. There is lack of high pressure or supercritical CO_2 reaction data.

1.6 Clay minerals

Clays and clay minerals are ubiquitous in soils, sediments, and sedimentary rocks ,especially in shale, mudstone, and siltstone. They play an important role in environmental processes such as nutrient cycling, contaminant migration, organic matter maturation, and petroleum production (Stucki & Kostka, 2006; Dong et al., 2009). Gradual chemical weathering of rocks by carbonic acid is a major pathway to form clay minerals.

Clay minerals are hydrous aluminum phyllosilicates sometimes containing other cations such as iron, magnesium, alkali metals. Isomorphous substitution in phyllosilicate sheets, for example, Al substitution for Si in the tetrahedral sheet, Mg/Fe(II) substitution for Al in the octahedral sheets, results permanent negative charge of clay mineral structure at neutral pH. The net negative charge of clay mineral structure must be compensated by adsorbed ions. Si/Al-O or Si/Al-OH bonds at clay mineral surface could gain protons at low pH and lose protons at high pH conditions. Therefore surface charge of clay mineral is pH dependent. Point of zero charge (PZC) is the pH value when surface charge of clay mineral equals to zero. When pH_{PZC}<PZC, clay mineral has a net positive surface capacity, while when pH_{PZC}>PZC, clay mineral has a net negative surface charge.

Table 1.2. Point of zero charge of some clay minerals. (Walther, 2009)

clay mineral	pH_{PZC}
Hematite	8.5
Goethite	7.3-7.8
Kaolinite	2-4.6
Quartz	2-3
Feldspars	2-2.4
Montmorillonite	2-3

Clay mineral structures are classified as 1:1 (kaolinite and serpentine) or 2:1 (vermiculite and montmorillonite) tetrahedral (T) sheets (Si, Al, Fe) to octahedral (O) sheets (Al, Fe, Mg). In each tetrahedron, one Si atom coordinates with four oxygen atoms; in each octahedron, one Al atom coordinates with six oxygen atoms (not considering isomorphous substitution). All nontronite (NAu-2), montmorillonite (SWy-2) and chlorite (CCa-2) have Tetrahedron-Octahedron-Tetrahedron (TOT) structures. TOT structure of montmorillonite is shown in Figure 1.6. Compared with montmorillonite, almost 100% Al^{3+} in octahedrons are replaced by Fe^{3+} in nontronite. In both montmorillonite and nontronite, there exist interlayer cations such as Ca^{2+}, Mg^{2+} or Na^{+} to balance the negative charge of phyllosilicate sheets; and the interlayer also contains water, which influence the swelling properties. Comparing with structure of montmorillonite, about 1/4 of Si^{4+} in tetrahedrons are replaced by Al^{3+} in chlorite. Another difference is that chlorite contains a brucite-like layer between TOT structures instead of exchangeable cations and water. This brucite-like layer is hydroxides of Mg, Al and Fe and holds net positive charge to balance negative charge of phyllosilicate sheets.

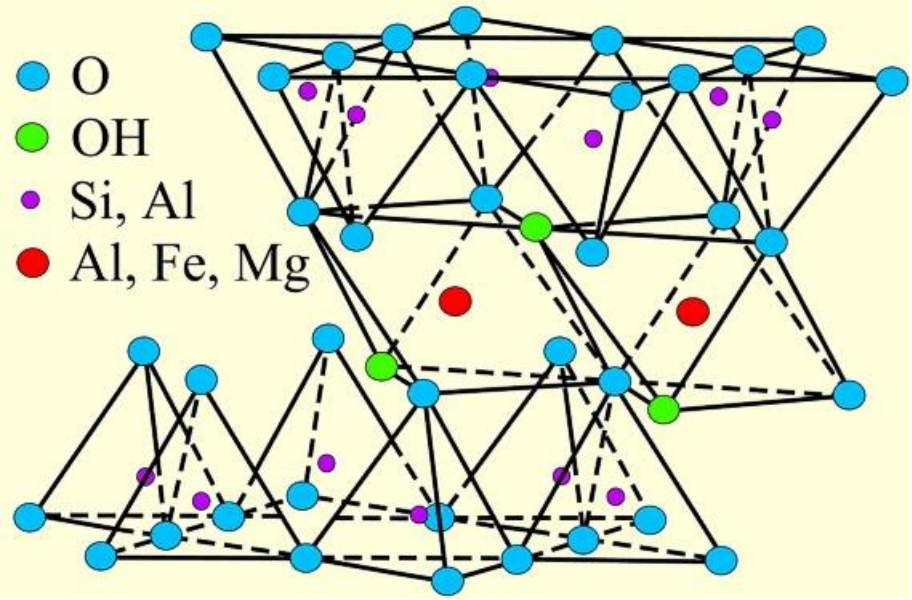

Figure 1.6. Illustration of structure of montmorillonite (Mineralogy, Petrology, and Geochemistry Across the Curriculum: Teaching Clay Mineralogy, A compilation by David Mogk, Dept. of Earth Sciences, Montana State University, http://serc.carleton.edu/NAGTWorkshops/mineralogy/clay_mineralogy.html)

Acid activated clay, usually bentonite (consisting mostly montmorillonite) has been used in industry as adsorbent. Strong acid like 1-10 M H_2SO_4 and HCl are used to expand porosity and surface area of clay at ~80 ℃. Most experimental studies on clay mineral dissolution were conducted with strong acid (>1M H_2SO_4 or HCl) under high temperature (70 ℃ to 95 ℃) for several hours (Okada et al. 2006; Steudel et al. 2009; Pentra ̌k et al. 2009, 2012; Wei et al. 2010). Steudel et al. (2009) found that substitution of Mg or Fe in the octahedral sheets and substitution of Al in the tetrahedral sheets promoted dissolution of non-swelling clay minerals including illite, sepiolite, kaolinite and magadiite in 1-10 M H_2SO_4 at 80 ℃ for several hours. They also concluded that the dissolution of the octahedral cations occurred in the following order: Mg>Fe>Al. Similar phenomena was also observed by Pentra ̌k et al. (2009). Compared with the mixed-layer illite/smectite mineral (Dolna ̌Ves, Slovakia), Ca-illite from Morris (Illinois, USA) with greater substitution of Mg and Fe for Al in the octahedral sheets and greater substitution of

Al for Si in the tetrahedral sheets dissolved to a greater extent in 6 mol/L HCl at 95 ℃ for 36 hours. However, under non-severe conditions clay minerals do not dissolve to any great extent. A conceptual model of clay mineral dissolution in H_2SO_4 was developed by Shaw & Henry (2009). At pH higher than 3, clay mineral structure was not interrupted and only ion exchange took place (Figure 1.7). However, hydrofluoric acid (HF) is effective for dissolving clay minerals because one dissolution product SiF_4 is volatile, making dissolution reaction has a more positive entropy change.

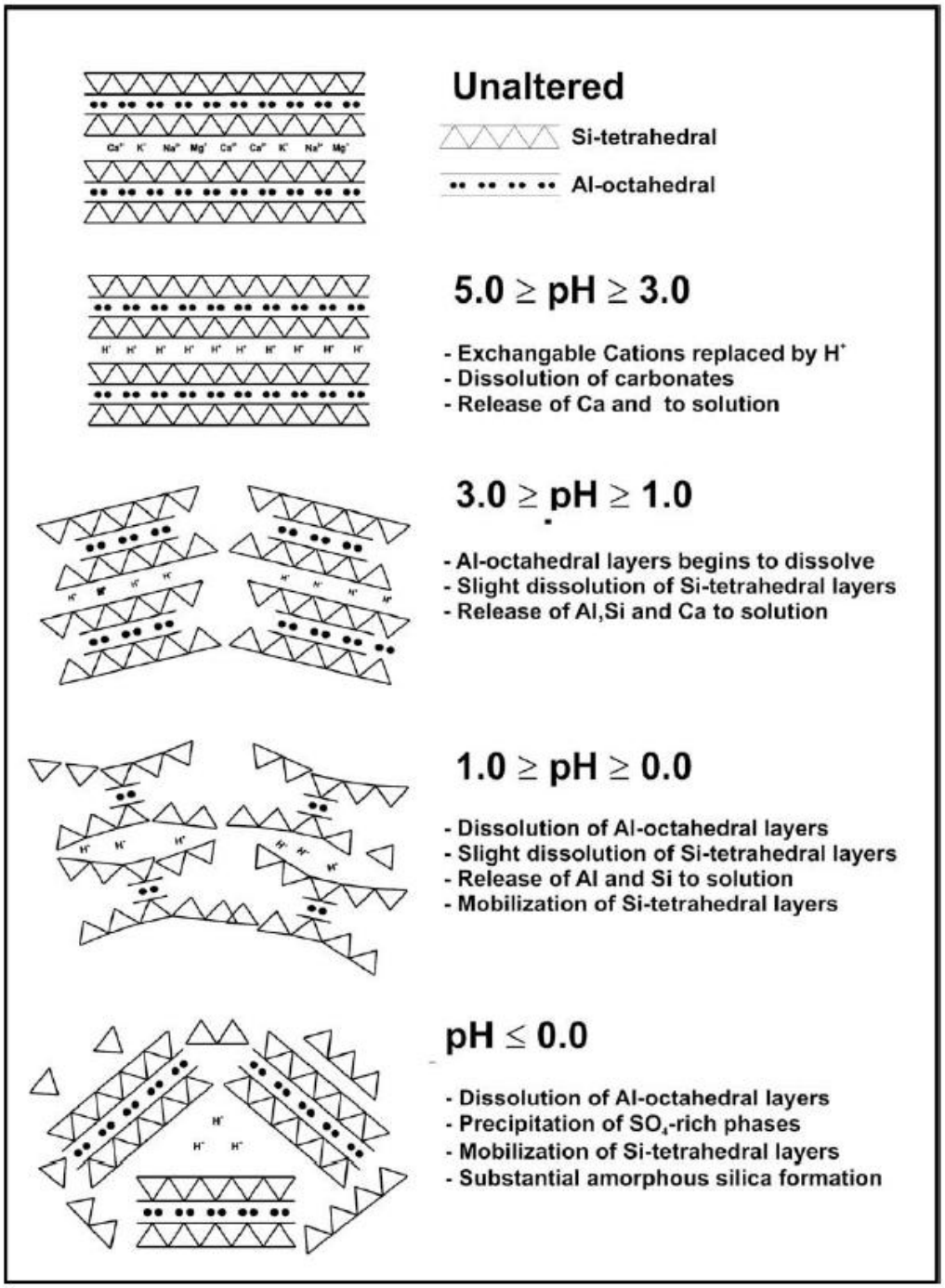

Figure 1.7. Conceptual model of clay mineral dissolution in H_2SO_4 between pH 5.0 and -3.0 (Shaw & Henry, 2009)

Iron is the fourth most abundant element in the Earth's crust and Fe in clay minerals often accounts for about half of the Fe pool in soils and sediments (Favre et al. 2006). Clay minerals are known to influence fate and transport of several contaminants (uranium, arsenic) through sorption process and by redox reactions with the Fe(III)-Fe(II) cycle (Haque et al 2008; Ilgen et al. 2009; Zhang et al 2009, 2011). Nontronite (NAu-2) specimen clay mineral contains ~20.7% Fe (wt.%) and 98% of Fe is Fe(III) (Bishop et al., 2011). Fe(III) in NAu-2 can be reduced biotically and abiotically. Microbes such as *Shewanella putrefaciens* strain CN32, methanogen *Methanosarcina mazei* and sulfate-reducing *Desulfovibrio vulgaris* ATCC29579, were capable to reduce 23.8%, 25% and 19.1% of total Fe in NAu-2, respectively (Bishop et al., 2011; Zhang et al., 2012; Liu et al., 2012). However, the citrate-bicarbonate-dithionite reduction method developed by Stucki et al. (1984) could chemically fully reduce NAu-2. Biotic and abiotic reduction pathways are different. Biotic reduction takes place first on edge or surface of clay mineral structure then moves inside (Komadel et al., 2006) (Figure 1.8 C), and not all Fe(III) is available to the microbes. For chemical reduction, Lear and Stucki (1987) proposed "pseudo random" reduction of Fe atoms in clay mineral structure: the produced Fe(II) atoms tend to be far away from each other (Figure 1.8D), based on UV-vis spectroscopy data. Clay mineral dissolves during reduction process and dissolution extent is dependent of reduction extent. Jaisi et al. (2008) reported that significant reductive dissolution occurred when reduction extent was higher than 30% (Figure 1.9). Fe(II) released from clay structure partitioned into surface-complexation sites (sodium acetate extractable), exchangeable sites (NH_4Cl extractable) and aqueous forms. There was around 65% Fe(II) left in clay structure for 71% reduced NAu-2. Increasing concentrations of dissolved Si was also observed as reduction extent of NAu-2 increased.

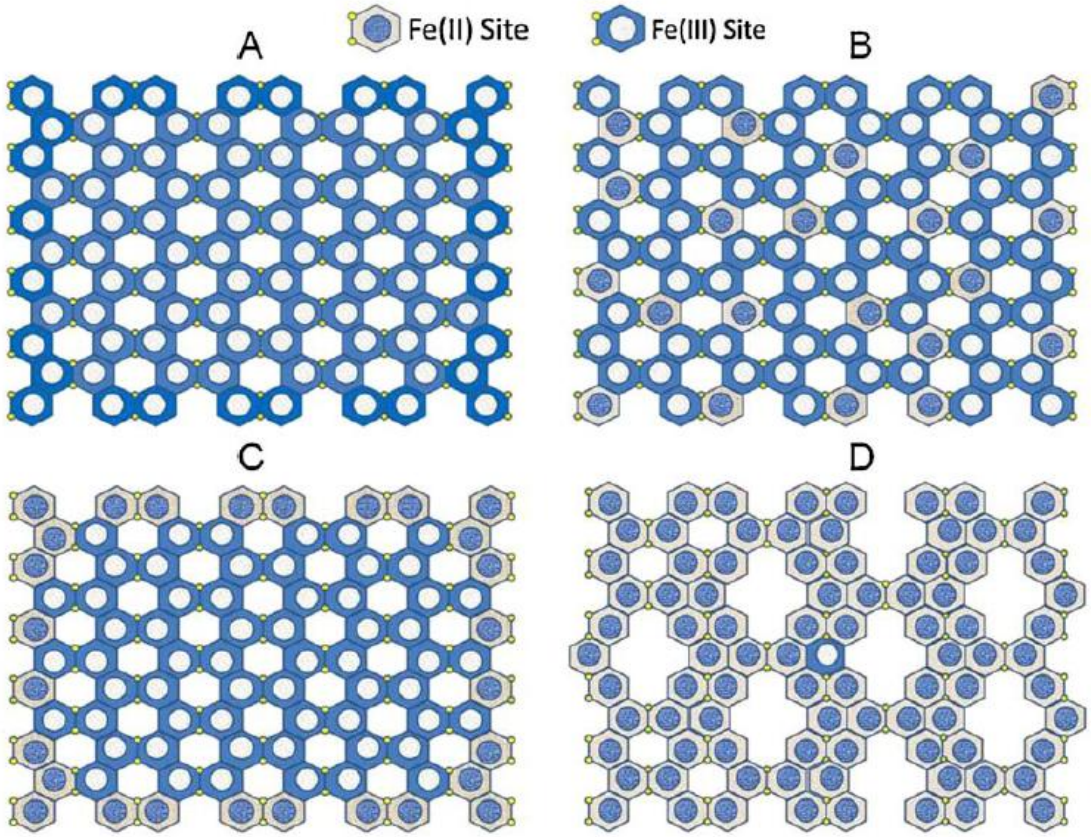

Figure 1.8. Illustration of distribution of Fe(II) and Fe(III) in the octahedral sheet of Garfield nontronite: (A) unaltered; (B) partially reduced by dithionite; (C) partially reduced by bacteria; (D) fully reduced by dithionite (Ribeiro et al. 2009; Stucki 2011). Patterns are projection down c* of dioctahedral layer silicates of nontronite, tetrahedral layers not shown. Fe atoms locate at center of each octahedron (hexagon in this projection pattern). Small yellow circles are OH groups.

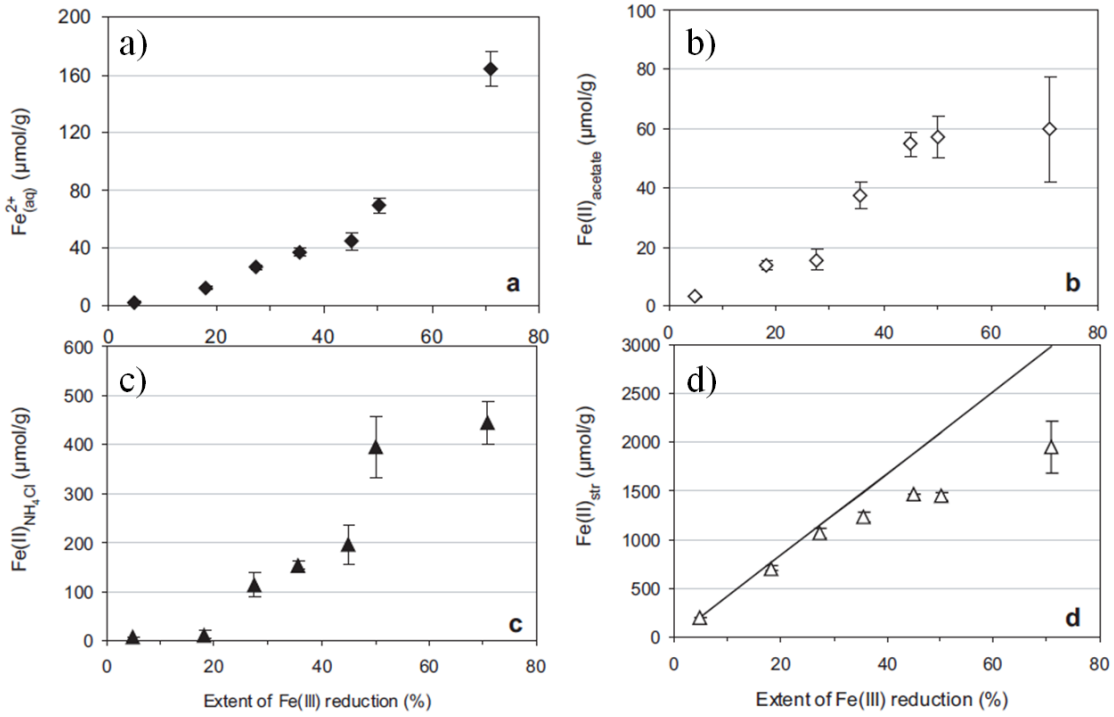

Figure 1.9. Fe(II) distribution of reductive dissolution of NAu-2 as a function of reduction extent. (a) dissolved Fe(II); (b) Sodium acetate extractable Fe(II); (c) NH_4Cl extractable Fe(II); (d) Fe(II) left in clay mineral structure

1.7 Uranium chemistry

Uranium is often dissolved in U(VI) form and precipitated as uraninite (UO_2), thus oxidation of U(IV) to U(VI) increases its solubility and mobility in environment. Redox reactions between uranium minerals and iron are important to influence the mobility of uranium. Generally, U(VI)/U(IV) and Fe(III)/Fe(II) have similar redox potentials at neutral pH. However, the exact redox potential in reaction systems is dependent on the exact species and the activity of each species (Figure 1.11). For example, Fe^{2+} (aq) is not facile to reduce U(VI), whereas some Fe(II)-bearing minerals such as microcrystalline hematite, goethite, smectite, and natural solids have been reported to reduce U(VI) at near-neutral pH (Liger et al., 1999; Jeon et al., 2005). On the other hand, oxidation of uraninite by Fe(III) in clay minerals have been observed. Structural

Fe(III) in nontronite NAu-2 could oxidize biogenic UO_2, while chemically reduced NAu-2 (27% 0.5 N HCl-extractable Fe(II)) did not reduce U(VI), both in 30 mM $NaHCO_3$ at pH=6.8 (Zhang et al., 2009). Through thermodynamic calculation approach, Ginder-Vogel et al. (2006) proved that at low pH, ferrihydrite, goethite and hematite can lead to biogenic UO_2 oxidation and increasing bicarbonate concentration will favor this redox reaction.

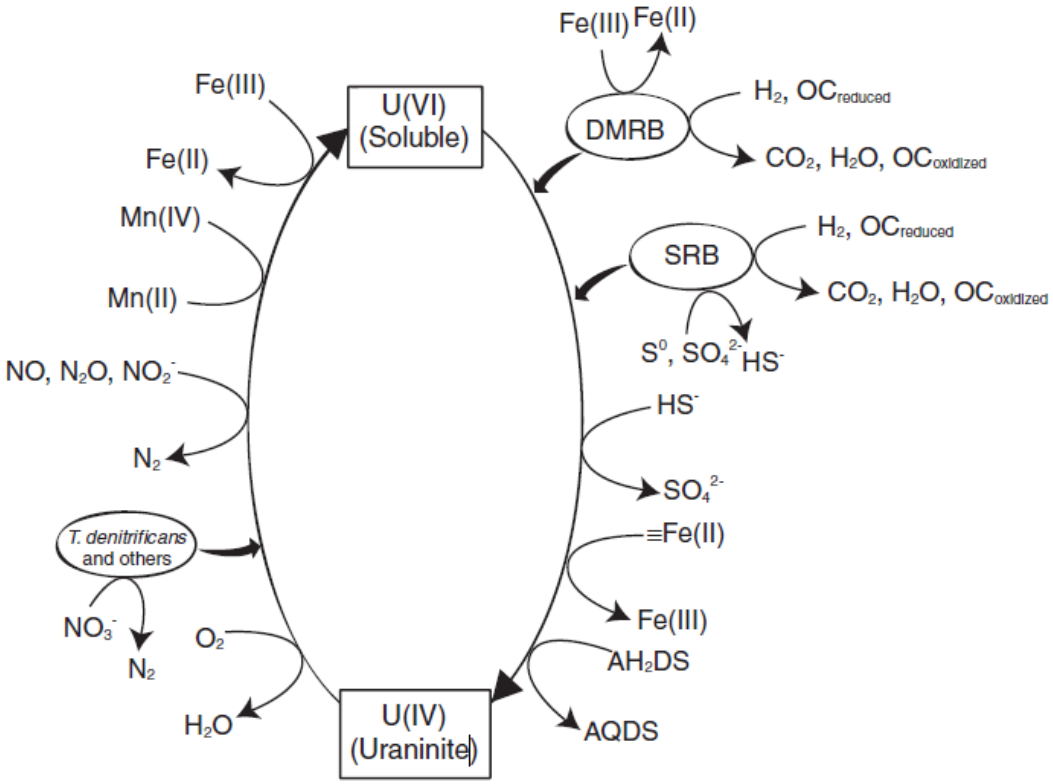

Figure 1.10. Uranium redox cycling with redox active reagents. Abbreviations: Dissimilatory Metal-Reducing Bacteria (DMRB), Sulfate-Reducing Bacteria (SRB), Surface Bound Iron (≡Fe), Reduced Organic Carbon ($OC_{reduced}$), Oxidized Organic Carbon ($OC_{oxidized}$), 9, 10-Anthraquinone-2, 6-Disulfonic Acid (AQDS), and Reduced AQDS (AH2DS). (Ginder-Vogel & Fendorf, 2008)

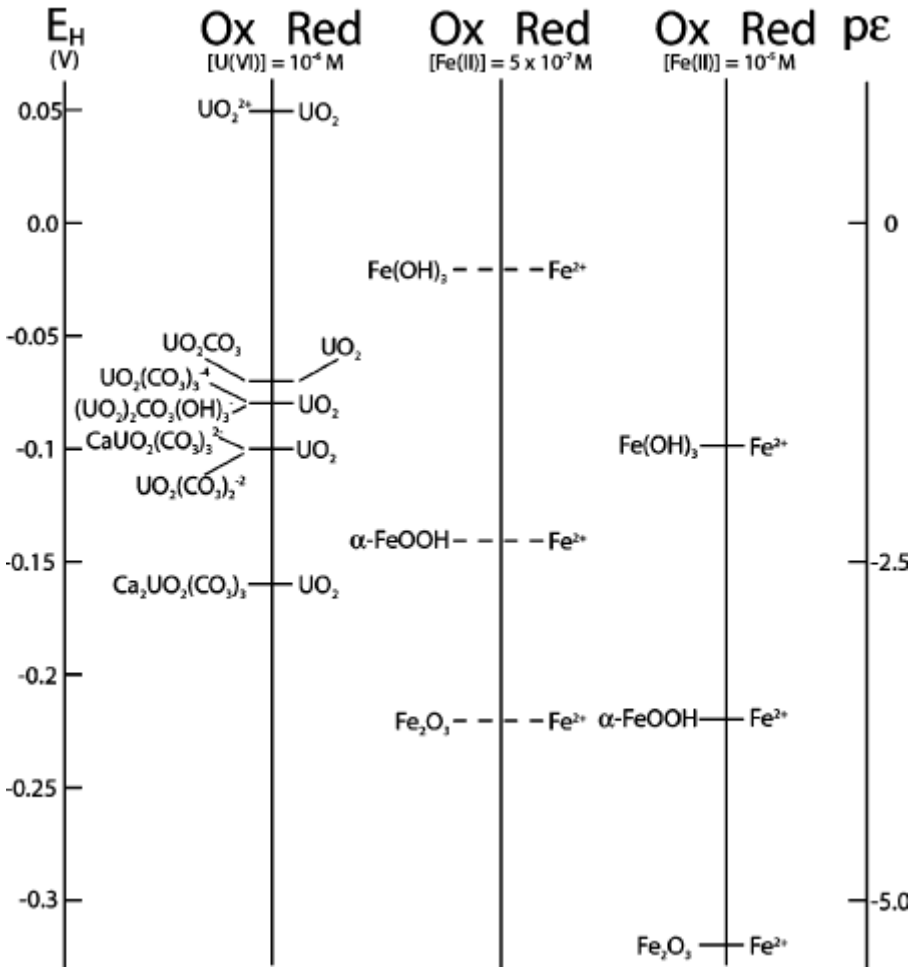

Figure 1.11. Fe(III)/Fe(II) and U(VI)/U(IV) redox couples at pH=7, concentrations of $3*10^{-3}$ M HCO_3^-, $1*10^{-6}$ M U(VI), $1*10^{-3}$ M Ca^{2+}, and either $5*10^{-7}$ or $1*10^{-5}$M Fe(II). (Ginder-Vogel et al. 2006)

Dissolution of uraninite into aqueous form has been found as the rate limiting step of oxidation of uraninite by ferrihydrite (Ginder-Vogel et al., 2010). Deceasing pH values and increasing bicarbonate concentrations facilitated dissolution of uraninite and promoted oxidation of uraninite both kinetically (Ginder-Vogel et al., 2010) and thermodynamically (Ginder-Vogel et al., 2006) (Figure 1.12). In carbon sequestration scenario, adding CO_2, which would increase acidity, might induce proton-driven and facilitate oxidation-driven dissolution of uranium.

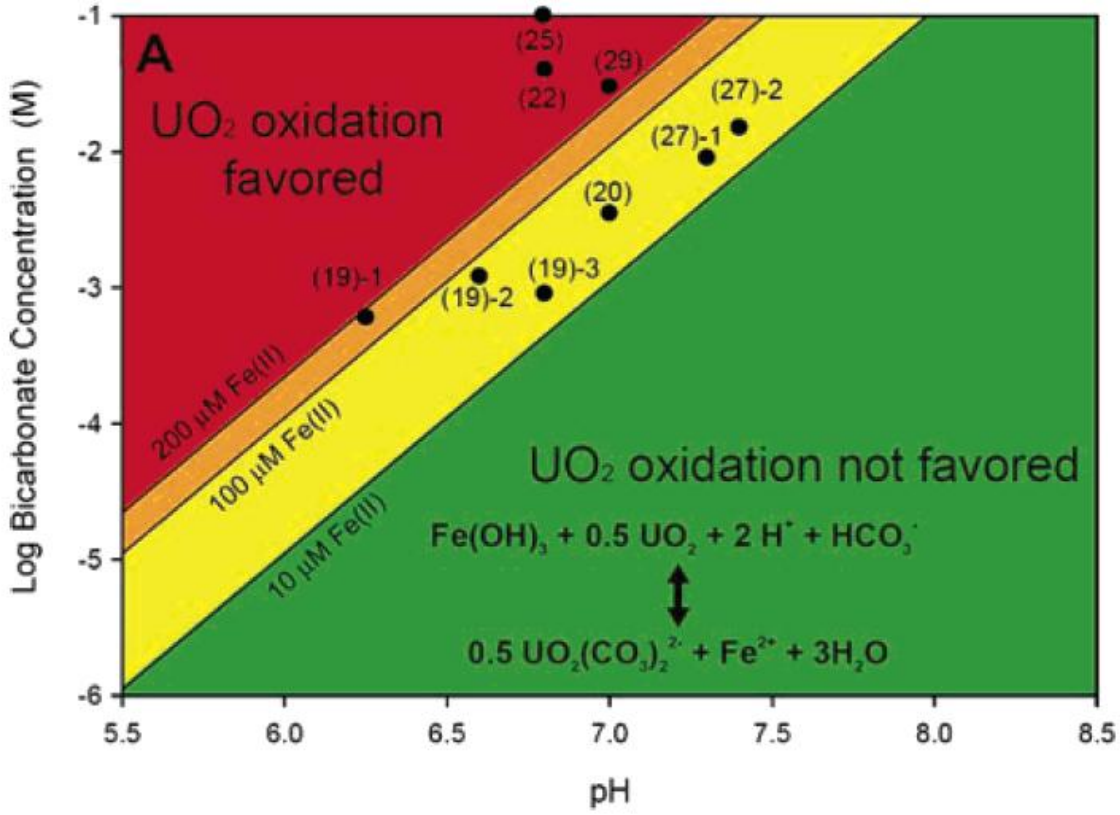

Figure 1.12. Thermodynamic demonstration of UO_2 (amorphous) oxidation by ferrihydrite with 0.126 µM U(VI) (aq) in equilibrium. Plots and numbers indicate data from reference of the original paper. (Ginder-Vogel et al., 2006)

1.8 Research objectives

1. Compare dissolution of nontronite (NAu-2), montmorillonite (SWy-2) and chlorite (CCa-2) in 1.0 M NaCl brine under high pressure CO_2 conditions (P_T = 9.66 bar, $P_{CO2} \geq 8.66$ bar CO_2) and ambient pressure conditions (P_T = 1.0 bar, N_2:H_2 = 95:5%).
2. Compare dissolution of NAu-2 in 1.0 M NaCl, 0.33 M $CaCl_2$ and 0.33 M Na_2SO_4 under high pressure CO_2 conditions and ambient pressure conditions.

3. Compare dissolution of partially reduced nontronite (R-NAu-2) with unaltered NAu-2 under high pressure CO_2 conditions and ambient pressure conditions.
4. Study NAu-2 and R-NAu-2 dissolution in 0.33 M Na_2SO_4, 1.40 M H_3PO_4 - 0.50 M H_2SO_4.
5. Study redox reactions between NAu-2, R-NAu-2 with U(VI) under high pressure CO_2 conditions and ambient pressure conditions, and the influence of U(VI) on dissolution of NAu-2 and R-NAu-2.
6. Study redox reactions between NAu-2 and U(IV) under high pressure CO_2 conditions and ambient pressure conditions, the influence of U(IV) on dissolution of NAu-2, and dissolution of uranium into aqueous phase.

Chapter 2

Materials and Methods

2.1 Experimental Materials

2.1.1 Clay minerals

Nontronite (NAu-2), Wyoming Montmorillonite (SWy-2), and Ripidolite (CCa-2) specimen clay minerals were purchased from the Clay Mineral Society and size fractionated for use in these experiments. As-received material was first grinded by mortar and pestle, and then the clay powder was soaked overnight in 0.5 M NaCl at a clay concentration of 33.3 g/L. The mineral suspension was transferred into 250 mL Nalgene centrifuge tubes and centrifuged at 110 rcf (relative centrifugal force) for 3 min to collect the ≤2 μm particle size fraction (remained in supernatant). The mineral pellet was resuspended, sonicated and the ≤2 μm particle size fraction was collected again. The ≤2 μm particle size fraction was then washed repeatedly with DI water until no Cl^- was detected by adding drops of AgCl solution into supernatant. Pellets were oven-dried at 80 ℃ until constant weight.

Table 2.1. Source clay mineral properties (Bishop et al., 2011)

clay	Structure	BET SA (m2/g)
NAu-2	$[Ca_{0.28}Na_{4.56}K_{0.42}]_{0.72}(Al_{0.23}Fe^{2+}_{0.06}Fe^{3+}_{3.76}Mg_{0.10}Ti_{0.06})(Si_{7.19}Al_{0.81}Fe_{0.33})O_{20}(OH)_4$	271
SWy-2	$(Ca_{0.16}Na_{0.24})[Al_{1.45}Fe^{2+}_{0.01}Fe^{3+}_{0.12}Mg_{0.44}][Si_{6.73}Al_{1.27}]O_{20}(OH)_4$	240
CCa-2	$[(Mg_{0.46}Fe^{2+}_{1.50}Fe^{3+}_{3.43}Ti_{0.44}Mn_{0.03})(Si_{5.51}Al_{2.49})O_{20}(OH)_4][(Mg_4Al_{1.81}(OH)_{12}]$	19

To produce partially reduced NAu-2 (R-NAu-2), 0.5 g of NAu-2 was suspended in 60 mL 0.1 M $MgCl_2$ in an Erlenmeyer flask capped with a rubber stopper and stirred overnight. 60 mL of 0.3 M sodium citrate solution and 30 mL of 1.0 M sodium bicarbonate solution were then added into the clay mineral suspension. The flask was placed into a water bath maintained at 70 °C, purged with oxygen-free N_2(g), and mixed using a magnetic stir bar. After 30 min at 70 °C, 1.0 g sodium dithionite was added into the suspension to reduce the clay-Fe(III) and allowed to react for 75 min. The reaction was stopped by immersing the flask into an ice bath, and the flask was continuously purged with N_2(g) until it cooled. The flask was moved into an anoxic (supplying gas: N_2:H_2 95:5 gas mix, maximum O_2 concentration recorded < 20 ppm) chamber (Coy, Grass Lakes, MI) immediately after cooling to room temperature. The reduced clay mineral suspension was washed sequentially in O_2-free 0.1 M NaCl, 0.01 M NaCl, 0.001 M NaCl solutions, and then washed three times in O_2-free Milli-Q water. Anoxic Milli-Q was prepared by boiling and purging with 99.99% N_2 for 1 to 2 h. Reduced NAu-2 suspensions were stored in the anoxic chamber. Concentrations of R-NAu-2 suspensions were determined by oven-drying 10 mL suspension at 80 ℃ till constant weight and weighing the remaining pellet.

2.1.2 Brine solutions

In this study, we use three synthetic brines. 1 M NaCl, 0.33 M $CaCl_2$ and 0.33 M Na_2SO_4 brines were prepared using ACS grade salt (BDH Sodium Chloride, BDH Calcium Chloride Dihydrate, EM SCIENCE Sodium Sulfate). Brine chemistry is very site dependent, governed by mineralogy in the sediment. According to Marcus Wigand et al. (2009) and Jamal Daneshfar et al. (2009), salinity of natural brine can be up to 100,000 mg/L.

2.1.3 Uranium solutions

Uranyl acetate dihydrate was dissolved in 30 mM $NaHCO_3$ (pH 6.8) under N_2 atmosphere to prepare a 0.90 mM U(VI) stock solution.

Biogenic uraninite (UO_2(s)) was produced by adding *Shewanella oneidensis* MR-1 (initial cell density 0.5-1 $*10^8$ cells/mL) with 1.0 mM uranyl acetate as the sole electron acceptor (with 5 mM sodium lactate in 30 mM $NaHCO_3$ buffer). After a 3 month incubation period, the cell-uraninite suspension was transferred into 10% NaOH solution and mixed for two days to digest cell material (Ginder-Vogel et al., 2006), then washed three times with 24 mM O_2-free $NaHCO_3$ and twice with O_2-free Milli-Q water. Final total uranium concentration was 0.666 mM and U(VI) concentration was 0.280 mM. Such high concentration of U(VI) was due to frequent washing, moving out of anoxic chamber and centrifuging processes.

2.1.4 *Shewanella oneidensis* strain MR-1 cell cultivation

Frozen cell suspension of *Shewanella oneidensis* MR-1 was thawed. 100 μL was transferred to a culture tube containing 5 mL Tryptic Soy Broth-without dextrose (TSB-D) and incubated aerobically for 24 h at room temperature on bench top. Then 1ml was transferred into 100ml TSB-D and incubated at 20 ℃ on rotating shaker at ~100 rpm. 16 hours later, cells were centrifuged down with glass beads at 3500 rcf at 15 ℃. Centrifuge tubes were refilled with PIPES and vortexed for 5 minutes. After twice more washing step, fresh PIPES was added and suspension was mixed in anoxic chamber overnight. Cells were centrifuged down at 3500 rcf for 10 minutes with centrifuge tube caps sealed and moved back into anoxic chamber. 5 mL PIPES was added after pouring off supernatant. Tubes were vortexed on high level for two minutes and then low level for 10 minutes. Concentrated cell suspensions were diluted 200-fold with Milli-Q

water and measured by absorbance at 410 nm on a Shimadzu UV-1601 spectrometer (Shimadzu Inc., Columbia, MD):

$$\text{Concentration of cells } (10^9 \text{cells/mL}) = \frac{A420*200}{7.5}$$

2.2 Experimental Methods

High pressure CO_2 conditions were established by adding a measured mass of dry ice (purchased from Penn State Bakery) to a pressure tube containing clay minerals, brine, with/without uranium. Reaction kinetics were measured over a 15 d period by sacrificing pressure tubes, analyzing the filtrate for dissolved mineral components and U, and analyzing the Fe(II/III) speciation in solution and the clay pellet. Reactors were 38 mL pressure tubes (Ace Glass, Inc.) that were rated to a maximum pressure of 150 psi (10.34 bar). Pressure tubes were acid washed using 10% - 15% nitric acid before use. All reactor preparation before adding dry ice was done inside an anoxic chamber. Reactors were filled with 10 mL of 0.5 g/L clay mineral brine suspensions (Table 2.2). Pressure tubes were moved out of anoxic chamber after tightening front seal plugs. For reactors designated for CO_2 atmosphere reaction, 0.8 g dry ice (weight when leaving balance) was added into each tube outside the anoxic chamber, and the plug was tightened immediately to prevent CO_2 loss. Due to operation difficulties of putting dry ice in anoxic chamber, pressure tubes need to be opened under aerobic condition. The opening time of each tube did not exceed 10 seconds, and all steps: weighing dry ice, moving dry ice to pressure tube, opening pressure tube, adding in dry ice and closing plugs were operated as fast and constant as possible. Considering very limited time of pressure tubes opening to atmosphere, and bubbling of CO_2 gas in the tube after adding dry ice, we assume there was at most 1 bar N_2 H_2 mix gas (95:5) left in the tube and there was no oxygen inside. After adding dry ice, initial

pressure (10 min after adding dry ice) reached 9.66 bar (measured by pressure gauge attached within seal plug, Ace Glass, Inc.), out of which ≥ 8.66 bar was partial pressure of CO_2. 15 days later the total pressure left was about 7.17 bar. All pressure tubes were placed on a rotating shaker (VWR 1000 Standard Orbital Shaker) at level 3.5 (~ 100 rpm) in a 20 ℃ temperature control room. Control reactors with no clay mineral in brine were also set up. All high pressure CO_2 pressure tubes had ambient pressure (P_T = 1.0 bar, N_2:H_2 = 95:5%) controls. Reactors were incubated for 15 d and samples were collected after 0, 1, 3, 6, 10 and 15 d. In no-uranium experiments, clay pellets were collected by centrifugation at 8000 rcf for 10 minutes and washed using Milli-Q water, oven-dried and grinded for Scanning Electron Microscope (SEM) and X-Ray Diffraction (XRD) analysis. Filtrated solution samples were prepared for ICP-AES analysis.

1.40 M H_3PO_4 - 0.50 M H_2SO_4 was selected for our dissolution of clay minerals in strong acid experiment. 1.40 M H_3PO_4 - 0.50 M H_2SO_4 is also used in Luan & Burgos' (2012) sequential extraction method designed for analyzing clay-uranium systems. Dissolution of clay minerals in strong acid experiment was conducted in Erlenmeyer flasks and ion concentrations in no-clay control were also measured.

Table 2.2. Summary of experimental components and conditions tested

conditions	high pressure CO_2			1.40 M H_3PO_4-0.50 M H_2SO_4	U(VI) high pressure CO_2	U(IV) high pressure CO_2
brine / clay	1 M NaCl	0.33 M $CaCl_2$	0.33 M Na_2SO_4	0.33 M Na_2SO_4	0.33 M Na_2SO_4	0.33 M Na_2SO_4
NAu-2	X	X	X	X	X	X
SWy-2	X					
CCa-2	X					
R-NAu-2			X	X	X	

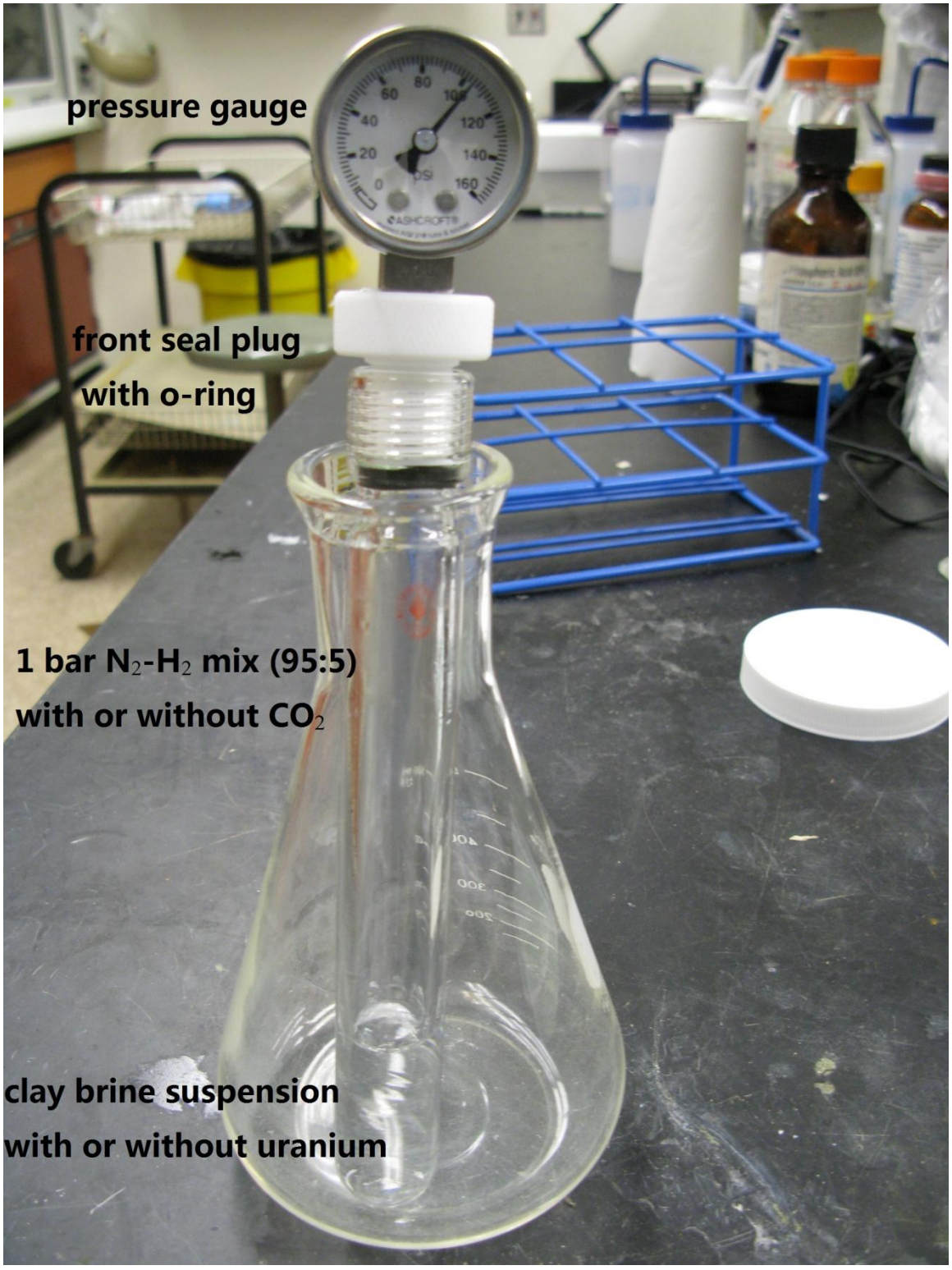

Figure 2.1. Picture of a pressure tube, taken after 15 days in experiment of 1.0 M NaCl brine under high pressure CO_2 condition, final pressure was ~ 104 psi (7.17 bar)

Clay-uranium experiments were initiated by mixing 1.0 g/L NAu-2 or R-NAu-2 in 0.66 M Na_2SO_4 brine suspension with U(VI) or U(IV) stock solution at a 1:1 volume ratio. Final concentrations in the pressure tubes were 0.5 g/L NAu-2 or R-NAu-2, 0.33 M Na_2SO_4, and 0.45 mM U(VI) for U(VI) reactions, or 0.333 mM uraninite-uranium (58% U(IV)) for U(IV) reactions. Total suspension volume in each pressure tube was approximately 10 mL. UO_2-only, and ambient pressure (P_T = 1.0 bar, N_2:H_2 = 95:5%) were also prepared with this experiment. All glassware, plasticware, syringes and needles used in these experiments were stored in an anoxic chamber (Coy, Grass Lakes, MI) for several days before use. Reactors were incubated for 15 d and samples were collected after 0, 1, 3, 6, 10 and 15 d. For each sample, 1 mL well-mixed suspension was centrifuged at 14000 rpm for 10 minutes; and dissolved Fe and U in the supernatant were measured. Another 0.2 mL aliquot was centrifuged. Fe and U in clay mineral were then measured based on a H_3PO_4-H_2SO_4-HF sequential extraction method developed in our laboratory (Luan & Burgos, 2012).

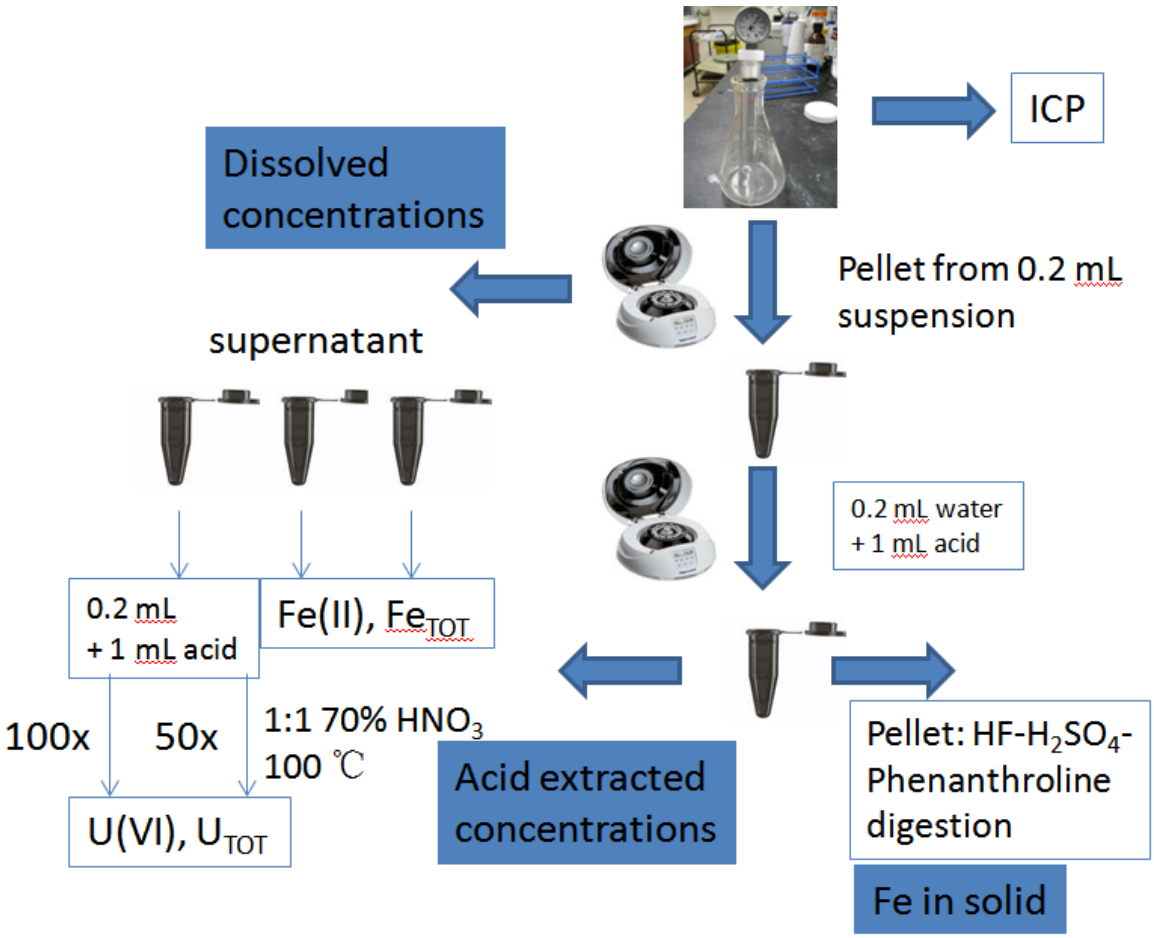

Figure 2.2. Illustration of sequential extraction method used for analyzing clay-U systems

2.3 Analytical Methods

2.3.1 ICP-AES analysis

Pressure tubes were sacrificed as a function of time for analysis. The tube plug was first opened to relieve pressure, the reactor contents were shaken by hand, and the whole suspension was poured into 20 mL plastic scintillation bottles (acid washed). After taking samples for Fe and U measurement, the sample suspension was passed through a 0.2 μm syringe filter, and the

filtrate was acidified with a few drops of 70% nitric acid (J.T. Baker, high purity for trace metal analysis), and stored at 4 ^{o}C until analysis.

Samples were diluted and analyzed using a Perkin-Elmer Optima 5300, Inductively Coupled Plasma Emission Spectrometry (ICP-AES).

2.3.2 pH

pH of clay mineral suspensions were measured for 10 g/L NAu-2 in 1.0 M NaCl reactions, 10 g/L NAu-2 in 2.0 M $CaCl_2$ reactions, and 10 g/L SWy-2 in 1.0 M NaCl reactions under both high pressure CO_2 and ambient pressure conditions. Pressure tubes were sacrificed as a function of time for analysis. The tube plug was first opened to relieve pressure, the reactor contents were shaken by hand, and the whole suspension was poured into 15 mL centrifuge tubes. pH probe was merged at 2 cm depth of suspension immediately, and pH values were automatically recorded to a laptop computer, which was connected to the pH meter (Mettler Toledo, S40 SevenMulti). pH values were recorded every 3 seconds. pH values at 120 seconds were used as our data to allow for stabilization time of pH probe.

2.3.3 XRD

Reacted clay pellets collected from suspension were washed by Milli-Q water till no Cl- detected by $AgNO_3$. Clay mineral samples were oven-dried in 80 ℃, grinded into powder and passed through No. 200 sieve. Samples were contained tightly in Special Glass Thin-Walled Capillary Tubes (Charles Supper Company) and analyzed using Rigaku Dmax-rapid Microdiffractometer (Rigaku Americas Corporation) equipped with Molybdenum source.

2.3.4 SEM

Size fractionated NAu-2, SWy-2 and CCa-2 samples, and NAu-2 samples after 15 d reaction in 2 M NaCl under 8.66 bar CO_2 condition were washed by Milli-Q water till no Cl- detected by $AgNO_3$. Clay mineral samples were oven-dried in 80 ℃, grinded into powder. Samples were analyzed using Hitachi S-3500N Scanning Electron Microscope.

2.3.5 Iron measurement

In no-uranium reaction systems, the conventional $HF{-}H_2SO_4$ digestion method was used to measure the structural clay-Fe(II) and clay-Fe_{TOT} concentrations. For one example, 0.2 mL well mixed clay mineral suspension were transferred into 1.5 mL brown centrifuge tube with screw cap, 0.48 mL 4.9 N H_2SO_4, 0.11 ml 10% (wt/wt) 1,10-phenanthroline (in 95% ethanol), and 0.055 mL 27.6 N HF were then added. A batch of tubes was placed into a microcentrifuge tube rack that floated (partially submerged) in a boiling water bath. After 30 min heating and 15 min cooling, 0.55 mL of 2.4 N H_3BO_3 solution was added into the tubes. 0.2 mL digested sample was transferred into 1 mL 10% sodium citrate solution in black 1.5 mL centrifuge tubes and the Fe(II) concentration was measured by absorbance at A510. 0.2 mL digested sample was added to 1 mL 10% sodium citrate with 2% hydroxylammonium sulfate, reacted overnight, and the total Fe concentration was measured by absorbance at 510 nm on a Shimadzu UV-1601 spectrometer (shimadzu Inc., Columbia, MD). Fe standard curves were prepared using ammonium ferric sulphate dodecahydrate.

In clay-uranium systems, Fe in supernatant was measured at 510nm directly after adding 0.2 mL solution into 1 mL 10% sodium citrate solution; Fe in clay pellet was measured based on Luan & Burgos' sequential extraction method (2012). Fe and U samples in solution were

collected by centrifuged down 1 ml clay-U suspension at 14000 rpm for 10 min. 0.2 mL supernatant was transferred into 1 mL 10% sodium citrate solution in black 1.5 mL centrifuge tubes and the dissolved Fe(II) concentration was measured by absorbance at 510 nm. Another 0.2 mL supernatant was added to 1 mL 10% sodium citrate with 2% hydroxylammonium sulfate, reacted overnight, and the total dissolved Fe concentration was measured by absorbance at 510 nm. Another 0.2 mL suspension was centrifuged down at 14000 rcf for 10 min; supernatant was drawn out carefully; 0.2 mL O_2-free Milli-Q water and 1.0 mL 1.40 M H_3PO_4-0.50 M H_2SO_4 were added. The 1.5 mL tubes were then shaken by hand. After extraction for 10 min, the samples were centrifuged down. Fe was also measured in this supernatant under same procedure as dissolved Fe. We refer to this quantity as 1.40 M H_3PO_4-0.50 M H_2SO_4 extractable Fe. All supernatant was carefully removed using 1 mL syringe with 25G needle. 0.2 mL O_2-free Milli-Q water was then added, and the tubes were shaken by hand. 0.48 mL 4.9 N H_2SO_4, 0.11 mL 10% (wt/wt) 1,10-phenanthroline (in 95% ethanol) and 0.055 mL 27.6 N HF were then added into each tube. The tube was capped and moved out of the anoxic chamber. A batch of tubes was placed into a microcentrifuge tube rack that floated (partially submerged) in a boiling water bath. After 30 min heating and 15 min cooling, 0.55 mL of 2.4 N H_3BO_3 solution was added into the each tube. 0.2 mL of digested sample was added to 1 mL 10% sodium citrate, and clay-Fe(II) was then measured by absorbance at 510 nm. Another 0.2 mL of digested sample was added to 1 mL 2% hydroxylammonium sulfate in 10% sodium citrate solution, reacted overnight, and total clay-Fe was then measured by absorbance at 510 nm. We refer to this quantity as Fe in solid.

2.3.6 Uranium measurement

All U measurements were performed with a KPA-11 (ChemChek, Richland, WA) equipped with an autosampler where the whole unit was operated within an anoxic chamber. The

KPA technique is valence state-specific, where it only measures luminescent hexavalent uranium (Schulman, 1984; Brina & Miller, 1992; Sowder et al. 1998) . A data cable was run from the KPA-11 to a personal computer just outside of the chamber. The anoxic chamber was supplied with a 95:5% N_2:H_2 gas mix. Recirculating fans equipped with Pd catalysts and silica gel were used to remove any O_2(g). It has been reported that these catalysts can maintain a P_{O2} of < $3.8*10^{-7}$ atm within the chambers (Jeon et al., 2004; Park & Dempsey, 2005). Concentrated Uraplex reagent was added to anoxic Milli-Q water and flushed with 99.99% N_2 for 20 min, sealed with a butyl rubber stopper and Al crimp-sealed. The autosampler pump withdrew Uraplex directly from this crimp-sealed bottle through a needle. Samples were commonly diluted with anoxic Milli-Q water to adjust sample concentrations to the most responsive and repeatable range for our KPA (ca. 0.42 nM to 4.2 μM final conc.) and to minimize any matrix effects that could be caused by dissolved components such as Fe^{3+} and PO_4^{3-} (Sowder et al. 1998). This anoxic Milli-Q water was also prepared outside of the chamber and crimp-sealed in serum bottles to avoid exposure to H_2. Samples were diluted into autosampler vials (such that they were nearly full and then sealed with parafilm) and then immediately loaded onto the autosampler tray. The diluted sample and Uraplex solution were fully exposed to the anoxic chamber atmosphere only during automated mixing just before sample analysis (< 20 s).

Dissolved uranium samples was diluted by adding 1 mL 1.40 M H_3PO_4 - 0.50 M H_2SO_4 into 0.2 mL supernatant. Diluted dissolved uranium samples and original "1.40 M H_3PO_4 - 0.50 M H_2SO_4 extracted" samples were further diluted 100-fold using O_2-free Milli-Q water before measured by KPA. 0.300 mL diluted "dissolved uranium" or "1.40 M H_3PO_4 - 0.50 M H_2SO_4 extracted" samples was mixed with 0.300 mL 70% HNO_3 and heated in boiling water bath for 45 min to oxidize all uranium to U(VI). After cooling to room temperature, oxidized uranium samples were further diluted 50-fold using Milli-Q water and then measured by KPA. U(IV) was calculated as difference between total uranium and U(VI).

Chapter 3

Results and Discussion

3.1 Unaltered clay mineral dissolution under high pressure CO_2 conditions

Most structural elements of all the unaltered clay minerals in all the brines tested did not dissolve to any great extent under high pressure CO_2 conditions (P_T = 9.66 bar, $P_{CO2} \geq$ 8.66 bar CO_2) or under ambient pressure conditions (P_T = 1 bar; N_2:H_2 = 95:5%). There was no more than a total of 10 mg/L of dissolved cations (sum of [Al], [Fe], [Mg] and [Si]) detected for these experiments, which accounted for less than 2% of the total clay mineral mass. Na or Ca, the cations of the brines, were not measured because of difficulty in accurately measuring mg/L level changes in concentrations with a background of >10 g/L. There were no obvious dissolution features observed shown in SEM images of nontronite NAu-2 before and after reaction in 2 M NaCl brine under high pressure CO_2 conditions for 15 d (Appendix B). No changes were observed in XRD patterns of NAu-2 before and after reaction in 2 M NaCl or 1 M $CaCl_2$ under high pressure CO_2 conditions (Appendix C). pH values of NAu-2 and montmorillonite SWy-2 suspensions under high pressure CO_2 or ambient pressure conditions dropped to as low as pH 3.98 (Table 3.1). Except for this one condition (1 d reaction in 1 M $CaCl_2$), pH values were >4.0 under high pressure CO_2 conditions and >5.5 under ambient pressure conditions. Based on conceptual model developed by Shaw and Hendry (2009), aluminosilicate structure of clay minerals did not dissolve until pH values were <3.0 in H_2SO_4. Under our experimental conditions, the effective acidity of H_2CO_3* (~0.25 M) was not strong enough to dissolve unaltered clay minerals to any great extent. It is important to mention possible interference during pH measurement. Suspended clay particles might block pores of liquid junction of the probe; high

ionic strength in the clay suspension also affected the liquid junction potential. Therefore pH measurement was not strictly accurate.

Table 3.1. pH values of nontronite NAu-2 and montmorillonite SWy-2 suspensions as a function of incubation time. Experiments were conducted under high pressure CO_2 conditions (P_T = 9.66 bar, $P_{CO2} \geq$ 8.66 bar CO_2) or ambient pressure conditions (P_T = 1 bar; N_2:H_2 = 95:5%). Sample pH was measured after the pressure tube had been opened for 2 min.

clay	brine	condition	time (d)	pH
10 g/L NAu-2	2 M NaCl	ambient	0	6.16
10 g/L NAu-2	2 M NaCl	ambient	15	5.85
10 g/L NAu-2	2 M NaCl	high pressure CO_2	1	4.43
10 g/L NAu-2	2 M NaCl	high pressure CO_2	3	4.50
10 g/L NAu-2	2 M NaCl	high pressure CO_2	7	4.52
10 g/L NAu-2	2 M NaCl	high pressure CO_2	15	4.68
10 g/L NAu-2	1 M $CaCl_2$	ambient	0	6.00
10 g/L NAu-2	1 M $CaCl_2$	ambient	15	5.51
10 g/L NAu-2	1 M $CaCl_2$	high pressure CO_2	1	3.98
10 g/L NAu-2	1 M $CaCl_2$	high pressure CO_2	3	4.12
10 g/L NAu-2	1 M $CaCl_2$	high pressure CO_2	7	4.07
10 g/L NAu-2	1 M $CaCl_2$	high pressure CO_2	15	4.15
10 g/L SWy-2	2 M NaCl	ambient	15	7.32
10 g/L SWy-2	2 M NaCl	high pressure CO_2	1	4.66
10 g/L SWy-2	2 M NaCl	high pressure CO_2	3	4.72
10 g/L SWy-2	2 M NaCl	high pressure CO_2	7	4.86
10 g/L SWy-2	2 M NaCl	high pressure CO_2	15	4.65

Concentrations of dissolved ions were typically quite low and difficult to quantify precisely in the highly concentrated background electrolytes. Dissolved concentrations in clay mineral suspensions were always compared to concentrations measured in no-clay control pressure tubes maintained under high pressure CO_2 and ambient conditions (Table 3.2; horizontal lines in Figures 3.1 – 3.5, 3.7, 3.8, 3.15, 3.16, 3.21, 3.22). Samples had to be diluted 20-fold to

avoid serious matrix effects (Todoli et al., 2002) for ICP-AES analysis, and after dilution the concentrations of all target ions were close to detection limits (~0.01 mg/L). As a result, it was difficult to demonstrate significant differences in dissolution between different clay minerals or brines, or make any detailed analysis of dissolution kinetics. Although ICP-MS has lower detection limits than ICP-AES, it also requires a comparable lower concentration of total dissolved solids in samples, therefore, ICP-MS to was not used to measure dissolved ions.

Table 3.2. Dissolved concentrations of Al, Fe, Mg and Si in brine-only, no-clay controls under high pressure CO_2 conditions (P_T = 9.66 bar, $P_{CO2} \geq$ 8.66 bar CO_2) or ambient pressure conditions (P_T = 1 bar; N_2:H_2 = 95:5%).

brine	condition	Al (mg/L)	Fe (mg/L)	Mg (mg/L)	Si (mg/L)
1.0 M NaCl	high pressure CO_2	0.09	0.00	0.03	1.72
	ambient	0.05	0.01	0.04	2.75
0.33 M $CaCl_2$	high pressure CO_2	0.45	0.00	1.29	2.51
	ambient	0.43	0.03	1.27	2.15
0.33 M Na_2SO_4	high pressure CO_2	0.07	0.00	0.20	1.84
	ambient	0.01	0.00	0.29	1.94

Al and Mg dissolved out of chlorite CCa-2 to a greater extent than NAu-2 or SWy-2 under high pressure CO_2 conditions (Figure 3.1). There were no significant differences in the dissolution of Fe and Si for these three clay minerals. Under ambient pressure conditions, Mg was the only element to dissolve to any significant extent as compared to the background concentration in the brine in the no-clay control (Figure 3.2). The greater extent of Mg dissolution from CCa-2 as compared to NAu-2 and SWy-2 is consistent with previous studies (May et al. 1995, Brandt et al. 2002). While all of these clay minerals have a 2:1 tetrahedral-octahedral-tetrahedral (TOT) layered structure, CCa-2 also contains a "brucite-like" layer bonded to one of the tetrahedral sheets. Brucite is magnesium hydroxide and, thus, this brucite-like layer contains Mg but also some Al and Fe. Brandt et al. (2002) reported that the brucite-like layer dissolved ~2 – 2.5 times faster than the TOT sheets resulting in higher concentrations of Mg and Al. The

different brines did not significantly influence the dissolution of NAu-2 under higher pressure CO_2 or ambient pressure conditions (Figures 3.3 and 3.4, respectively).

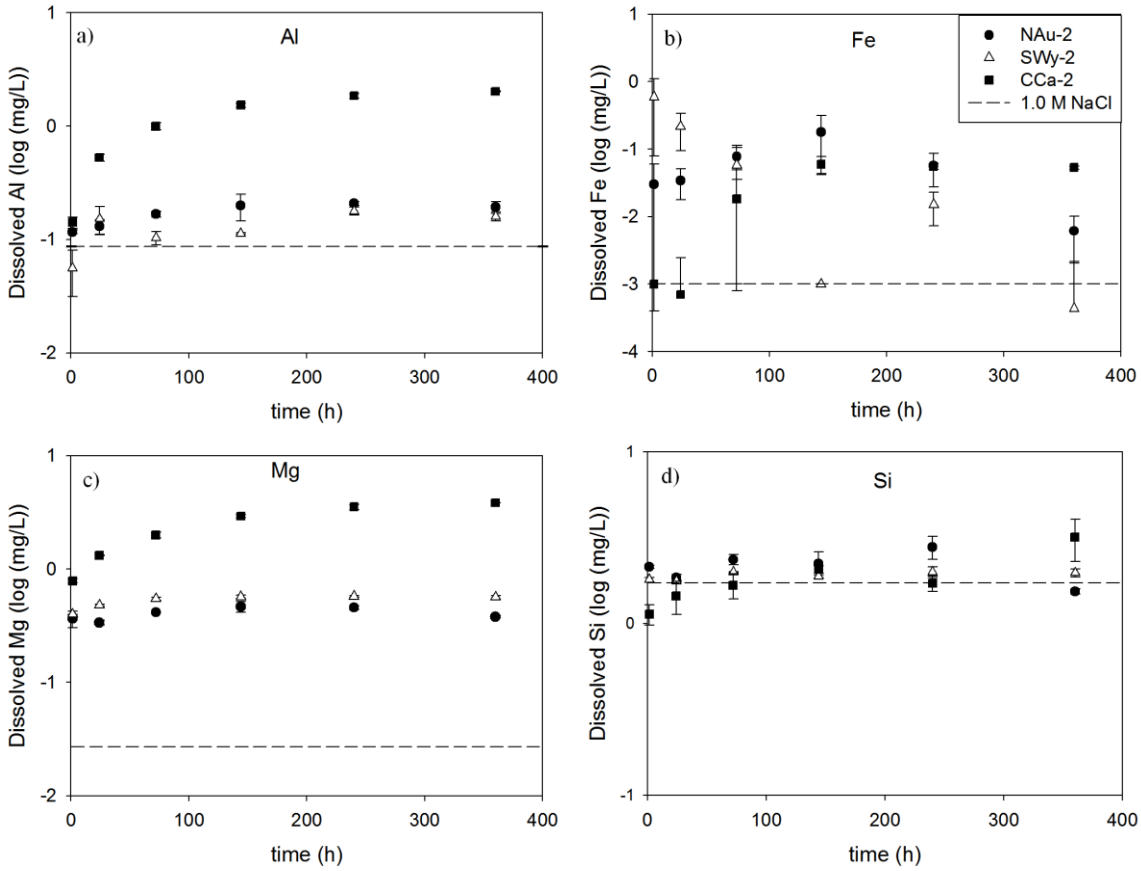

Figure 3.1. Dissolution of nontronite NAu-2, montmorillonite SWy-2 and chlorite CCa-2 (all 0.5 g/L) in 1.0 M NaCl under high pressure CO_2 conditions (P_T = 9.66 bar, $P_{CO2} \geq$ 8.66 bar CO_2). Average concentrations of ions in brine-only, no-clay, high pressure CO_2 controls are shown as dashed lines.

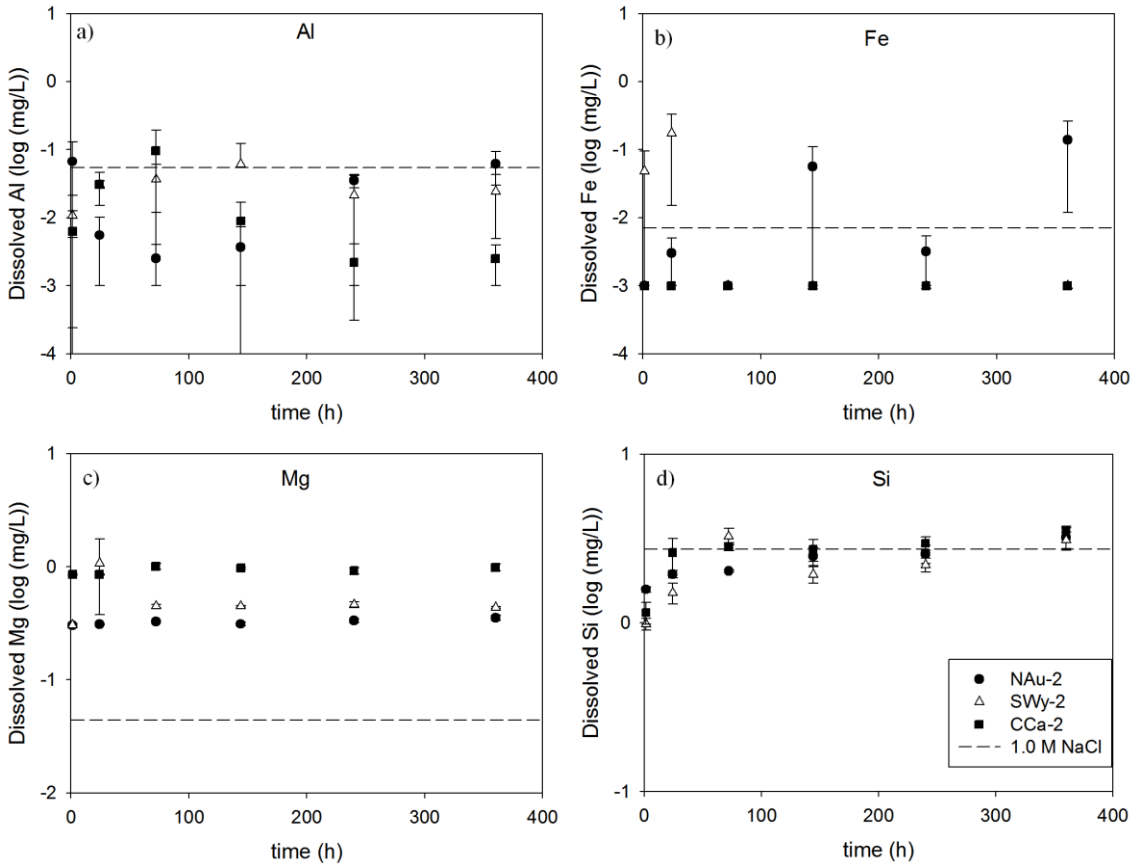

Figure 3.2. Dissolution of nontronite NAu-2, montmorillonite SWy-2 and chlorite CCa-2 (all 0.5 g/L) in 1.0 M NaCl under ambient pressure conditions (P_T = 1.0, N_2:H_2 = 95:5%). Average concentrations of ions in brine-only, no-clay, ambient pressure controls are shown as dashed lines.

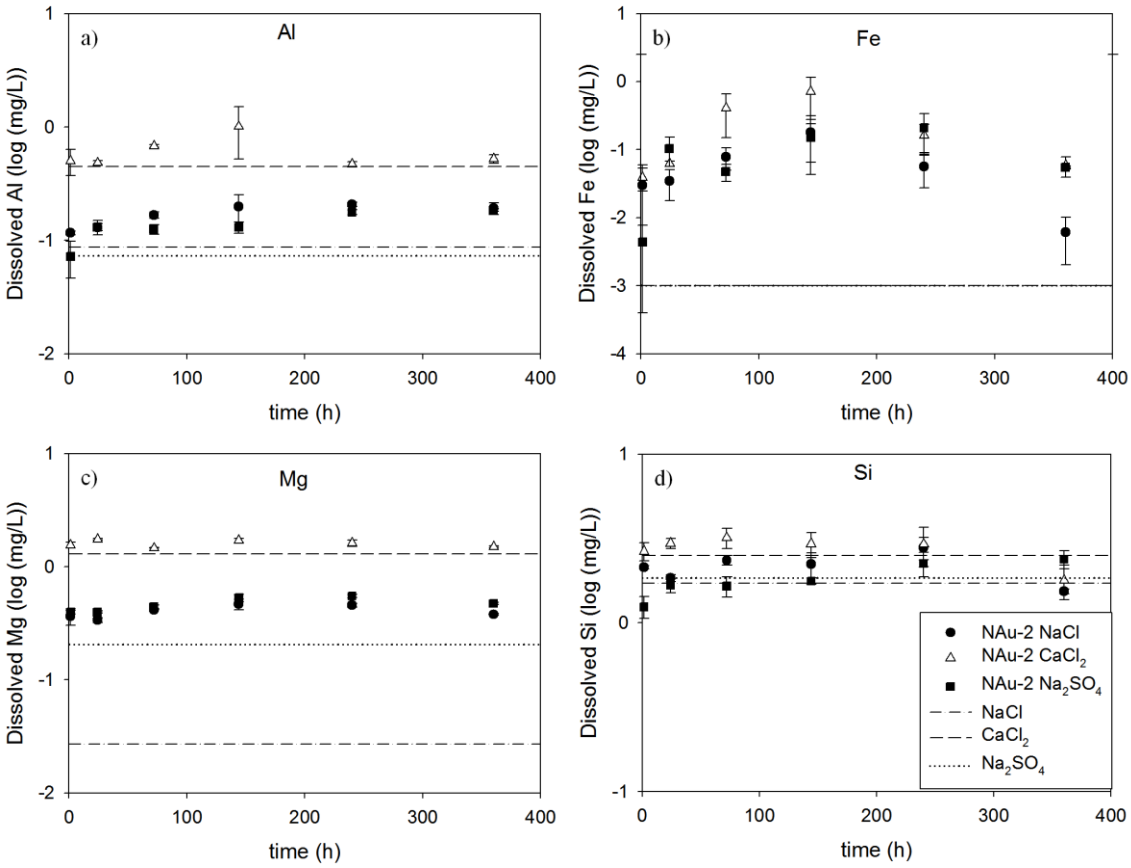

Figure 3.3. Dissolution of nontronite NAu-2 (0.5 g/L) in 1.0 M NaCl, 0.33 M $CaCl_2$ and 0.33 M Na_2SO_4 under high pressure CO_2 conditions (P_T = 9.66 bar, $P_{CO2} \geq$ 8.66 bar CO_2). Average concentrations of ions in brine-only, no-clay, high pressure CO_2 controls are shown as dashed lines.

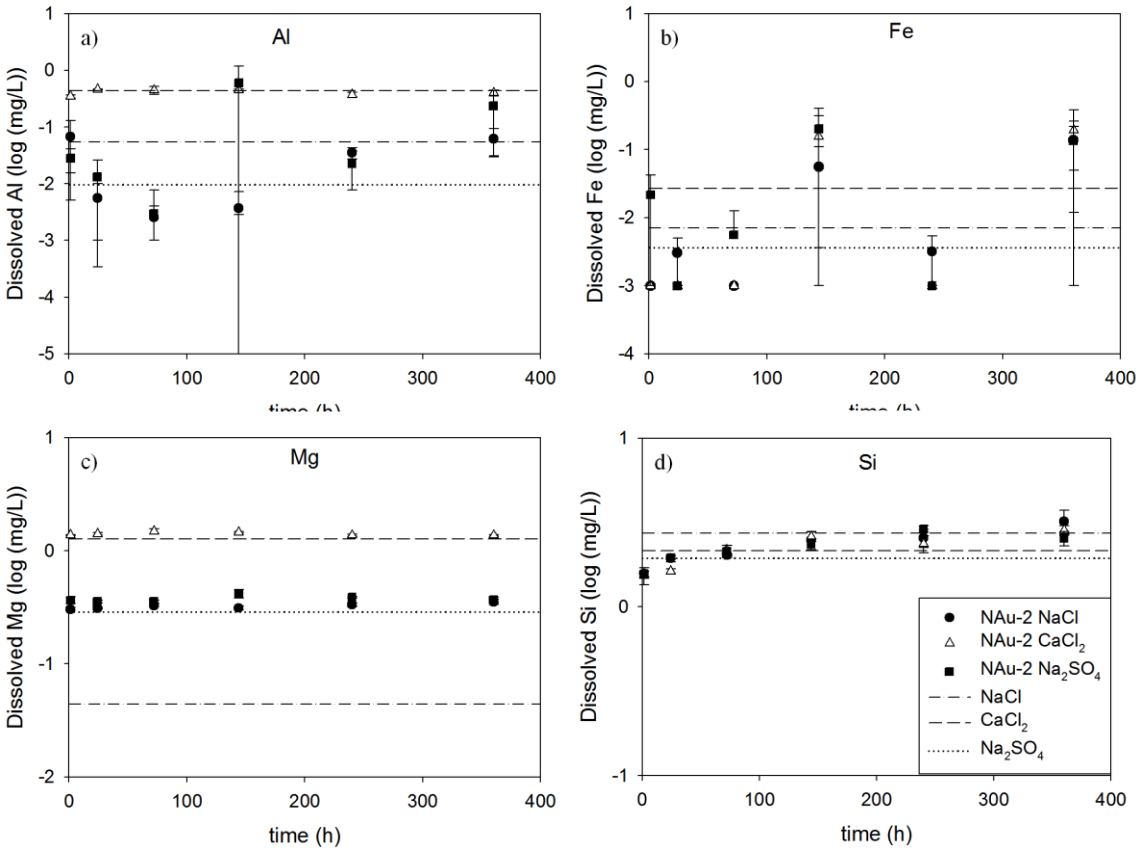

Figure 3.4. Dissolution of nontronite NAu-2 (0.5 g/L) in 1.0 M NaCl, 0.33 M $CaCl_2$ and 0.33 M Na_2SO_4 under ambient pressure conditions (P_T = 1.0, N_2:H_2 = 95:5%). Average concentrations of ions in brine-only, no-clay, ambient pressure controls are shown as dashed lines.

3.2 Dissolution of partially reduced NAu-2 (R-NAu-2)

Compared to unaltered NAu-2, partially reduced nontronite (R-NAu-2, ~48% $Fe(II)/Fe_{TOT}$) dissolved to a greater extent under both high pressure CO_2 and ambient pressure conditions (Figure 3.5). Based on results obtained under high pressure CO_2 conditions, carbonic acid significantly increased the dissolution of Fe, Mg and Si from R-NAu-2. A total of ~66 mg/L of dissolved cations (sum of Al, Fe, Mg and Si) after 15 d reaction period accounted for ~13% of the total clay mineral mass. Under ambient pressure conditions, there are higher concentrations of Mg and Si dissolved from R-NAu-2. Reduction of structural clay-Fe(III) to structural clay-Fe(II) will result in a charge imbalance (caused by Fe^{3+} being replaced by Fe^{2+}) that must be compensated within the clay mineral structure and/or through exchange of adsorbed ions. Previous studies have shown that substitution of Fe^{2+} and Mg^{2+} for Al^{3+} in the octahedral sheet and substitution of Al^{3+} for Si^{4+} in the tetrahedral sheet increased the solubility of illite and smectite in 1 – 10 M HCl and 1 – 10 M H_2SO_4 at 80 ℃ - 90 ℃ (Steudel et al., 2009; Pentrak et al., 2010).

Previous studies on the reduction of nontronite and natural clay-sized sediment fractions have presented differing conclusions on how reduction affects clay mineral structure, which affects solubility. Microbe usually reduced no more than 25% NAu-2 (Zhang et al., 2012; Liu et al., 2012) which does not affect clay mineral structure to a high extent (Stucki, 2011). However, Bishop et al. (2011) found that the NAu-2 showed a change from 92% smectite + 8% I–S (illite–smectite) for the unreduced sample to a 94% 28:72 I–S + 6% illite for the bioreduced sample (25% $Fe(II)/Fe_{TOT}$) based on XRD data of ethylene glycolated clay mineral samples. Chemical reduction of smectite might change its structure and lead to reductive dissolution when reduction extent is high (Jaisi et al., 2008). Jaisi et al. (2008) reported that after dithionite reduction, 100% Fe(II) stayed in NAu-2 structure when reduction extend was < 30%, while only 65% stayed in

clay mineral structure when 71% Fe(III) was reduced. Wu et al. (2012) used citrate-dithionite-bicarbonate extraction method to remove iron oxides in a weathered shale saprolite sediment to collect pure iron-bearing clay minerals under 80 ℃ for 3 times, 15 minutes each time (totally <20% reduction), and found only minimal alteration of phyllosilicate structure proved by XRD patterns.

Another reason for enhanced dissolution is release of sorbed ions. ~5% reductive dissolution was observed during bioreduction process of NAu-2 and the dissolved Fe(II) could be adsorbed onto clay mineral surface or interlayer region and became active in dissolution or other reactions (Yang et al., 2012). Jaisi et al. (2008) reported that for 50% reduced NAu-2 by dithionite, 3% Fe(II) located at ion-exchangeable sites, 20% located at surface complexation sites and 73% stayed in clay mineral structure. In our study, under ambient pressure conditions, Mg and Si concentration in R-NAu-2 suspension was higher than that in unaltered NAu-2 suspension, even at first sampling point (1.33 h), indicating relatively fast releasing of sorbed ions into 0.33 M Na_2SO_4.

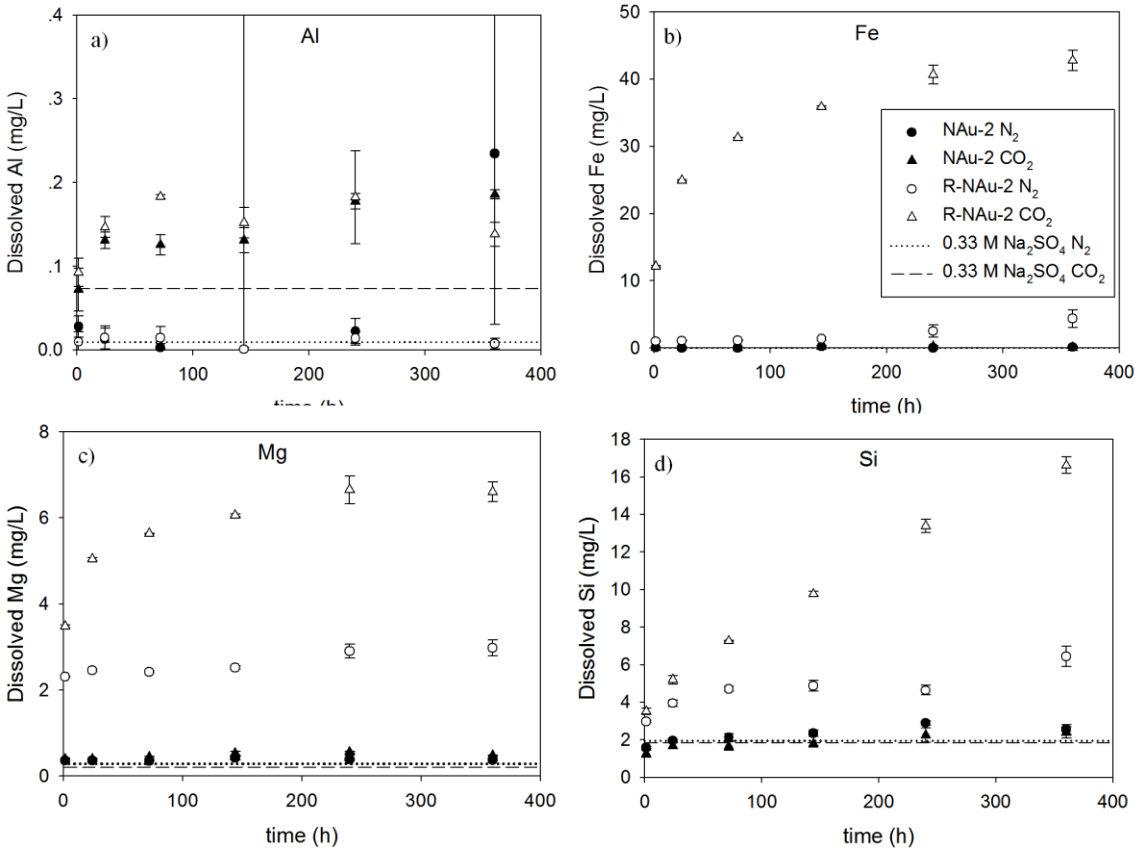

Figure 3.5. Dissolution of nontronite NAu-2 and reduced nontronite (R-NAu-2) (both 0.5 g/L) in 0.33 M Na_2SO_4 under high pressure CO_2 (P_T = 9.66 bar, $P_{CO2} \geq$ 8.66 bar CO_2) and ambient pressure conditions (P_T = 1.0, N_2:H_2 = 95:5%). Average concentrations of ions in brine-only, no-clay controls are shown as dashed lines.

Dissolution of Al and Si from montmorillonite and nontronite in acid has been described as a pseudo first order reaction at a fixed pH value (Osthaus, 1955; Zysset & Schindler, 1996; Rozalen et al., 2008).

$$\frac{d[Si]}{dt} = k * M \quad [3\text{-}1]$$

M is the clay mass concentration (g/L). [Si] has unit of g/L. k (h^{-1}) is the pseudo first order rate constant. In this study, we assume dissolution is congruent (not strictly congruent for all elements in clay, merely constant [Si]/[dissolved clay mass] is sufficient) in order to calculate remaining clay mass based on [Si]. For NAu-2 and R-NAu-2, Si accounts for 21.2% clay mass (exact ratio does not matter for calculating reaction half life).

$$M = 0.5 - [Si]/0.212 \quad [3\text{-}2]$$

$$\ln(0.106 - [Si]) = -4.72 * kt + a \quad [3\text{-}3]$$

$$t_{\frac{1}{2}} = \frac{0.147}{k} \quad [3\text{-}4]$$

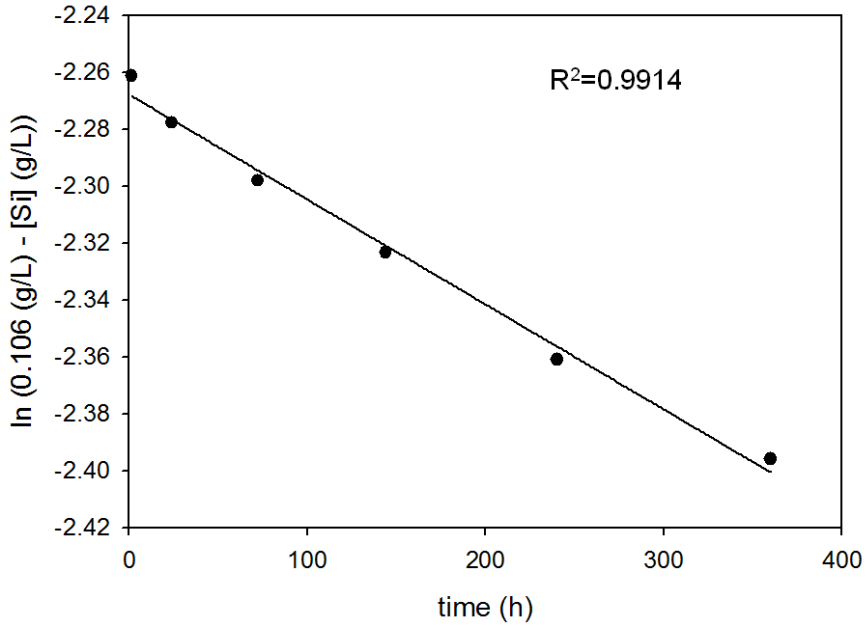

Figure 3.6. Regression line for pseudo first order dissolution of Si from 0.5 g/L reduced nontronite (R-NAu-2) in 0.33 M Na_2SO_4 under high pressure CO2 conditions (P_T = 9.66 bar, P_{CO2} ≥ 8.66 bar CO_2)

This dissolution reaction data fits pseudo first order kinetics model very well with R^2 = 0.9914. Dissolution of Si from 0.5 g/L reduced nontronite (R-NAu-2) in 0.33 M Na_2SO_4 under high pressure CO_2 conditions (P_T = 9.66 bar, $P_{CO2} \geq$ 8.66 bar CO_2) has half life from 1664h – 2157 h (95% confidence interval). Based on our experiment, reduced nontronite is not a stable mineral in geological carbon sequestration reservoir, considering proposed storage time of thousands of years. However, further study needs to be performed under conditions in real carbon sequestration site, where the form of clay minerals or temperature, pressure conditions differs a lot from our experiment conditions.

3.3 Clay mineral dissolution in 1.40 M H_3PO_4 - 0.50 M H_2SO_4

A stronger acid such as 1.40 M H_3PO_4 - 0.50 M H_2SO_4 dissolved both NAu-2 and R-NAu-2 to a significantly greater extent as compared to high pressure CO_2 conditions. (Figures 3.7 and 3.8, respectively). The combination and concentrations of H_3PO_4 - H_2SO_4 were selected because of their use in clay-uranium extractions (Luan & Burogs, 2012) that were employed in our clay-uranium experiments. Stronger acid concentrations are also very relevant to geologic CO_2 sequestration because impurities of SO_x or NO_x can significantly increase the acidity of aquifers near injection area (Knauss et al., 2005; Xu et al., 2007; Wang et al., 2011).

The high pressure CO_2 conditions did not significantly dissolve NAu-2 (Figure 3.1) but did dissolve Fe, Mg and Si from R-NAu-2 (Figure 3.5). In comparison, H_3PO_4 - H_2SO_4 dissolved Al, Fe, Mg and Si from both NAu-2 and R-NAu-2. The solubilization of Al reflects the ability of the stronger acid to attack the octahedral sheet within the TOT structure. A total of ~65 mg/L and 225 mg/L of dissolved cations (sum of [Al], [Fe], [Mg] and [Si]) after 3 d reaction period accounted for ~13% and 45% of the total NAu-2 and R-NAu-2 mass, respectively. Dissolved concentrations of Al, Fe, Mg and Si were all significantly higher after reaction of H_3PO_4 - H_2SO_4 with R-NAu-2 (Figure 3.8) as compared to NAu-2 (Figure 3.7), which was consistent with reactions under high pressure CO_2 conditions.

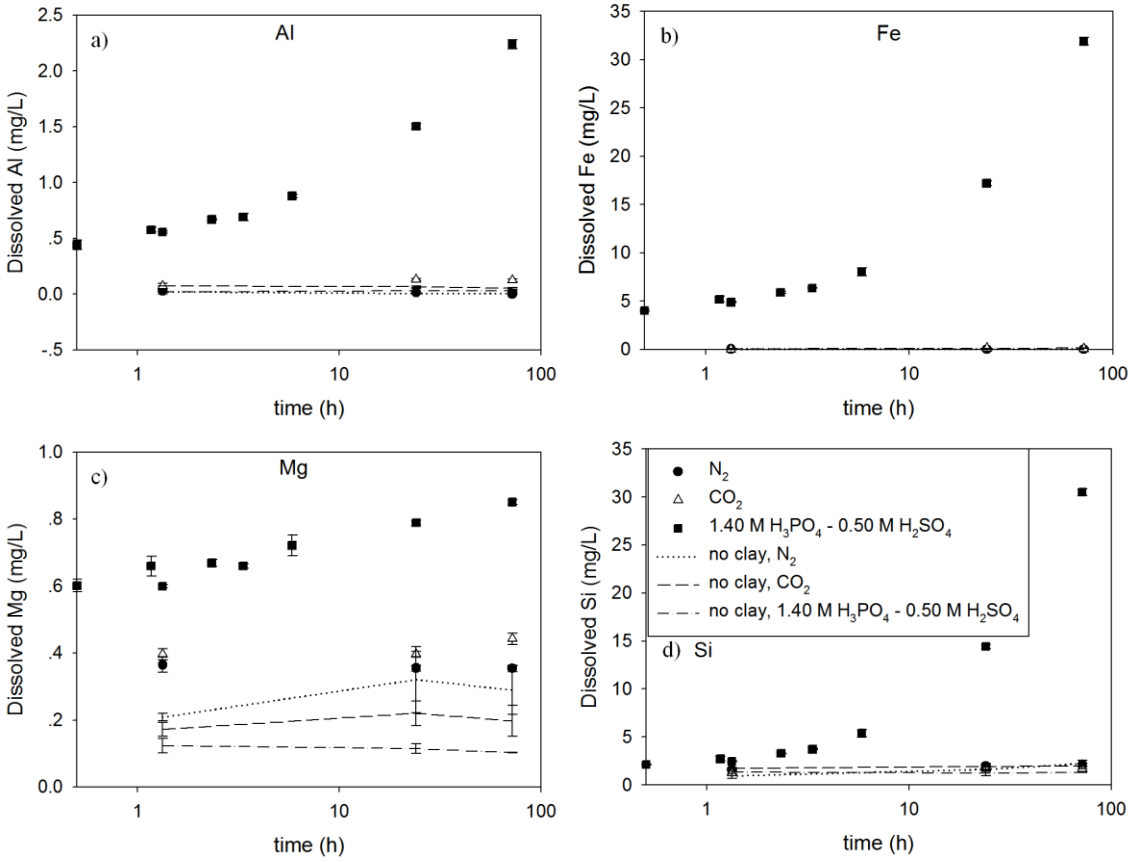

Figure 3.7. Dissolution of nontronite NAu-2 in 1.40 M H_3PO_4 - 0.50 M H_2SO_4 versus high pressure CO_2 conditions. (P_T = 9.66 bar, $P_{CO2} \geq$ 8.66 bar CO_2) and ambient pressure conditions (P_T = 1.0, N_2:H_2 = 95:5%). Experiments conducted with 0.5 g/L NAu-2 in 0.33 M Na_2SO_4. Average concentrations of ions in brine-only, no-clay controls are shown as dashed and dotted lines.

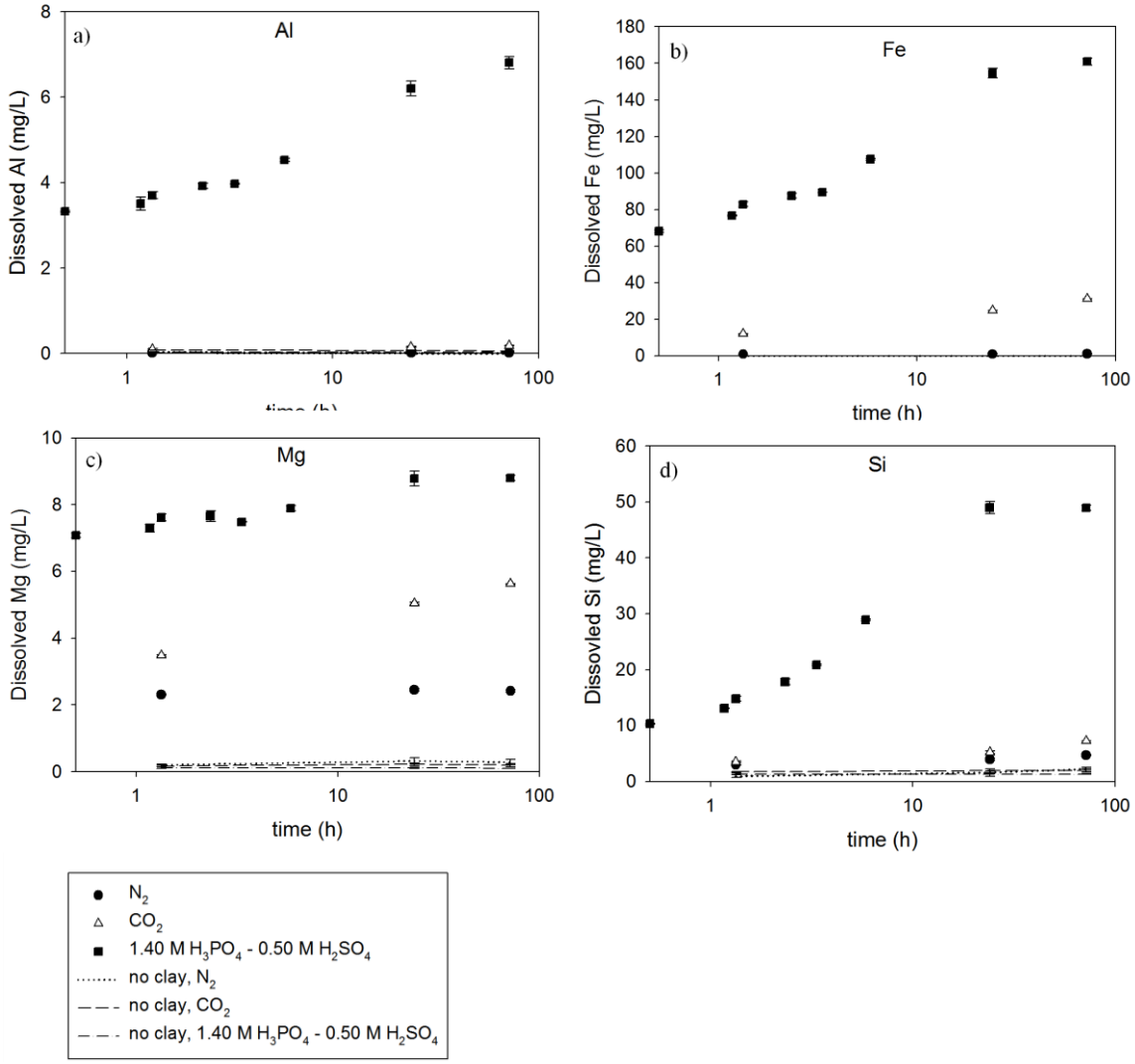

Figure 3.8. Dissolution of reduced nontronite R-NAu-2 in 1.40 M H_3PO_4 - 0.50 M H_2SO_4 versus high pressure CO_2 conditions. (P_T = 9.66 bar, $P_{CO2} \geq$ 8.66 bar CO_2) and ambient pressure conditions (P_T = 1.0, N_2:H_2 = 95:5%). Experiments conducted with 0.5 g/L R-NAu-2 in 0.33 M Na_2SO_4. Average concentrations of ions in brine-only, no-clay controls are shown as dashed and dotted lines.

Dissolution kinetics of nontronite (NAu-2) and reduced nontronite (R-NAu-2) in 1.40 M H_3PO_4 - 0.50 M H_2SO_4 in 0.33 M Na_2SO_4 is calculated using equation 3-1 to 3-4, under same assumption of congruent dissolution (not strictly congruent for all elements in clay, merely constant [Si]/[dissolved clay mass] is sufficient). Dissolution reaction data of both NAu-2 and R-NAu-2 fit pseudo first order kinetics model very well with R^2 = 0.9957 and 0.9951, respectively. For R-NAu-2, only first six data points were used for regression because all clay mineral was dissolved before 24 hours (exclude the last two data points). Half life of dissolution reaction was 147 h – 168 h (95% confidence interval) for NAu-2, and 16.2 h – 19.7 h (95% confidence interval) for R-NAu-2.

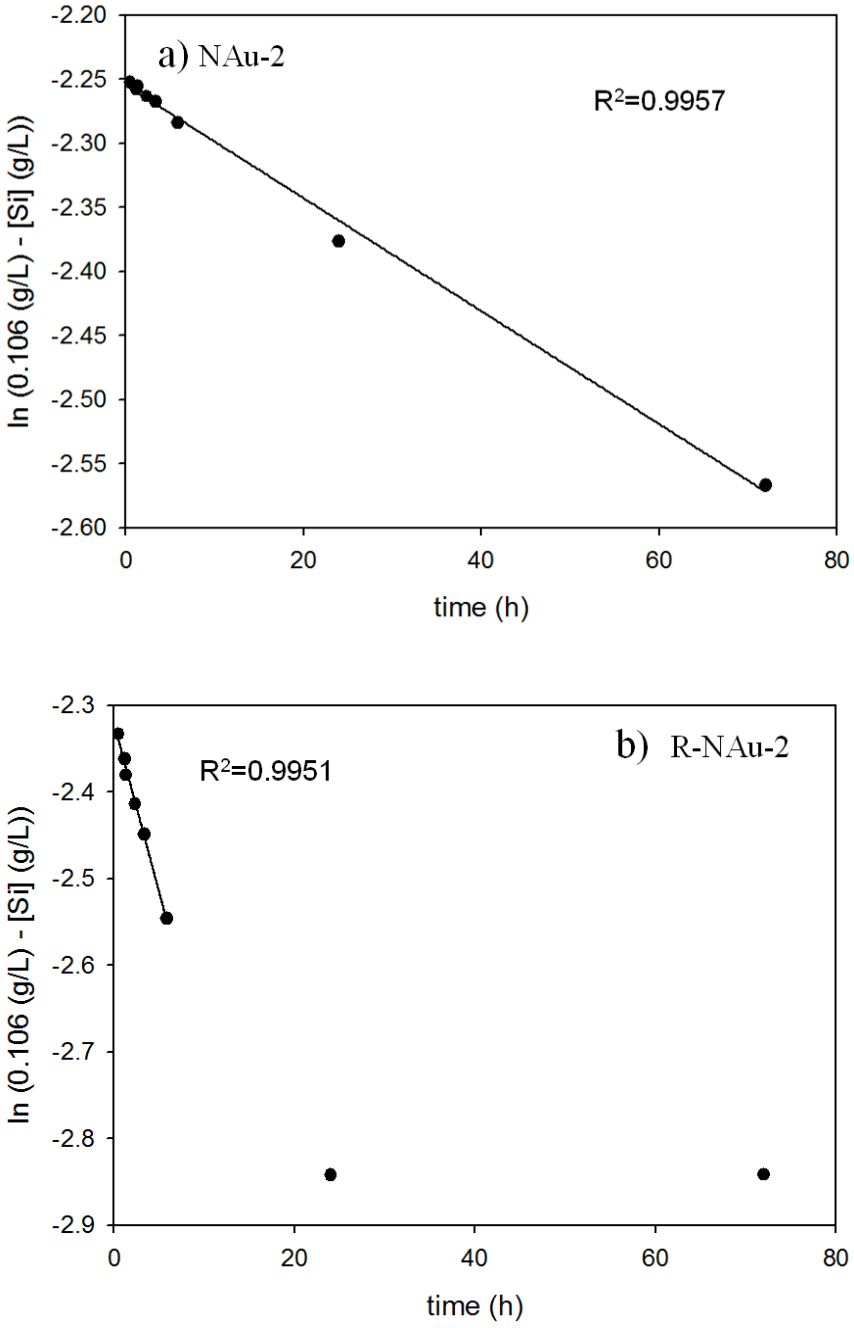

Figure 3.9. Regression line for pseudo first order dissolution of Si from 0.5 g/L (a) nontronite NAu-2, (b) reduced nontronite R-NAu-2 in 1.40 M H_3PO_4 - 0.50 M H_2SO_4 in 0.33 M Na_2SO_4

Dissolution of NAu-2 and R-NAu-2 in 1.40 M H_3PO_4 - 0.50 M H_2SO_4 was incongruent (Figure 3.10). The theoretical ratio of elements in clay mineral was calculated based on Table 2.1 (Bishop et al., 2011), which might not be accurate for different batches of specimen clay mineral samples or partially reduced clay minerals. However, the declining slope of Mg/Al, Fe/Si, Al/Si and the non-steep slope of Fe/Al demonstrated that the sequence of dissolution was: Mg>Fe≈Al>Si. This is consistent with results reported by Rozale ́n et al. (2008), Pentra ́k et al. (2009) and Steudel et al. (2009). Incongruent dissolution might be caused by sorption and/or precipitation released ions (Zysset & Schindler, 1996; Rozale ́n et al., 2008).

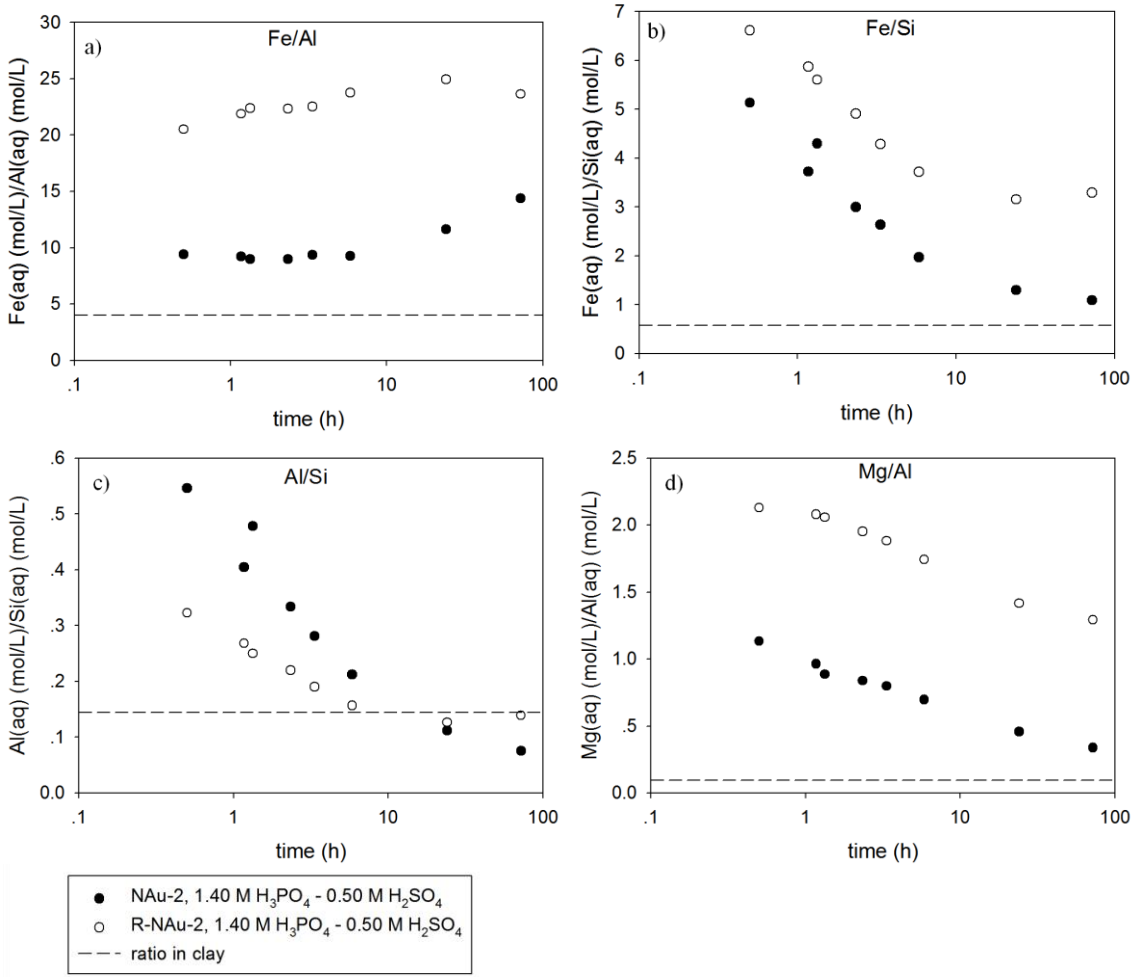

Figure 3.10. Ratios of dissolved Fe/Al, Fe/Si, Al/Si and Mg/Al ((mol/L)/(mol/L)) from nontronite NAu-2 and reduced nontronite R-NAu-2 (both 0.5 g/L) in 0.33 M Na_2SO_4 under ambient pressure conditions (P_T = 1.0, N_2:H_2 = 95:5%) in 1.40 M H_3PO_4 - 0.50 M H_2SO_4. Theoretical element ratios in clay mineral are shown as dashed lines.

The speciation of dissolved Fe(II/III) and clay-Fe(II/III) were also measured during these dissolution experiments (Figure 3.11). For both NAu-2 and R-NAu-2, the $Fe(II)/Fe_{TOT}$ ratio was higher in the dissolved fraction as compared to the iron remaining in the clay mineral structure. This indicates that Fe(II) was easier to dissolve, consistent with observation that R-NAu-2 dissolved more than NAu-2. The overall $Fe(II)/Fe_{TOT}$ ratio was calculated based on the $Fe(II)/Fe_{TOT}$ ratios in solution and in the clay mineral structure and the mass of each fractional compartment. While the $Fe(II)/Fe_{TOT}$ ratios in the aqueous and solid fractions changed slightly over time, the overall $Fe(II)/Fe_{TOT}$ ratios were stable over the reaction period. A stable $Fe(II)/Fe_{TOT}$ ratio demonstrates that the clay minerals were not participating in redox reactions and that all dissolution was acid-driven.

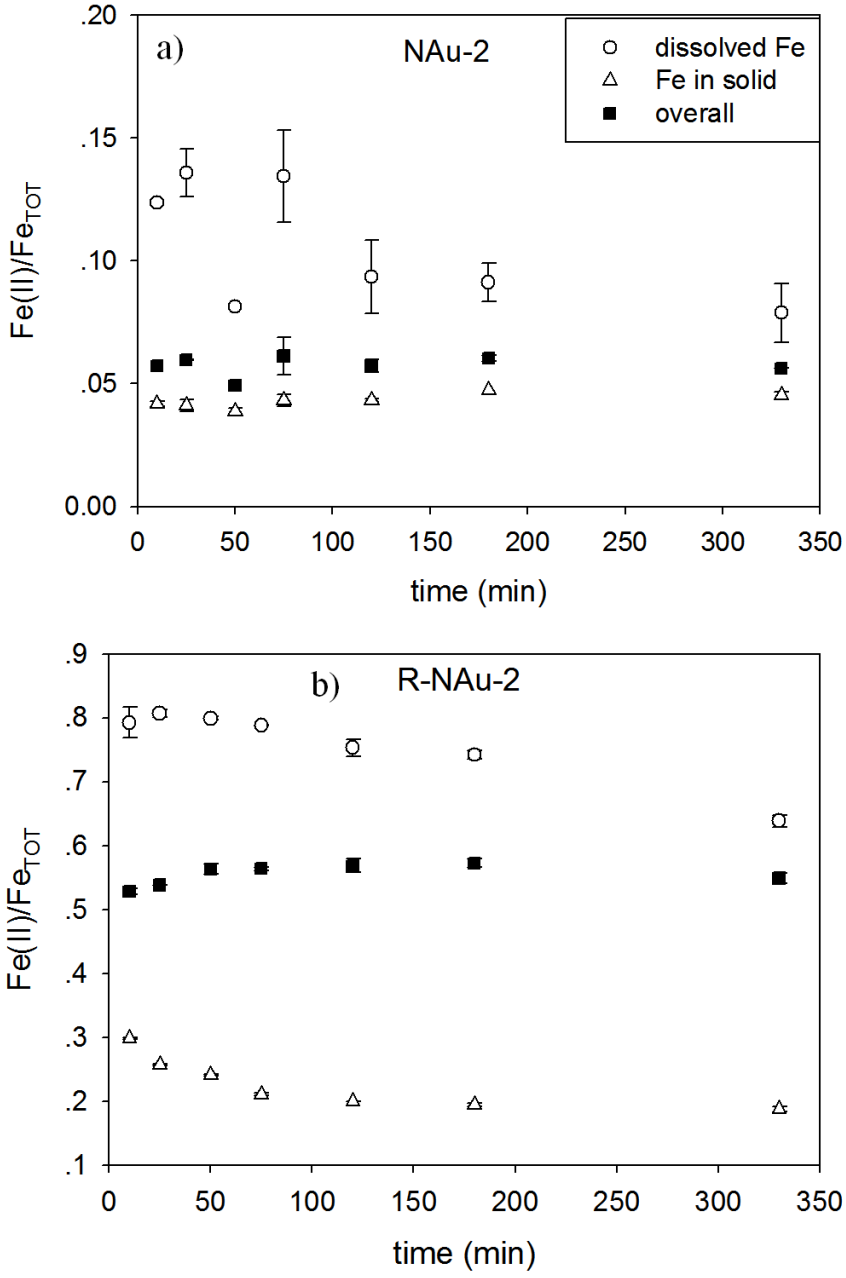

Figure 3.11. Speciation of Fe(II/III) during dissolution of nontronite in 1.40 M H_3PO_4 - 0.50 M H_2SO_4. Experiments conducted with 0.5 g/L NAu-2 (a) or R-NAu-2 (b) in 0.33 mM Na_2SO_4 under ambient pressure conditions (P_T = 1.0, N_2:H_2 = 95:5%) in 1.40 M H_3PO_4 - 0.50 M H_2SO_4.

3.3 Reactions between NAu-2, R-NAu-2 and uranium

3.3.1 Reactions between NAu-2, R-NAu-2 and U(VI)

Experiments were conducted with nontronite and uranium to investigate possible redox reactions between Fe in clay mineral and uranium, and how this redox reaction may affect clay mineral dissolution and uranium(aq) under high pressure CO_2 conditions. Experiments were conducted with reduced NAu-2, which contained 48% Fe(II)/Fe_{TOT}, and uranyl (U(VI)(aq)) to determine if redox reactions between Fe(II) and U(VI) would lead to oxidative stabilization of the clay mineral and decrease dissolved uranium concentration. Experiments were conducted with unaltered NAu-2, which contained a high percentage clay-Fe(III), and uraninite (nominally UO_2(s) but actually a mixed-valence suspension of 58% U(IV) and 42% U(VI)) to determine if redox reactions between Fe(III) and U(IV) would lead to reductive dissolution of NAu-2 and oxidative dissolution of uranium. Experiments were also conducted with unaltered NAu-2 and U(VI) to measure the effect of the contaminant on clay mineral dissolution under conditions when redox reactions between clay-Fe and U were not favorable.

In the clay-with-uranium experiments, H_3PO_4-H_2SO_4 was used to extract and separate U from the clay pellet before digesting the clay mineral in HF-H_2SO_4-phenanthroline (Luan & Burgos, 2012). This sequential extraction procedure was required to avoid analytical interferences caused by valence cycling between clay-Fe(II/III) and U(IV/VI) in conventional "parallel" extractions (e.g., $NaHCO_3$ for U(VI) (Zhou & Gu, 2005) and HF-H_2SO_4 for clay-Fe(II) (Stucki & Anderson, 1981; Komadel & Stucki, 1988).

Based on measurements of the speciation of clay-Fe(II/III) and concentrations of U(VI), U(VI) did not participate in any redox reactions with NAu-2 or R-NAu-2 under any pressure condition. There were no significant differences in the overall Fe(II)/Fe_{TOT} ratios between with-U(VI) experiment and no-uranium experiments for both NAu-2 and R-NAu-2 under either high pressure CO_2 or ambient pressure conditions (Figure 3.12 (a)). Sum of dissolved U(VI) and H_3PO_4-H_2SO_4-extracted U(VI) concentrations were constantly close to 0.45 mM, which was the initial U(VI) concentration in reaction system (Figure 3.12 (b)), reflecting ~ 100% U(VI)/U_{TOT}. This is consistent with results reported by Zhang et al. (2009) where they found chemically reduced NAu-2 (27% 0.5 N HCl-extractable Fe(II)) did not reduce U(VI) in 30 mM $NaHCO_3$ at pH=6.8.

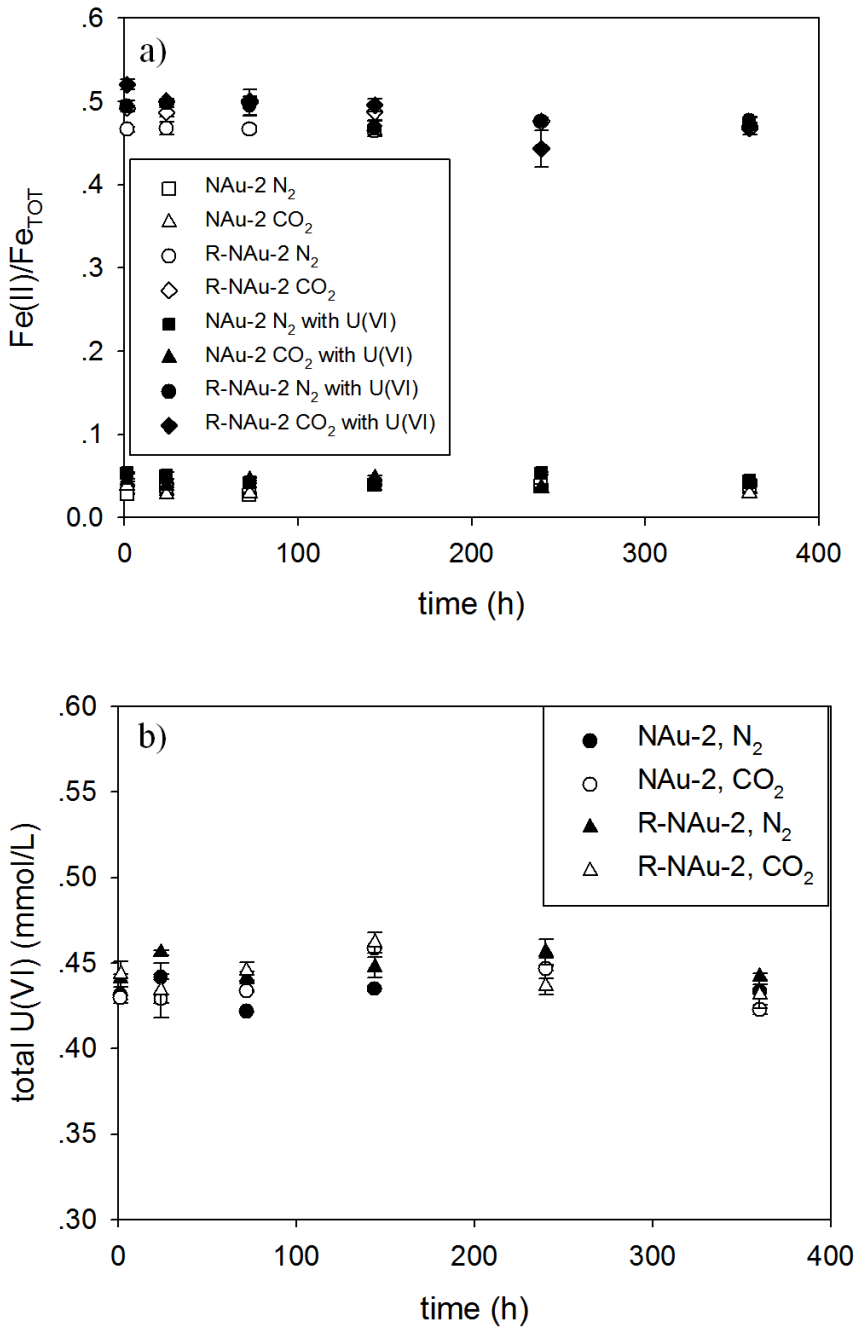

Figure 3.12. (a) Overall $Fe(II)/Fe_{TOT}$ ratios in reactions with or without U(VI) and (b) sum of dissolved U(VI) and H_3PO_4-H_2SO_4-extractable U(VI) concentrations. Experiments conducted with 0.5 g/L NAu-2 or R-NAu-2 in 0.33 M Na_2SO_4 under high pressure CO_2 conditions (P_T = 9.66 bar, $P_{CO2} \geq 8.66$ bar CO_2) or ambient pressure conditions (P_T = 1.0 bar, N_2:H_2 = 95:5%).

Fe(II) was predominant in the dissolved and 1.40 M H_3PO_4-0.50 M H_2SO_4 extracted fractions yet the Fe(II)/Fe_{TOT} ratios remained constant (Figure 3.13) under both pressure conditions. These results are consistent with results obtained without U in 1.40 M H_3PO_4 - 0.50 M H_2SO_4 under ambient pressure conditions where Fe(II) was preferably dissolved from R-NAu-2 (Figure 3.11 (b)). However, these dissolved Fe(II)/Fe_{TOT} ratios are closer to 1, higher than Fe(II)/Fe_{TOT} ratios in no-U 1.40 M H_3PO_4-0.50 M H_2SO_4 experiment, indicating acidity is not strong enough to extract as much Fe(III) as 1.40 M H_3PO_4-0.50 M H_2SO_4.

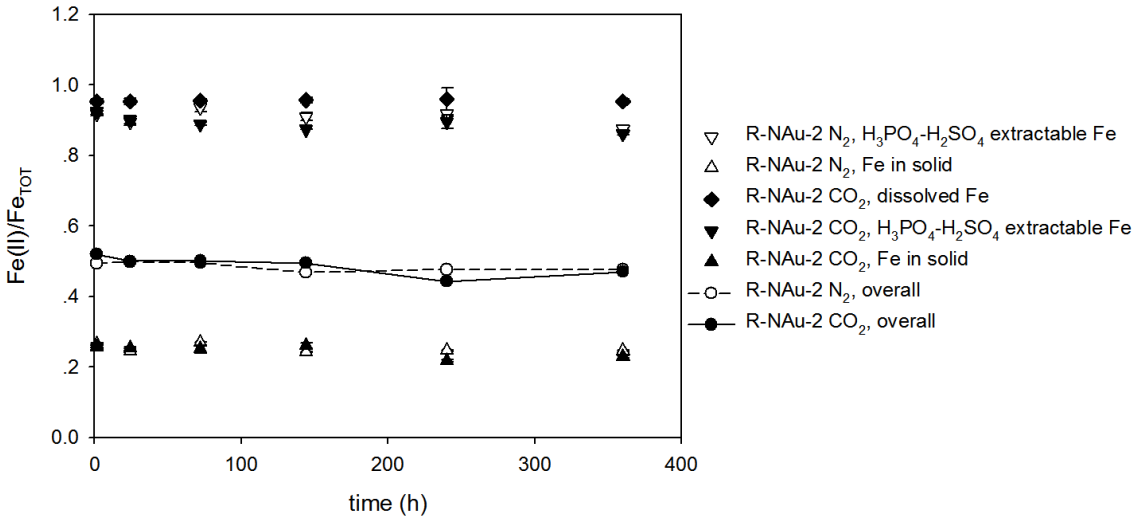

Figure 3.13. Fe(II)/Fe_{TOT} ratios in dissolved, 1.40 M H_3PO_4 - 0.50 M H_2SO_4 extractable and solid fractions for R-NAu-2 dissolution. The dissolved Fe under ambient pressure conditions (P_T = 1.0 bar, N_2:H_2 = 95:5%) was non-measurable. Experiments conducted with 0.5 g/L R-NAu-2 in 0.33 M Na_2SO_4 with 0.45 mM Uranium (VI).

In experiments conducted with U(VI), unaltered NAu-2 did not dissolve to any measureable extent under high pressure CO_2 or ambient pressure conditions, which is consistent with no-uranium experiments. 10 minutes 1.40 M H_3PO_4 - 0.50 M H_2SO_4 extraction dissolved 4.6% Fe out of NAu-2 under both pressure conditions (Figure 3.14 (a), (b)). R-NAu-2 also did not dissolve to any great extent under ambient pressure conditions, while dissolved Fe concentrations increased significantly under high pressure CO_2 conditions, from 4.5% at 1.33 hours to 19.9% of

total Fe after 360 hours incubation (Figure 3.14 (c), (d)). H_3PO_4-H_2SO_4 was able to extract far more Fe from reduced NAu-2 as compared to unaltered NAu-2. These results are consistent with results obtained without U under high pressure CO_2 conditions (Figure 3.5).The sum of dissolved and H_3PO_4-H_2SO_4-extractable Fe concentrations remained relatively constant at 36% of total Fe, and essentially the same under both pressure conditions. These results demonstrate that a long-term weak H_2CO_3 extraction followed by a short-term H_3PO_4-H_2SO_4-extraction dissolved the same amount of clay-Fe as compared to a short-term H_3PO_4-H_2SO_4-extraction alone.

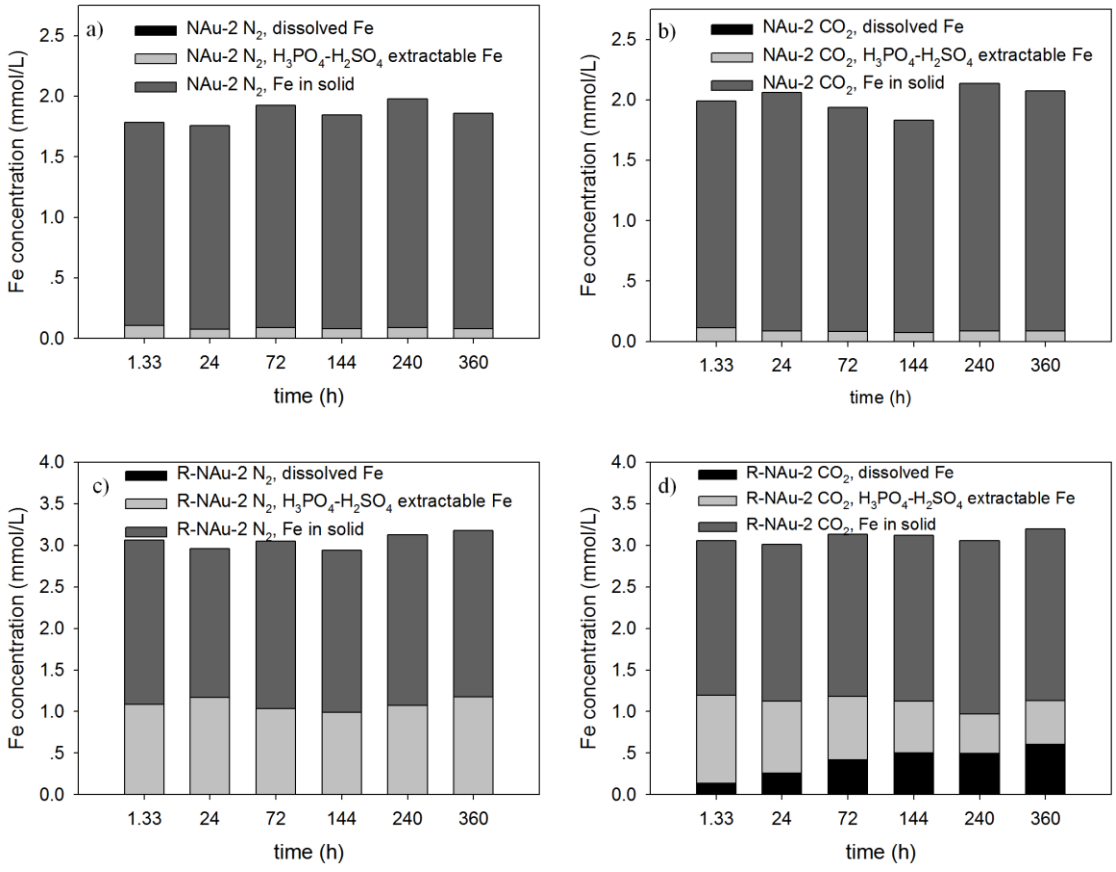

Figure 3.14. Fe distribution in dissolved, 1.40 M H_3PO_4 - 0.5 M H_2SO_4 extractable and solid fractions. (a) NAu-2 U(VI) reaction under ambient pressure conditions (P_T = 1.0 bar, N_2:H_2 = 95:5%), (b) NAu-2 U(VI) reaction under high pressure CO_2 conditions (P_T = 9.66 bar, $P_{CO2} \geq$ 8.66 bar CO_2), (c) R-NAu-2 U(VI) reaction under ambient pressure conditions, (d) R-NAu-2 U(VI) reaction under high pressure CO_2 conditions. Experiments conducted with 0.5 g/L clay mineral in 0.33M Na_2SO_4 with 0.45 mM Uranium (VI).

U(VI) decreased the extent of dissolution of Al, Fe and Mg from R-NAu-2 under high pressure CO_2 conditions (Figure 3.15). However, under ambient pressure conditions (Figure 3.17), there was no significant differences with or without U(VI) in dissolution of Al, Fe and Mg from R-NAu-2. The sorption of U(VI) may have blocked protons from accessing and dissolving the clay mineral surface. Dissolution of Si out of R-NAu-2 under both pressure conditions was slightly enhanced by U(VI), indicating possible influence of U(VI) on tetrahedral sheets of clay mineral structure.

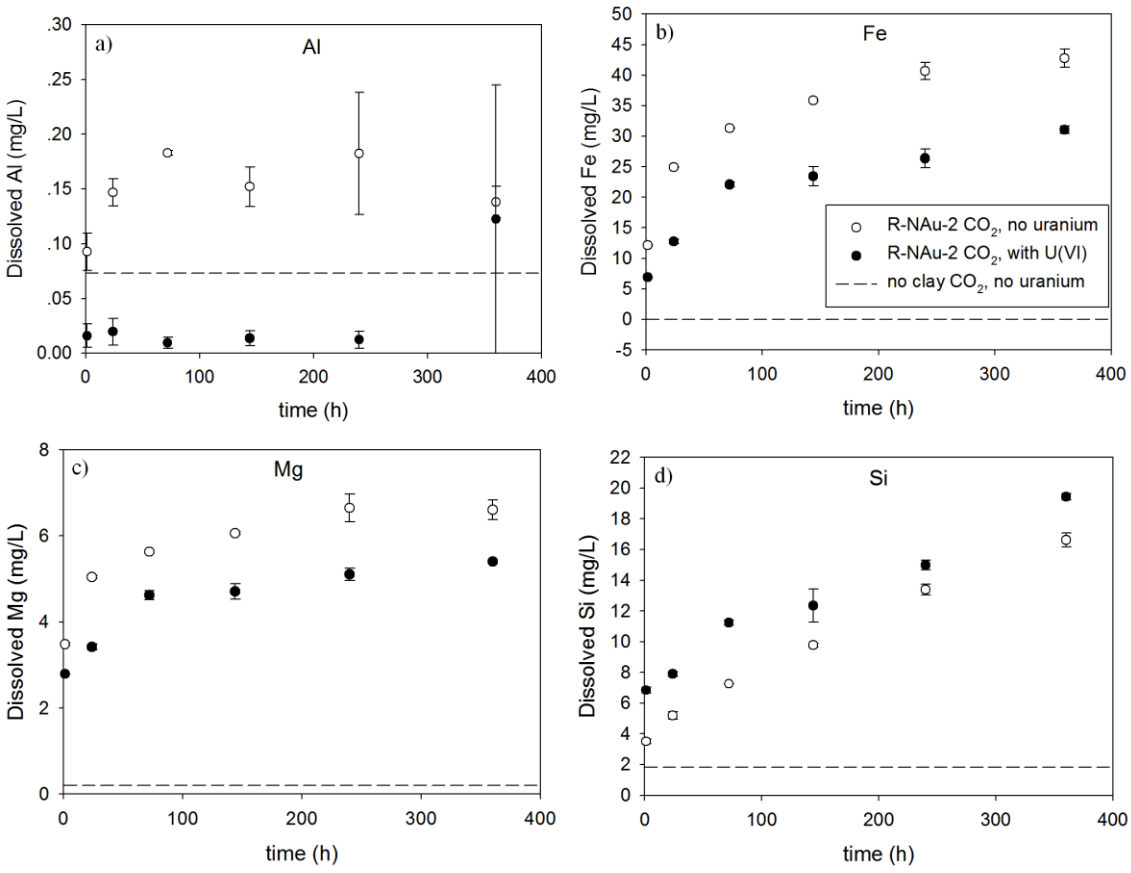

Figure 3.15. Dissolution of reduced nontronite R-NAu-2 (0.5 g/L) in 0.33 M Na_2SO_4 with and without 0.45 mM U(VI) under high pressure CO_2 (P_T = 9.66 bar, $P_{CO2} \geq$ 8.66 bar CO_2). Average concentrations of ions in brine-only, no-clay controls are shown as dashed lines.

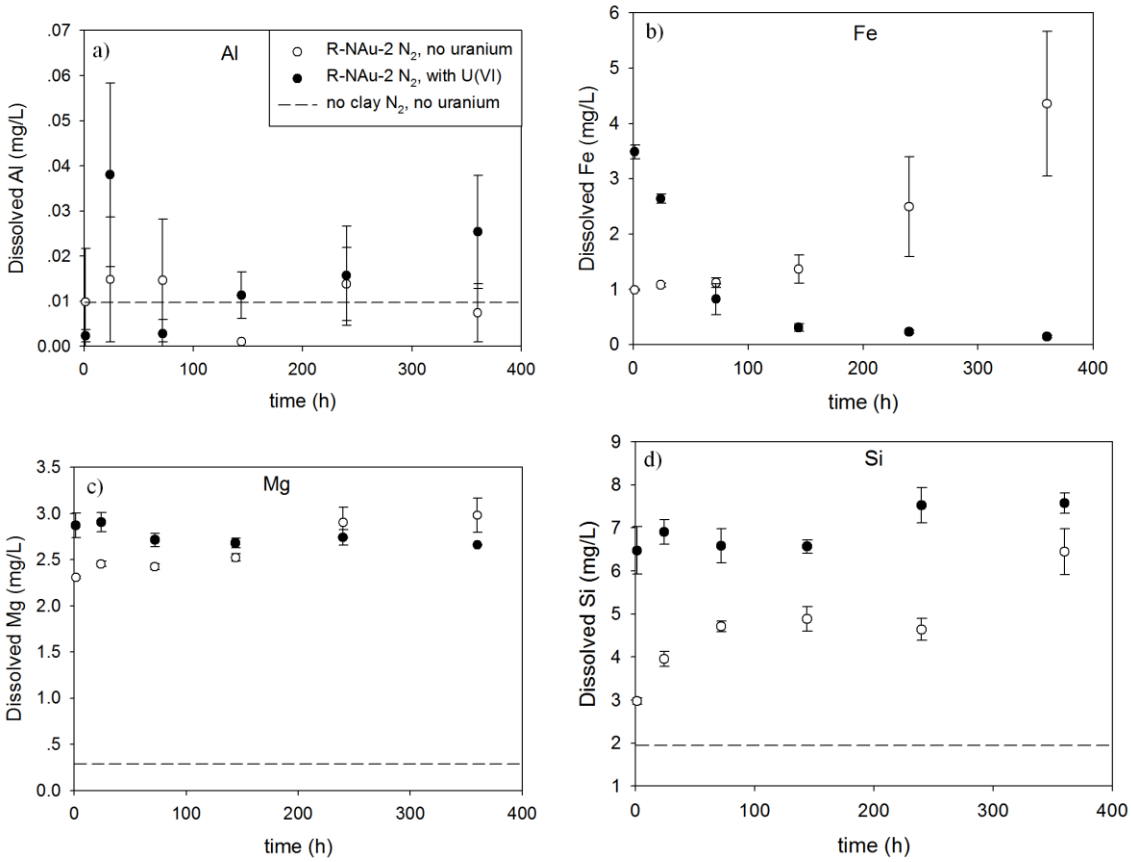

Figure 3.16. Dissolution of reduced nontronite R-NAu-2 (0.5 g/L) in 0.33 M Na_2SO_4 with and without 0.45 mM U(VI) under ambient pressure conditions (P_T = 1.0 bar, N_2:H_2 = 95:5%). Average concentrations of ions in brine-only, no-clay controls are shown as dashed lines.

3.3.2 Reactions between NAu-2 and U(IV)

Under both high pressure CO_2 conditions (P_T = 9.66 bar, $P_{CO2} \geq$ 8.66 bar CO_2) and ambient pressure conditions (P_T = 1.0 bar, N_2:H_2 = 95:5%), Fe(III) in NAu-2 was reduced (Figure 3.17 (a)) and U(IV) was oxidized (Figure 3.18). The extent of redox reactions between U(IV) and Fe(III) was greater under high pressure CO_2 conditions than under ambient pressure conditions. After 360 hours, overall Fe(II)/Fe_{TOT} ratio increased to 18.1% under high pressure CO_2 conditions, and increased to 10.5% under ambient pressure conditions from initial value of 3.9%. Dissolved Fe was only measurable under high pressure CO_2 conditions, and Fe(II) was predominant (Figure 3.17 (b)). Higher Fe(II) ratios under high pressure CO_2 conditions compared to ambient pressure conditions were also observed in 1.40 M H_3PO_4 - 0.50 M H_2SO_4 extractable and solid Fe (Figure 3.17 (c), (d)). Under high pressure CO_2 conditions, lower pH value and higher bicarbonate concentrations facilitated dissolution of both uraninite and NAu-2, and promoted oxidation of uraninite both kinetically (Ginder-Vogel et al., 2010) and thermodynamically (Ginder-Vogel et al., 2006) (Figure 1.12). U(VI) concentrations in no-clay controls also increased with large standard errors, which might be caused by leakage of O_2 into pressure tubes and/or in anaerobic chamber. However, U(VI) concentrations in no-clay controls were still lower than experiments conducted with NAu-2, reflecting NAu-2 was the major oxidant of U(IV).

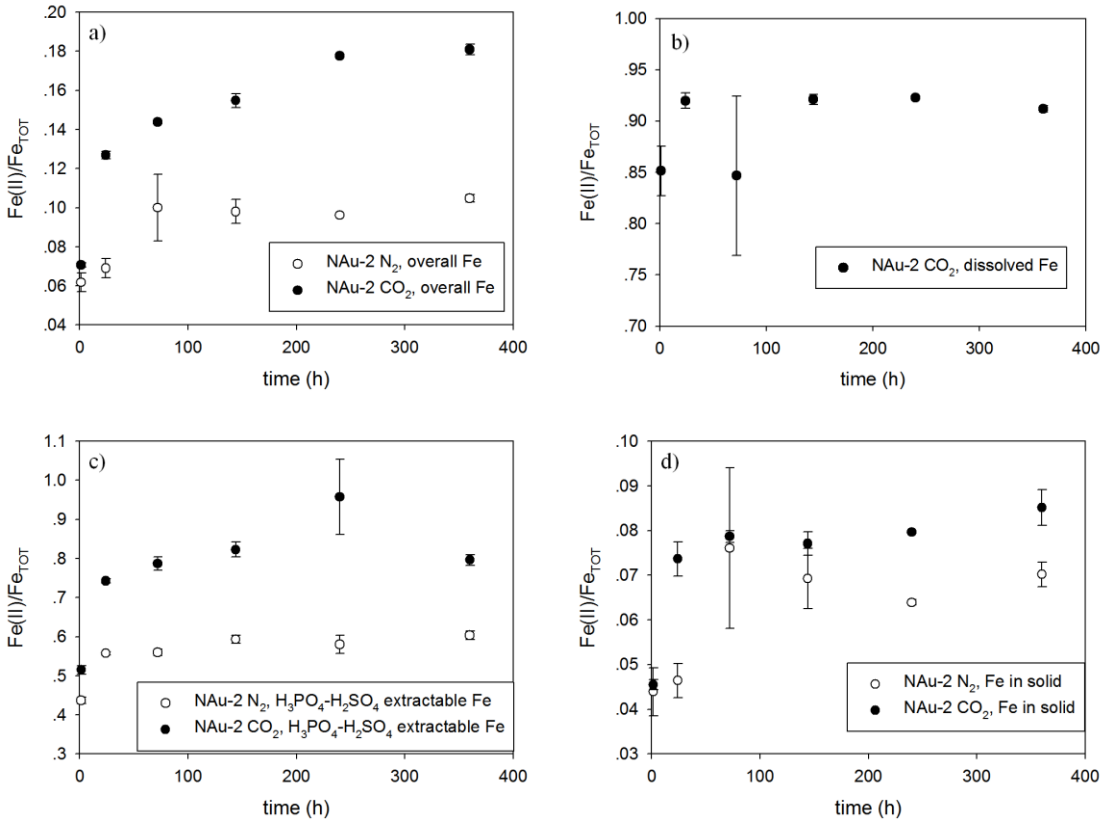

Figure 3.17. Fe(II)/Fe_{TOT} ratios of (a) overall Fe, (b) dissolved Fe, (c) 1.40 M H_3PO_4 - 0.50 M H_2SO_4 extractable Fe, (d) Fe in solid. Experiments conducted with 0.5g/L NAu-2, 0.33 mM uraninite-U (58% U(IV)) in 0.33 M Na_2SO_4 brine under high pressure CO_2 conditions (P_T = 9.66 bar, $P_{CO2} \geq$ 8.66 bar CO_2) and ambient pressure conditions (P_T = 1.0 bar, N_2:H_2 = 95:5%).

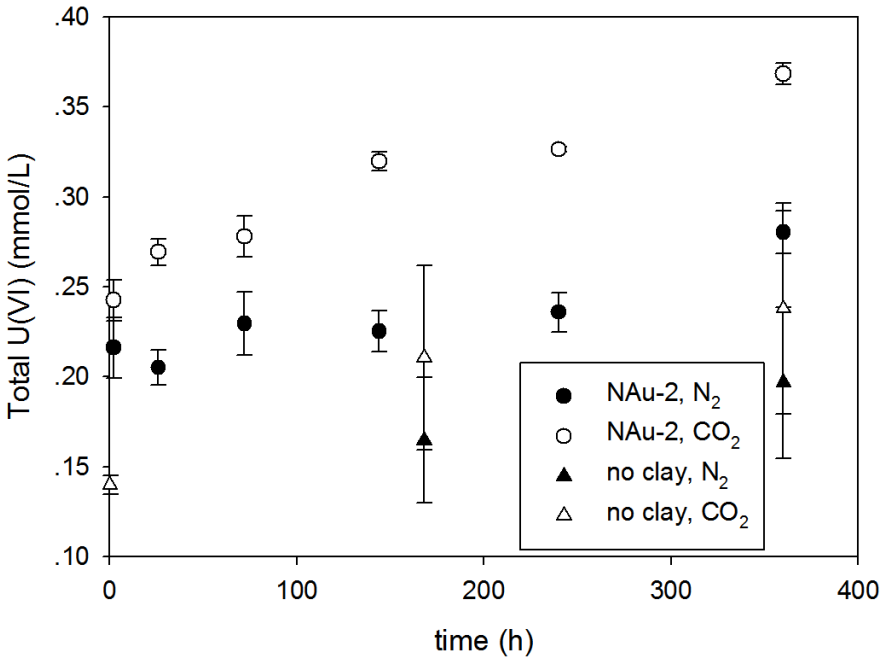

Figure 3.18. Total U(VI) concentrations (sum of dissolved U(VI) and 1.40 M H_3PO_4 - 0.50 M H_2SO_4 extracted U(VI)). Experiments conducted with 0.5g/L NAu-2, 0.33 mM uraninite-U (58% U(IV)) in 0.33 M Na_2SO_4 brine under high pressure CO_2 conditions (P_T = 9.66 bar, $P_{CO2} \geq$ 8.66 bar CO_2) and ambient pressure conditions (P_T = 1.0 bar, N_2:H_2 = 95:5%). Total U(VI) concentrations in no-clay controls are also presented.

ΔFe(II):ΔU(VI) ratios were close to 2:1, the theoretical stoichiometry of redox reaction between Fe(III) and U(IV) (Figure 3.19), but ΔU(VI) was systematically high relative to ΔFe(II), indicating systematic errors during experiment. This could be caused by leakage of oxygen into pressure tubes and/or in anoxic chamber which oxidized part of U(IV). Initial Fe(II)/Fe_{TOT} ratio was the average overall Fe(II)/Fe_{TOT} values in no-uranium NAu-2-0.33 M Na_2SO_4 experiment under both high pressure CO_2 and ambient pressure conditions. Initial U(VI) concentration was total U(VI) concentration at sampling time 0 in no-clay controls of NAu-2-U(IV)-0.33 M Na_2SO_4 experiment.

$$2\ Fe(III) + U(IV) = 2\ Fe(II) + U(VI)$$

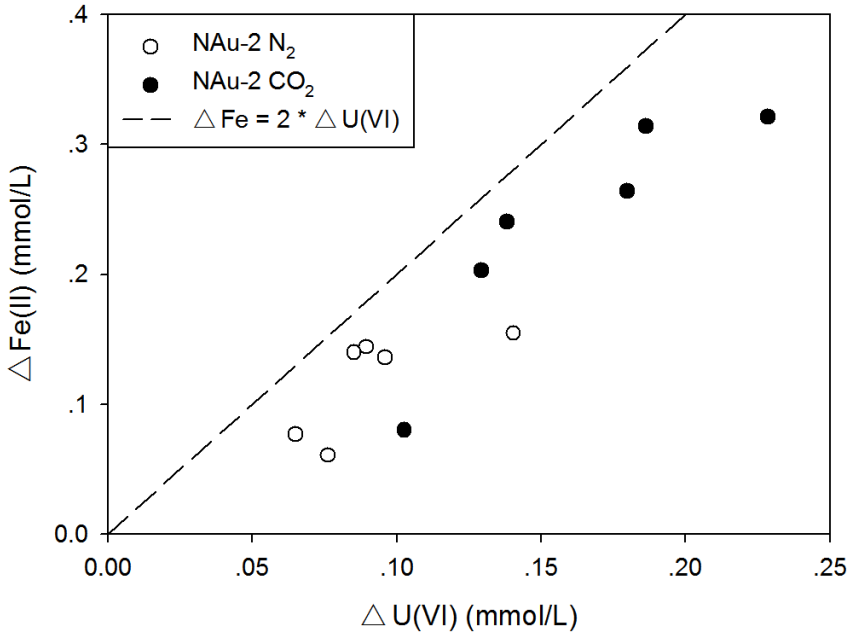

Figure 3.19. Increase of Fe(II) versus increase of U(VI). Experiments conducted with 0.5g/L NAu-2, 0.33 mM uraninite-U (58% U(IV)) in 0.33 M Na_2SO_4 brine under high pressure CO_2 conditions (P_T = 9.66 bar, $P_{CO2} \geq$ 8.66 bar CO_2) (●) and ambient pressure conditions (P_T = 1.0 bar, N_2:H_2 = 95:5%) (○). Dashed line represents theoretical 2:1 ratio of this redox reaction.

As before in experiments conducted without U, and experiments with U(VI), unaltered NAu-2 did not dissolve to any measureable extent under ambient pressure conditions (P_T = 1.0 bar, N_2:H_2 = 95:5%) (Figure 3.20 (a)). However, under high pressure CO_2 conditions (P_T = 9.66 bar, $P_{CO2} \geq$ 8.66 bar CO_2), reduction of structural Fe by U(IV) enhanced NAu-2 dissolution (Figure 3.20 (b)), which is consistent with previous results where R-NAu-2 had higher solubility than unaltered NAu-2 in carbonic acid ([H_2CO_3*]≈0.25 M]) and 1.40 M H_3PO_4-0.50 M H_2SO_4. The dissolution extent was increasing as a function of reaction time for the following reasons: 1. NAu-2 was kept being reduced; 2. NAu-2 with high Fe(II)/Fe_{TOT} had higher solubility in acid; 3. carbonic acid dissolved Fe(II), and made more Fe(III) available to redox reaction. Thus, CO_2 enabled a self-enhancing dissolution-reduction process of NAu-2. Compared with experiments

with NAu-2/R-NAu-2 and U(VI) (Figure 3.14), the sum of dissolved and H_3PO_4-H_2SO_4-extractable Fe concentrations increased under either conditions, which was attributed to continuous reduction of NAu-2 by U(IV).

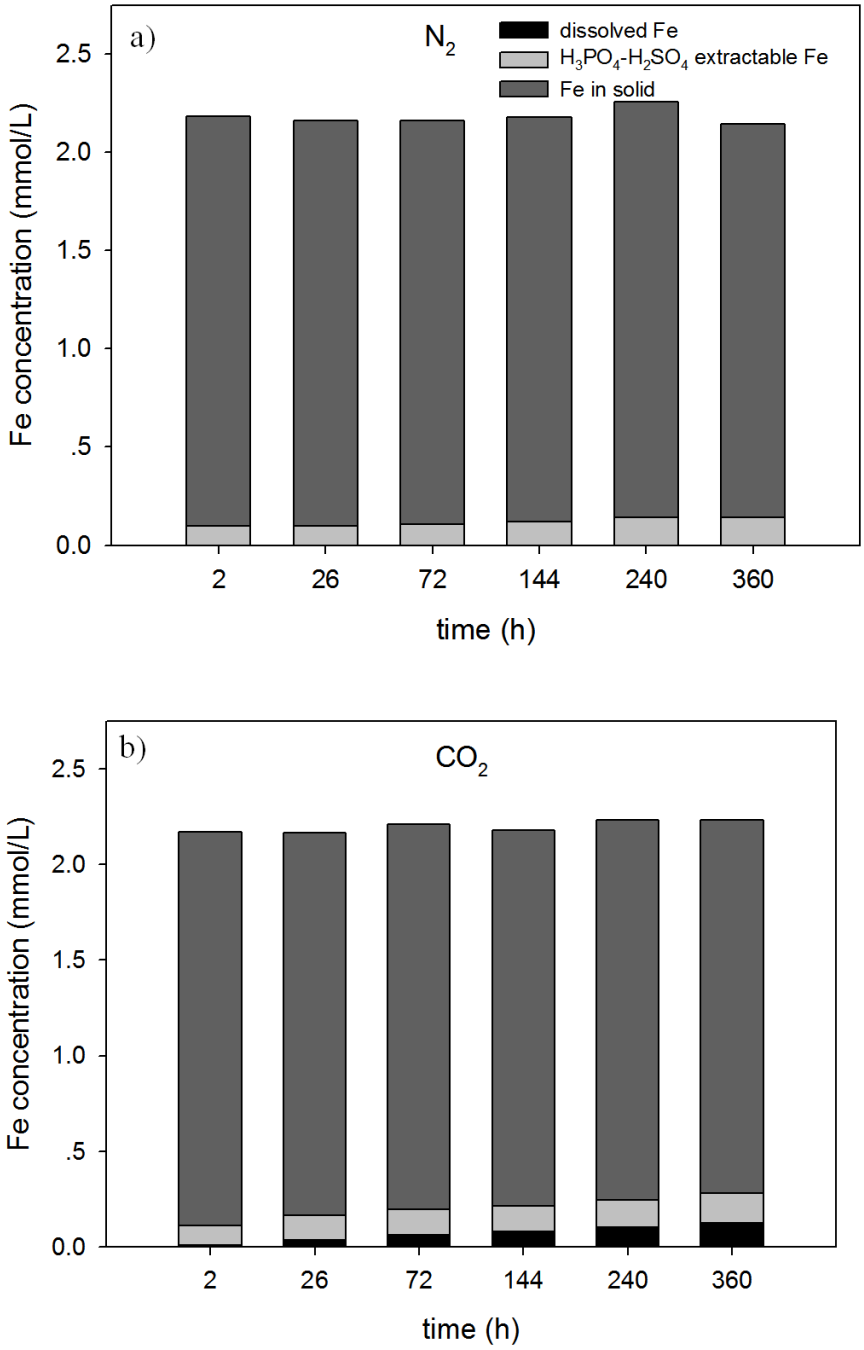

Figure 3.20. Fe distribution in dissolved, 1.40 M H_3PO_4-0.50 M H_2SO_4 extractable and solid forms. (a) under ambient pressure conditions (P_T = 1.0 bar, N_2:H_2 = 95:5%), (b) under high pressure CO_2 conditions (P_T = 9.66 bar, $P_{CO2} \geq$ 8.66 bar CO_2). Experiments conducted with 0.5g/L NAu-2, 0.33 mM uraninite-U (58% U(IV)) in 0.33 M Na_2SO_4.

Except enhanced dissolution of Fe in the presence of U(IV) under high pressure CO2 conditions (Figure 3.21 (b)), no other significant influence of U(IV) or U(VI) on dissolution of unaltered NAu-2 was observed, due to very low solubility of unaltered NAu-2 under high pressure CO_2 conditions (Figure 3.21) and ambient pressure conditions (Figure 3.22).

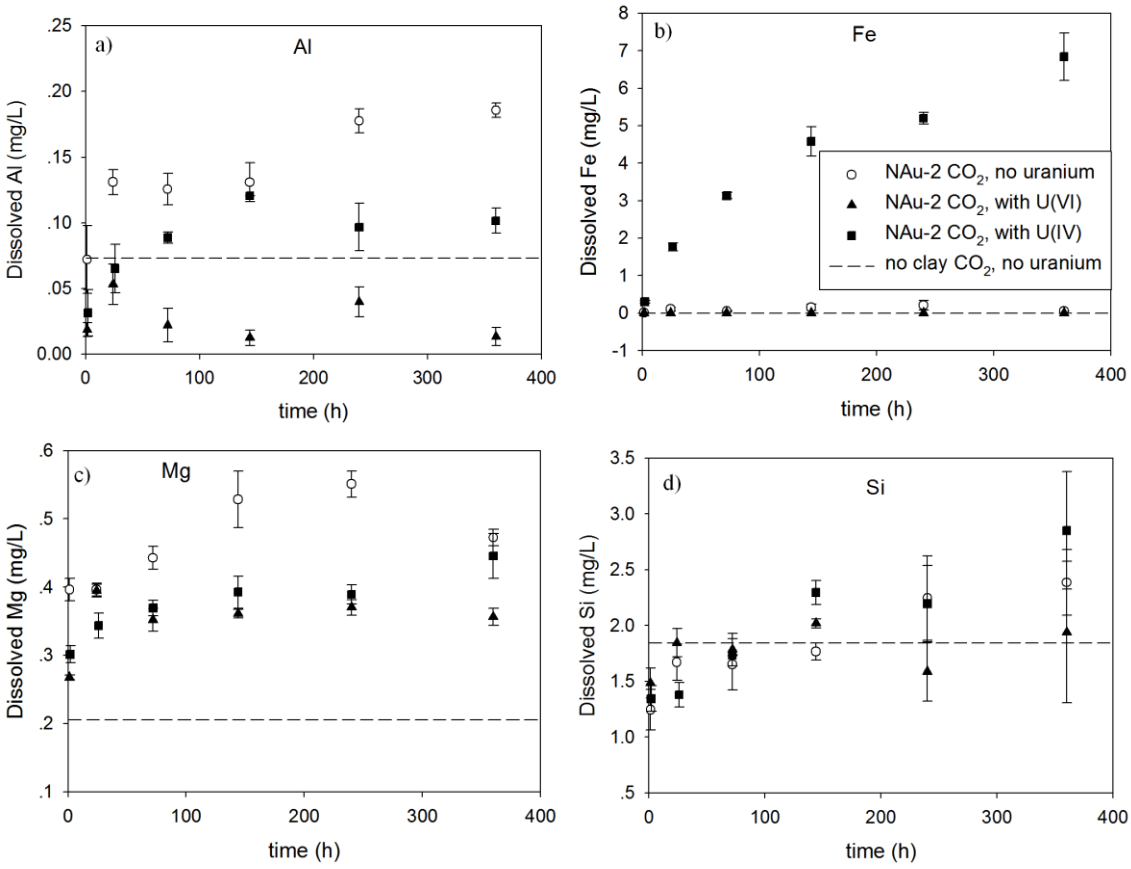

Figure 3.21. Dissolution of nontronite NAu-2 (0.5 g/L) in 0.33 M Na_2SO_4 with 0.45 mM U(VI) or with 0.33 mM uraninite-U (58% U(IV)) under high pressure CO_2 conditions (P_T = 9.66 bar, P_{CO2} ≥ 8.66 bar CO_2). Average concentrations of ions in brine-only, no-clay controls are shown as dashed lines.

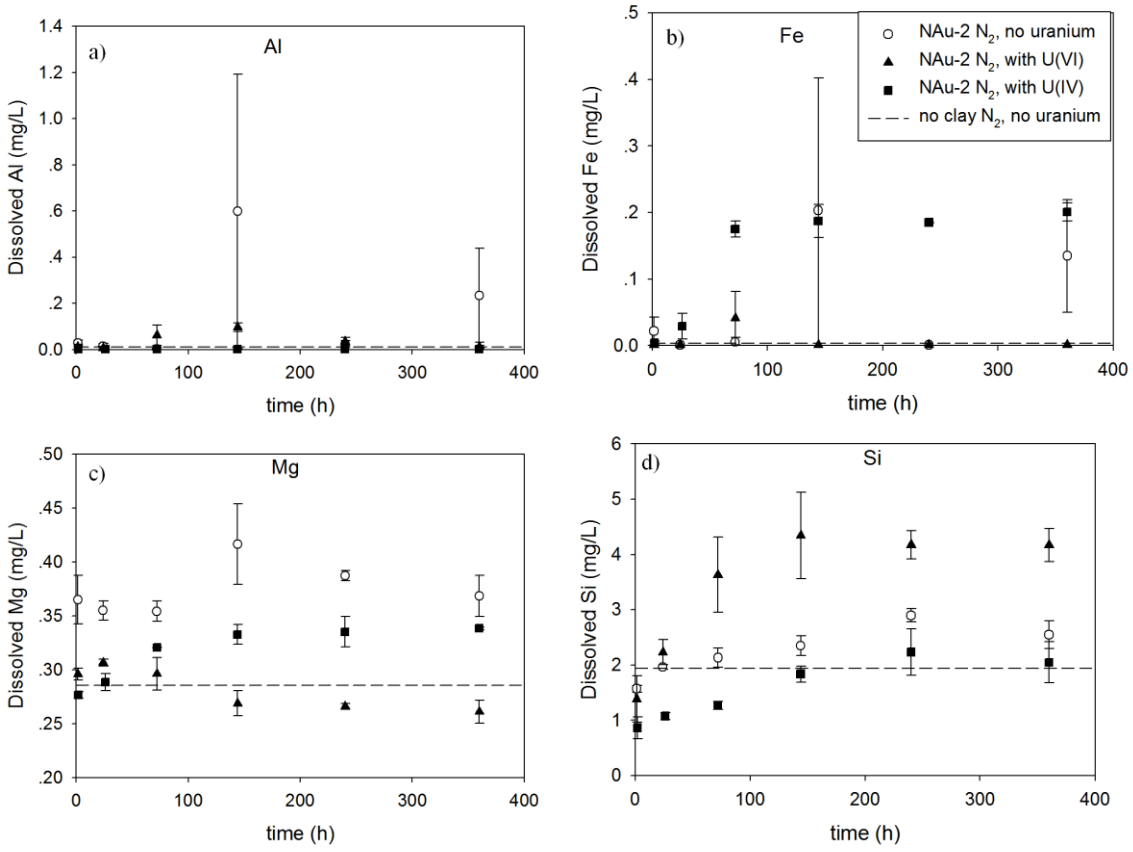

Figure 3.22. Dissolution of nontronite NAu-2 (0.5 g/L) in 0.33 M Na_2SO_4 with 0.45 mM U(VI) or with 0.33 mM uraninite-U (58% U(IV)) under under ambient pressure conditions (P_T = 1.0 bar, N_2:H_2 = 95:5%). Average concentrations of ions in brine-only, no-clay controls are shown as dashed lines.

Concentrations of uranium in brine were significantly higher under high pressure CO_2 conditions as compared with ambient pressure conditions (Figure 3.23), which was caused by acid-driven and oxidation-driven dissolution. This is similar with in situ recovery mining of uranium, where O_2 or other oxidizing reagents such as H_2O_2, together with CO_2, is pumped with water into a confined aquifer with permeable uranium ore. Oxidation-driven, acid-driven and bicarbonate-driven dissolution of uranium enriches recovered water. If geological carbon sequestration takes place in aquifers with uranium ore and nontronite, similar monitoring and remediation of uranium contamination must be carried out. In our experiment, no clay washing

operation was made to avoid loss of uranium or iron, so it was possible that the supernatant of clay mineral suspension was not removed completely. Due to high uranium concentration in supernatant under high pressure CO_2 condition, the concentration of uranium measured in acid extraction might be false high, making total uranium concentration also false high. (Figure 3.23 (b))

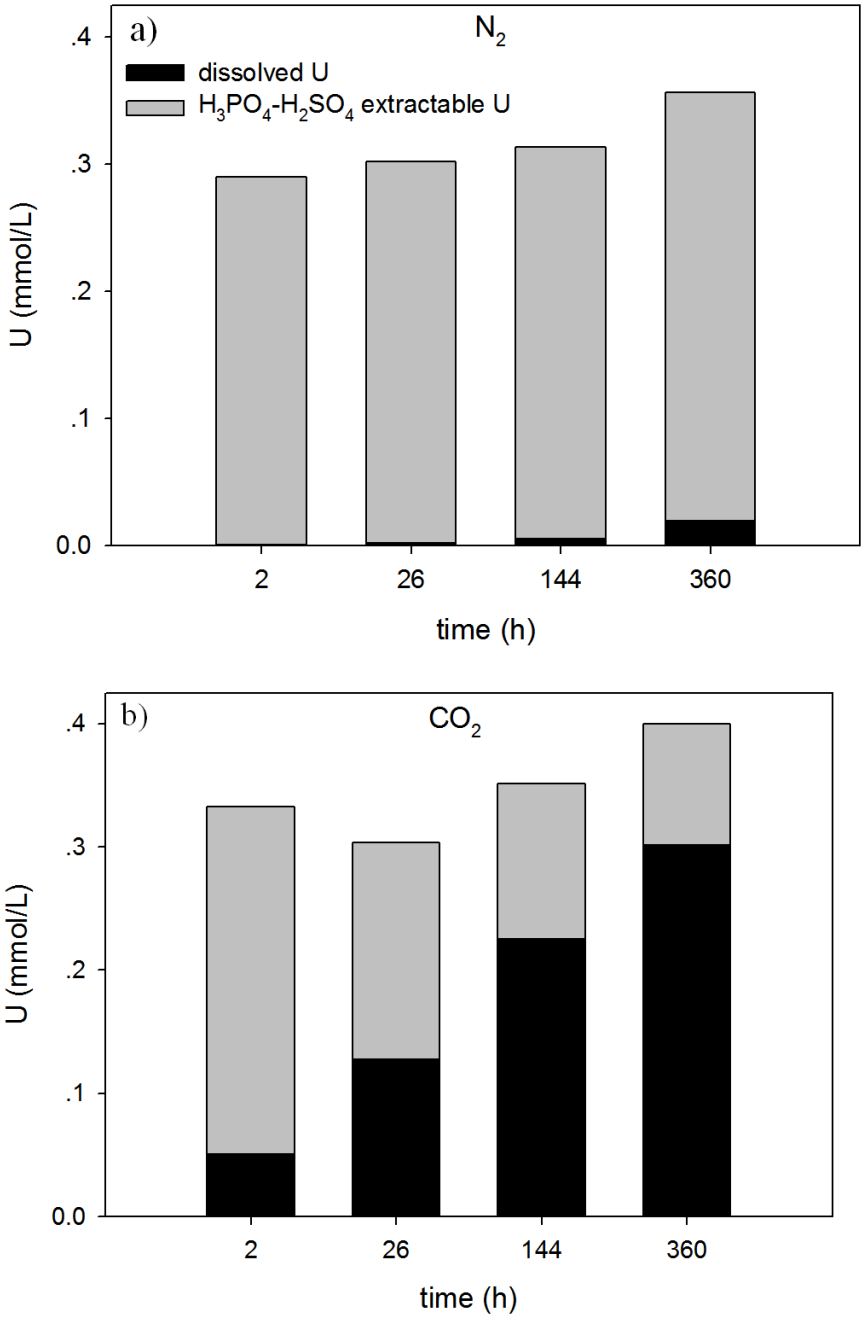

Figure 3.23. U distribution in dissolved and 1.40 M H_3PO_4 - 0.50 M H_2SO_4 extractable fractions. (a) under ambient pressure conditions (P_T = 1.0 bar, N_2:H_2 = 95:5%), (b) under high pressure CO_2 conditions (P_T = 9.66 bar, $P_{CO2} \geq$ 8.66 bar CO_2). Experiments conducted with 0.5g/L NAu-2, 0.33 mM uraninite-U (58% U(IV)) in 0.33 M Na_2SO_4.

U(VI) was the predominant dissolved uranium species under high pressure CO_2 conditions (Figure 3.24), indicating fast oxidation of U(aq) and oxidation-driven dissolution of uraninite. While 1.40 M H_3PO_4 - 0.50 M H_2SO_4 extractable uranium, which was originally in solid or sorbed forms before acid extraction, was relatively slowly oxidized. This also explains high pressure CO_2 enhanced oxidation of U(IV) (Figure 3.18), by increasing dissolved uranium concentration.

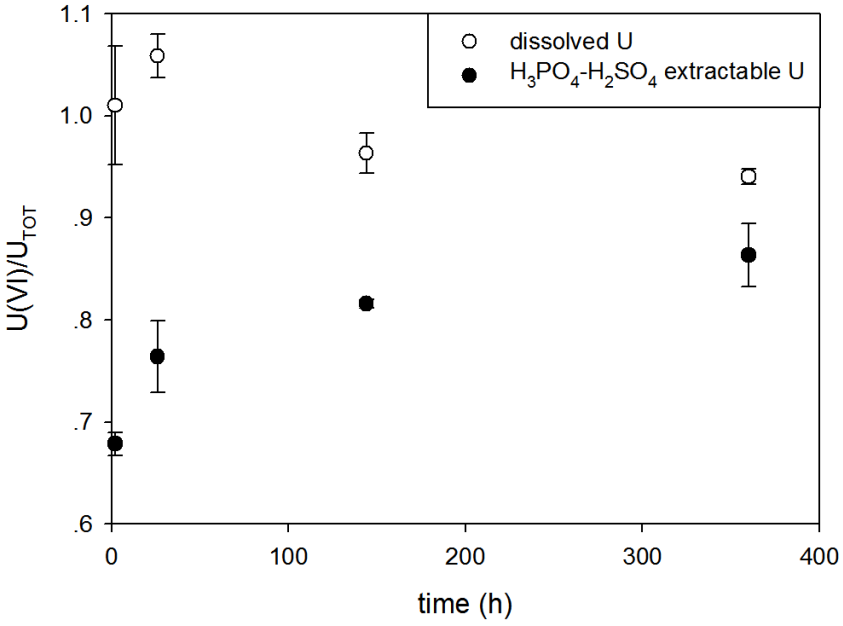

Figure 3.24. $U(VI)/U_{TOT}$ ratios of dissolved and 1.40 M H_3PO_4 - 0.50 M H_2SO_4 extractable U. Experiments conducted with 0.5g/L NAu-2, 0.33 mM uraninite-U (58% U(IV)) in 0.33 M Na_2SO_4 under high pressure CO_2 conditions (P_T = 9.66 bar, $P_{CO2} \geq$ 8.66 bar CO_2).

Chapter 4

Conclusions

- Unaltered NAu-2, or SWy-2 or CCa-2 did not dissolve to any great extent under high pressure CO_2 conditions (P_T = 9.66 bar, $P_{CO2} \geq$ 8.66 bar CO_2) in all 1.0 M NaCl, 0.33 M $CaCl_2$ or 0.33 M Na_2SO_4.
- Partially reduced NAu-2 (R-NAu-2) dissolved to a significant greater extent than unaltered NAu-2 in 0.33 M Na_2SO_4 under high pressure CO_2 conditions, and in 1.40 M H_3PO_4 - 0.50 M H_2SO_4 under ambient pressure conditions (P_T = 1.0 bar, N_2:H_2 = 95:5%).
- Fe(II) in clay mineral structure is unstable compared to Fe(III), dissolved Fe had higher Fe(II)/Fe_{TOT} ratios than Fe in solid for both NAu-2 and R-NAu-2.
- Long-term weak H_2CO_3 extraction followed by a short-term H_3PO_4-H_2SO_4 extraction dissolved the same amount (~ 36%) of clay-Fe as compared to a short-term H_3PO_4-H_2SO_4 extraction alone.
- No redox reactions observed between NAu-2/R-NAu-2 with U(VI).
- U(VI) decreased the extent of dissolution of Al, Fe and Mg from R-NAu-2 under high pressure CO_2 conditions, possibly by sorption to clay mineral and blocking acid attacking sites; U(VI) slightly enhanced dissolution of Si from R-NAu-2 under high pressure CO_2 conditions and ambient pressure conditions.
- Unaltered NAu-2 oxidized UO_2 under both high pressure CO_2 conditions and ambient pressure conditions, and CO_2 enhanced this redox reaction.

- UO_2 enhanced dissolution of Fe from NAu-2 under high pressure CO_2 conditions.
- CO_2 mobilized uranium into dissolved form through acid-driven and oxidation-driven dissolution, which could lead to environmental risks in this geochemical settings when leakage of carbon sequestration happens.

References

1 Andre, L., Audigane, P., Azaroual, M. & Menjoz, A. Numerical modeling of fluid-rock chemical interactions at the supercritical CO2-liquid interface during CO2 injection into a carbonate reservoir, the Dogger aquifer (Paris Basin, France). *Energy Conversion and Management* **48**, 1782-1797, doi:10.1016/j.enconman.2007.01.006 (2007).

2 Aydin, G., Karakurt, I. & Aydiner, K. Evaluation of geologic storage options of CO2: Applicability, cost, storage capacity and safety. *Energy Policy* **38**, 5072-5080, doi:10.1016/j.enpol.2010.04.035 (2010).

3 Bachmaf, S. & Merkel, B. J. Sorption of uranium(VI) at the clay mineral-water interface. *Environmental Earth Sciences* **63**, 925-934, doi:10.1007/s12665-010-0761-6 (2011).

4 Bachu, S. & Bennion, B. Effects of in-situ conditions on relative permeability characteristics of CO(2)-brine systems. *Environmental Geology* **54**, 1707-1722, doi:10.1007/s00254-007-0946-9 (2008).

5 Barnett, M. O., Jardine, P. M., Brooks, S. C. & Selim, H. M. Adsorption and transport of uranium(VI) in subsurface media. *Soil Science Society of America Journal* **64**, 908-917 (2000).

6 Bearat, H. *et al.* Carbon sequestration via aqueous olivine mineral carbonation: Role of passivating layer formation. *Environmental Science & Technology* **40**, 4802-4808, doi:10.1021/es0523340 (2006).

7 Bishop, M. E., Dong, H. L., Kukkadapu, R. K., Liu, C. X. & Edelmann, R. E. Bioreduction of Fe-bearing clay minerals and their reactivity toward pertechnetate (Tc-99). *Geochimica Et Cosmochimica Acta* **75**, 5229-5246, doi:10.1016/j.gca.2011.06.034 (2011).

8 Borch, T., Roche, N. & Johnson, T. E. Determination of contaminant levels and remediation efficacy in groundwater at a former in situ recovery uranium mine. *Journal of Environmental Monitoring* **14**, 1814-1823, doi:10.1039/c2em30077j (2012).

9 Brandt, F., Bosbach, D., Krawczyk-Barsch, E., Arnold, T. & Bernhard, G. Chlorite dissolution in the acid pH-range: A combined microscopic and macroscopic approach. *Geochimica Et Cosmochimica Acta* **67**, 1451-1461, doi:10.1016/s0016-7037(02)01293-0 (2003).

10 Brina, R. & Miller, A. G. DIRECT DETECTION OF TRACE LEVELS OF URANIUM BY LASER-INDUCED KINETIC PHOSPHORIMETRY. *Analytical Chemistry* **64**, 1413-1418, doi:10.1021/ac00037a020 (1992).

11 Burgos, W. D. *et al.* Characterization of uraninite nanoparticles produced by Shewanella oneidensis MR-1. *Geochimica Et Cosmochimica Acta* **72**, 4901-4915, doi:10.1016/j.gca.2008.07.016 (2008).

12 Daneshfar, J., Hughes, R. G. & Civan, F. Feasibility Investigation and Modeling Analysis of CO(2) Sequestration in Arbuckle Formation Utilizing Salt Water

Disposal Wells. *Journal of Energy Resources Technology-Transactions of the Asme* **131**, 10, doi:10.1115/1.3124115 (2009).

13 Dong, H. L. Clay-Microbe Interactions and Implications for Environmental Mitigation. *Elements* **8**, 113-118, doi:10.2113/gselements.8.2.113 (2012).

14 Dong, H. L., Jaisi, D. P., Kim, J. & Zhang, G. X. Microbe-clay mineral interactions. *American Mineralogist* **94**, 1505-1519, doi:10.2138/am.2009.3246 (2009).

15 Favre, F., Stucki, J. W. & Boivin, P. Redox properties of structural Fe in ferruginous smectite. A discussion of the standard potential and its environmental implications. *Clays and Clay Minerals* **54**, 466-472, doi:10.1346/ccmn.2006.0540407 (2006).

16 Gasda, S. E., Bachu, S. & Celia, M. A. Spatial characterization of the location of potentially leaky wells penetrating a deep saline aquifer in a mature sedimentary basin. *Environmental Geology* **46**, 707-720, doi:10.1007/s00254-004-1073-5 (2004).

17 Gaus, I., Azaroual, M. & Czernichowski-Lauriol, I. Reactive transport modelling of the impact of CO2 injection on the clayey cap rock at Sleipner (North Sea). *Chemical Geology* **217**, 319-337, doi:10.1016/j.chemgeo.2004.12.016 (2005).

18 Gherardi, F., Xu, T. F. & Pruess, K. Numerical modeling of self-limiting and self-enhancing caprock alteration induced by CO2 storage in a depleted gas reservoir. *Chemical Geology* **244**, 103-129, doi:10.1016/j.chemgeo.2007.06.009 (2007).

19 Giammar, D. E., Bruant, R. G. & Peters, C. A. Forsterite dissolution and magnesite precipitation at conditions relevant for deep saline aquifer storage and sequestration of carbon dioxide. *Chemical Geology* **217**, 257-276, doi:10.1016/j.chemgeo.2004.12.013 (2005).

20 Ginder-Vogel, M., Criddle, C. S. & Fendorf, S. Thermodynamic constraints on the oxidation of biogenic UO2 by Fe(III) (hydr) oxides. *Environmental Science & Technology* **40**, 3544-3550, doi:10.1021/es052305p (2006).

21 Ginder-Vogel, M. & Fendorf, S. in *Adsorption of Metals by Geomedia Ii: Variables, Mechanisms, and Model Applications* Vol. 7 *Developments in Earth and Environmental Sciences* (eds M. O. Barnett & D. B. Kent) 293-319 (Elsevier Science Bv, 2008).

22 Ginder-Vogel, M., Stewart, B. & Fendorf, S. Kinetic and Mechanistic Constraints on the Oxidation of Biogenic Uraninite by Ferrihydrite. *Environmental Science & Technology* **44**, 163-169, doi:10.1021/es902452u (2010).

23 Haque, N., Morrison, G., Cano-Aguilera, I. & Gardea-Torresdey, J. L. Iron-modified light expanded clay aggregates for the removal of arsenic(V) from groundwater. *Microchemical Journal* **88**, 7-13, doi:10.1016/j.microc.2007.08.004 (2008).

24 House, K. Z., Schrag, D. P., Harvey, C. F. & Lackner, K. S. Permanent carbon dioxide storage in deep-sea sediments. *Proceedings of the National Academy of Sciences of the United States of America* **103**, 12291-12295, doi:10.1073/pnas.0605318103 (2006).

25 Ilgen, A. G., Newville, M. & Trainor, T. P. Role of dissolved iron(II) and structural iron in clay mineral mediated redox transformations of arsenic and antimony. *Abstracts of Papers of the American Chemical Society* **237**, 1 (2009).

26 IPCC. Special Report on Carbon Dioxide Capture and Storage. (2005).

27 IPCC. Summary for Policymakers. Climate Change 2007: The Physical Science Basis. Contribution of Working Group I to the Fourth Assessment Report of the Intergovernmental Panel on Climate Change. (2007).

28 Izgec, O., Demiral, B., Bertin, H. & Akin, S. CO2 injection into saline carbonate aquifer formations II: Comparison of numerical simulations to experiments. *Transport in Porous Media* **73**, 57-74, doi:10.1007/s11242-007-9160-1 (2008).

29 Jaisi, D. P., Dong, H. L. & Liu, C. X. Influence of biogenic Fe(II) on the extent of microbial reduction of Fe(III) in clay minerals nontronite, illite, and chlorite. *Geochimica Et Cosmochimica Acta* **71**, 1145-1158, doi:10.1016/j.gca.2006.11.027 (2007).

30 Jaisi, D. P., Dong, H. L. & Morton, J. P. Partitioning of Fe(II) in reduced nontronite (NAu-2) to reactive sites: Reactivity in terms of Tc(VII) reduction. *Clays and Clay Minerals* **56**, 175-189, doi:10.1346/ccmn.2008.0560204 (2008).

31 Jaisi, D. P., Kukkadapu, R. K., Eberl, D. D. & Dong, H. L. Control of Fe(III) site occupancy on the rate and extent of microbial reduction of Fe(III) in nontronite. *Geochimica Et Cosmochimica Acta* **69**, 5429-5440, doi:10.1016/j.gca.2005.07.008 (2005).

32 Jeon, B. H., Dempsey, B. A., Burgos, W. D., Barnett, M. O. & Roden, E. E. Chemical reduction of U(VI) by Fe(II) at the solid-water interface using natural and synthetic Fe(III) oxides. *Environmental Science & Technology* **39**, 5642-5649, doi:10.1021/es0487527 (2005).

33 Jeon, B. H., Dempsey, B. A., Royer, R. A. & Burgos, W. D. Low-temperature oxygen trap for maintaining strict anoxic conditions. *Journal of Environmental Engineering-Asce* **130**, 1407-1410, doi:10.1061/(asce)0733-9372(2004)130:11(1407) (2004).

34 Kaszuba, J. P., Janecky, D. R. & Snow, M. G. Carbon dioxide reaction processes in a model brine aquifer at 200 degrees C and 200 bars: implications for geologic sequestration of carbon. *Applied Geochemistry* **18**, 1065-1080, doi:10.1016/s0883-2927(02)00239-1 (2003).

35 Kaszuba, J. P., Janecky, D. R. & Snow, M. G. Experimental evaluation of mixed fluid reactions between supercritical carbon dioxide and NaCl brine: Relevance to the integrity of a geologic carbon repository. *Chemical Geology* **217**, 277-293, doi:10.1016/j.chemgeo.2004.12.014 (2005).

36 Keating, E. H., Fessenden, J., Kanjorski, N., Koning, D. J. & Pawar, R. The impact of CO2 on shallow groundwater chemistry: observations at a natural analog site and implications for carbon sequestration. *Environmental Earth Sciences* **60**, 521-536, doi:10.1007/s12665-009-0192-4 (2010).

37 Kharaka, Y. K. *et al.* Gas-water-rock interactions in Frio Formation following CO2 injection: Implications for the storage of greenhouse gases in sedimentary basins. *Geology* **34**, 577-580, doi:10.1130/g22357.1 (2006).

38 Kharaka, Y. K. *et al.* Changes in the chemistry of shallow groundwater related to the 2008 injection of CO2 at the ZERT field site, Bozeman, Montana. *Environmental Earth Sciences* **60**, 273-284, doi:10.1007/s12665-009-0401-1 (2010).

39 Knauss, K. G., Johnson, J. W. & Steefel, C. I. Evaluation of the impact of CO2, co-contaminant gas, aqueous fluid and reservoir rock interactions on the geologic

sequestration of CO2. *Chemical Geology* **217**, 339-350, doi:10.1016/j.chemgeo.2004.12.017 (2005).

40 Komadel, P. & Stucki, J. W. QUANTITATIVE ASSAY OF MINERALS FOR FE-2+ AND FE-3+ USING 1,10-PHENANTHROLINE .3. A RAPID PHOTOCHEMICAL METHOD. *Clays and Clay Minerals* **36**, 379-381, doi:10.1346/ccmn.1988.0360415 (1988).

41 Kutchko, B. G., Strazisar, B. R., Lowry, G. V., Dzombak, D. A. & Thaulow, N. Rate of CO(2) attack on hydrated Class H well cement under geologic sequestration conditions. *Environmental Science & Technology* **42**, 6237-6242, doi:10.1021/es800049r (2008).

42 Lear, P. R. & Stucki, J. W. INTERVALENCE ELECTRON-TRANSFER AND MAGNETIC EXCHANGE IN REDUCED NONTRONITE. *Clays and Clay Minerals* **35**, 373-378, doi:10.1346/ccmn.1987.0350507 (1987).

43 Liger, E., Charlet, L. & Van Cappellen, P. Surface catalysis of uranium(VI) reduction by iron(II). *Geochimica Et Cosmochimica Acta* **63**, 2939-2955, doi:10.1016/s0016-7037(99)00265-3 (1999).

44 Liteanu, E. & Spiers, C. J. Influence of pore fluid salt content on compaction creep of calcite aggregates in the presence of supercritical CO2. *Chemical Geology* **265**, 134-147, doi:10.1016/j.chemgeo.2008.12.010 (2009).

45 Little, M. G. & Jackson, R. B. Potential Impacts of Leakage from Deep CO2 Geosequestration on Overlying Freshwater Aquifers. *Environmental Science & Technology* **44**, 9225-9232, doi:10.1021/es102235w (2010).

46 Liu, D. *et al.* Microbial reduction of structural iron in interstratified illite-smectite minerals by a sulfate-reducing bacterium. *Geobiology* **10**, 150-162, doi:10.1111/j.1472-4669.2011.00307.x (2012).

47 Liu, D. *et al.* Reduction of structural Fe(III) in nontronite by methanogen Methanosarcina barkeri. *Geochimica Et Cosmochimica Acta* **75**, 1057-1071, doi:10.1016/j.gca.2010.11.009 (2011).

48 Lu, J. M., Partin, J. W., Hovorka, S. D. & Wong, C. Potential risks to freshwater resources as a result of leakage from CO2 geological storage: a batch-reaction experiment. *Environmental Earth Sciences* **60**, 335-348, doi:10.1007/s12665-009-0382-0 (2010).

49 Luan, F. B. & Burgos, W. D. Sequential Extraction Method for Determination of Fe(II/III) and U(IV/VI) in Suspensions of Iron-Bearing Phyllosilicates and Uranium. *Environmental Science & Technology* **46**, 11995-12002, doi:10.1021/es303306f (2012).

50 NETL. US Department of Energy, Office of Fossil Energy, National Energy Technology Laboratory (2008a) Carbon Sequestration Atlas of the United States and Canada, 2nd edn. US Department of Energy, National Energy Technology Laboratory, Morgantown, West Virginia. (2008).

51 Okada, K., Arimitsu, N., Karneshima, Y., Nakajima, A. & MacKenzie, K. J. D. Solid acidity of 2 : 1 type clay minerals activated by selective leaching. *Applied Clay Science* **31**, 185-193, doi:10.1016/j.clay.2005.10.014 (2006).

52 Olajire, A. A. CO2 capture and separation technologies for end-of-pipe applications - A review. *Energy* **35**, 2610-2628, doi:10.1016/j.energy.2010.02.030 (2010).

53 Osthaus, B. Kinetic Studies on Montmorillonites and Nontronite by the Acid-Dissolution Technique. *Clays and Clay Minerals* **4**, 301-321 (1955).

54 Park, B. & Dempsey, B. A. Heterogeneous oxidation of Fe(II) on ferric oxide at neutral pH and a low partial pressure of 0(2). *Environmental Science & Technology* **39**, 6494-6500, doi:10.1021/es0501058 (2005).

55 Pentrak, M., Czimerova, A., Madejova, J. & Komadel, P. Changes in layer charge of clay minerals upon acid treatment as obtained from their interactions with methylene blue. *Applied Clay Science* **55**, 100-107, doi:10.1016/j.clay.2011.10.012 (2012).

56 Pentrak, M., Madejova, J. & Komadel, P. Effect of chemical composition and swelling on acid dissolution of 2: 1 clay minerals. *Philosophical Magazine* **90**, 2387-2397, doi:10.1080/14786430903559433 (2010).

57 Peper, S. M. *et al.* Kinetic study of the oxidative dissolution of UO2 in aqueous carbonate media. *Industrial & Engineering Chemistry Research* **43**, 8188-8193, doi:10.1021/ie049457y (2004).

58 Rameback, H. *et al.* Transport and leaching of technetium and uranium from spent UO2 fuel in compacted bentonite clay. *Journal of Nuclear Materials* **277**, 288-294, doi:10.1016/s0022-3115(99)00152-x (2000).

59 Ribeiro, F. R., Fabris, J. D., Kostka, J. E., Komadel, P. & Stucki, J. W. Comparisons of structural iron reduction in smectites by bacteria and dithionite: II. A variable-temperature Mossbauer spectroscopic study of Garfield nontronite. *Pure and Applied Chemistry* **81**, 1499-1509, doi:10.1351/pac-con-08-11-16 (2009).

60 Rimmele, G., Barlet-Gouedard, V. & Renard, F. Evolution of the Petrophysical and Mineralogical Properties of Two Reservoir Rocks Under Thermodynamic Conditions Relevant for CO2 Geological Storage at 3 km Depth. *Oil & Gas Science and Technology-Revue D Ifp Energies Nouvelles* **65**, 565-580, doi:10.2516/ogst/2009071 (2010).

61 Rosenbauer, R. J., Koksalan, T. & Palandri, J. L. Experimental investigation of CO2-brine-rock interactions at elevated temperature and pressure: Implications for CO2 sequestration in deep-saline aquifers. *Fuel Processing Technology* **86**, 1581-1597, doi:10.1016/j.fuproc.2005.01.011 (2005).

62 Rozalen, M. L. *et al.* Experimental study of the effect of pH on the kinetics of montmorillonite dissolution at 25 degrees C. *Geochimica Et Cosmochimica Acta* **72**, 4224-4253, doi:10.1016/j.gca.2008.05.065 (2008).

63 Schulman, S. G. Molecular luminescence spectroscopy. Methods and applications: Part 1. Wiley: New York, 1984.

64 Shaw, S. A. & Hendry, M. J. Geochemical and mineralogical impacts of H2SO4 on clays between pH 5.0 and-3.0. *Applied Geochemistry* **24**, 333-345, doi:10.1016/j.apgeochem.2008.10.011 (2009).

65 Shiraki, R. & Dunn, T. L. Experimental study on water-rock interactions during CO2 flooding in the Tensleep Formation, Wyoming, USA. *Applied Geochemistry* **15**, 265-279, doi:10.1016/s0883-2927(99)00048-7 (2000).

66 Shukla, R., Ranjith, P., Haque, A. & Choi, X. A review of studies on CO2 sequestration and caprock integrity. *Fuel* **89**, 2651-2664, doi:10.1016/j.fuel.2010.05.012 (2010).

67 Siirila, E. R., Navarre-Sitchler, A. K., Maxwell, R. M. & McCray, J. E. A quantitative methodology to assess the risks to human health from CO2 leakage into groundwater. *Advances in Water Resources* **36**, 146-164, doi:10.1016/j.advwatres.2010.11.005 (2012).

68 Sowder, A. G., Clark, S. B. & Fjeld, R. A. The effect of sample matrix quenching on the measurement of trace uranium concentrations in aqueous solutions using kinetic phosphorimetry. *Journal of Radioanalytical and Nuclear Chemistry* **234**, 257-260, doi:10.1007/bf02389781 (1998).

69 Spycher, N. & Pruess, K. A Phase-Partitioning Model for CO2-Brine Mixtures at Elevated Temperatures and Pressures: Application to CO2-Enhanced Geothermal Systems. *Transport in Porous Media* **82**, 173-196, doi:10.1007/s11242-009-9425-y (2010).

70 Sterpenich, J. *et al.* Experimental ageing of oolitic limestones under CO2 storage conditions Petrographical and chemical evidence. *Chemical Geology* **265**, 99-112, doi:10.1016/j.chemgeo.2009.04.011 (2009).

71 Steudel, A., Batenburg, L. F., Fischer, H. R., Weidler, P. G. & Emmerich, K. Alteration of non-swelling clay minerals and magadiite by acid activation. *Applied Clay Science* **44**, 95-104, doi:10.1016/j.clay.2009.02.001 (2009).

72 Steudel, A., Batenburg, L. F., Fischer, H. R., Weidler, P. G. & Emmerich, K. Alteration of swelling clay minerals by acid activation. *Applied Clay Science* **44**, 105-115, doi:10.1016/j.clay.2009.02.002 (2009).

73 Stucki, J. W. THE QUANTITATIVE ASSAY OF MINERALS FOR FE2+ AND FE3+ USING 1,10-PHENANTHROLINE .2. A PHOTOCHEMICAL METHOD. *Soil Science Society of America Journal* **45**, 638-641 (1981).

74 Stucki, J. W. A review of the effects of iron redox cycles on smectite properties. *Comptes Rendus Geoscience* **343**, 199-209, doi:10.1016/j.crte.2010.10.008 (2011).

75 Stucki, J. W. & Anderson, W. L. THE QUANTITATIVE ASSAY OF MINERALS FOR FE2+ AND FE3+ USING 1,10-PHENANTHROLINE .1. SOURCES OF VARIABILITY. *Soil Science Society of America Journal* **45**, 633-637 (1981).

76 Stucki, J. W. & Kostka, J. E. Microbial reduction of iron in smectite. *Comptes Rendus Geoscience* **338**, 468-475, doi:10.1016/j.crte.2006.04.010 (2006).

77 Todoli, J. L., Gras, L., Hernandis, V. & Mora, J. Elemental matrix effects in ICP-AES. *Journal of Analytical Atomic Spectrometry* **17**, 142-169, doi:10.1039/b009570m (2002).

78 Torrero, M. E., Baraj, E., DePablo, J., Gimenez, J. & Casas, I. Kinetics of corrosion and dissolution of uranium dioxide as a function of pH. *International Journal of Chemical Kinetics* **29**, 261-267, doi:10.1002/(sici)1097-4601(1997)29:4<261::aid-kin4>3.0.co;2-s (1997).

79 Walther, J. V. Essentials Of Geochemistry (Second Edition). (2009).

80 Wang, J. S., Ryan, D., Anthony, E. J. & Wigston, A. Effects of Impurities on Geological Storage of Carbon Dioxide. *Prepared for the IEA Greenhouse Gas R&D Programme* (2011).

81 Wang, S. & Jaffe, P. R. Dissolution of a mineral phase in potable aquifers due to CO2 releases from deep formations; effect of dissolution kinetics. *Energy Conversion and Management* **45**, 2833-2848, doi:10.1016/j.enconman.2004.01.002 (2004).

82 Wei, T. Y., Pan, Y. F., Lu, G. Q., Tong, Z. F. & Xiao, H. N. Activated Clay Prepared by Waste Acid Recycling: Technology and Mechanism. *Environmental Engineering Science* **27**, 531-535, doi:10.1089/ees.2009.0375 (2010).

83 Wigand, M., Carey, J. W., Schutta, H., Spangenberg, E. & Erzinger, J. Geochemical effects of CO2 sequestration in sandstones under simulated in situ conditions of deep saline aquifers. *Applied Geochemistry* **23**, 2735-2745, doi:10.1016/j.apgeochem.2008.06.006 (2008).

84 Wigand, M., Kaszuba, J. P., Carey, J. W. & Hollis, W. K. Geochemical effects of CO2 sequestration on fractured wellbore cement at the cement/caprock interface. *Chemical Geology* **265**, 122-133, doi:10.1016/j.chemgeo.2009.04.008 (2009).

85 Wilkin, R. T. & Digiulio, D. C. Geochemical Impacts to Groundwater from Geologic Carbon Sequestration: Controls on pH and Inorganic Carbon Concentrations from Reaction Path and Kinetic Modeling. *Environmental Science & Technology* **44**, 4821-4827, doi:10.1021/es100559j (2010).

86 Wolf, G. H., Chizmeshya, A. V. G., Diefenbacher, J. & McKelvy, M. J. In situ observation of CO2 sequestration reactions using a novel microreaction system. *Environmental Science & Technology* **38**, 932-936, doi:10.1021/es0346375 (2004).

87 Wu, T. *et al.* Isolation and Microbial Reduction of Fe(III) Phyllosilicates from Subsurface Sediments. *Environmental Science & Technology* **46**, 11618-11626, doi:10.1021/es302639n (2012).

88 Xu, T. F., Apps, J. A. & Pruess, K. Numerical simulation of CO2 disposal by mineral trapping in deep aquifers. *Applied Geochemistry* **19**, 917-936, doi:10.1016/j.apgeochem.2003.11.003 (2004).

89 Yang, J. J. *et al.* Effects of redox cycling of iron in nontronite on reduction of technetium. *Chemical Geology* **291**, 206-216, doi:10.1016/j.chemgeo.2011.10.013 (2012).

90 Zerai, B., Saylor, B. Z. & Matisoff, G. Computer simulation of CO2 trapped through mineral precipitation in the Rose Run Sandstone, Ohio. *Applied Geochemistry* **21**, 223-240, doi:10.1016/j.apgeochem.2005.11.002 (2006).

91 Zhang, G. X. *et al.* Microbial reduction of chlorite and uranium followed by air oxidation. *Chemical Geology* **283**, 242-250, doi:10.1016/j.chemgeo.2011.01.021 (2011).

92 Zhang, G. X. *et al.* Microbial reduction of iron(III)-rich nontronite and uranium(VI). *Geochimica Et Cosmochimica Acta* **73**, 3523-3538, doi:10.1016/j.gca.2009.03.030 (2009).

93 Zhang, J. *et al.* Microbial reduction of Fe(III) in illite-smectite minerals by methanogen Methanosarcina mazei. *Chemical Geology* **292**, 35-44, doi:10.1016/j.chemgeo.2011.11.003 (2012).

94 Zheng, L. G., Apps, J. A., Zhang, Y. Q., Xu, T. F. & Birkholzer, J. T. On mobilization of lead and arsenic in groundwater in response to CO2 leakage from deep geological storage. *Chemical Geology* **268**, 281-297, doi:10.1016/j.chemgeo.2009.09.007 (2009).

95 Zhou, P. & Gu, B. H. Extraction of oxidized and reduced forms of uranium from contaminated soils: Effects of carbonate concentration and pH. *Environmental Science & Technology* **39**, 4435-4440, doi:10.1021/es0483443 (2005).

96 Zysset, M. & Schindler, P. W. The proton promoted dissolution kinetics of K-montmorillonite. *Geochimica Et Cosmochimica Acta* **60**, 921-931, doi:10.1016/0016-7037(95)00451-3 (1996).

Appendix A – Tabulated data for Figures

Table A:1. Data corresponding to Figure 3.1

NCN	average concentration				NCN	standard error			
time (h)	Al (mg/L)	Fe (mg/L)	Mg (mg/L)	Si (mg/L)	time (h)	Al (mg/L)	Fe (mg/L)	Mg (mg/L)	Si (mg/L)
1.33	0.1164	0.0301	0.3648	2.1313	1.33	4.45E-03	0.0297	0.0615	0.0464
24	0.1305	0.0344	0.3363	1.8437	24	0.0192	0.0168	0.0174	0.0922
72	0.1675	0.0778	0.4151	2.352	72	0.0104	0.0282	7.88E-04	0.1608
144	0.1984	0.1781	0.4653	2.2301	144	0.053	0.1349	0.0486	0.3775
240	0.2079	0.0568	0.4574	2.7922	240	8.20E-03	0.0294	0.0174	0.4268
360	0.1922	6.13E-03	0.3783	1.5391	360	0.0231	4.08E-03	7.48E-03	0.0524
SCN	average concentration				SCN	standard error			
time (h)	Al (mg/L)	Fe (mg/L)	Mg (mg/L)	Si (mg/L)	time (h)	Al (mg/L)	Fe (mg/L)	Mg (mg/L)	Si (mg/L)
1.33	0.0559	0.5901	0.397	1.7998	1.33	0.0245	0.5108	2.59E-03	0.0509
24	0.1522	0.2174	0.4776	1.7623	24	0.0425	0.122	9.16E-03	0.027
72	0.1036	0.0576	0.5453	1.9944	72	0.0141	0.0568	0.0172	0.0157
144	0.1128	1.00E-03	0.5679	1.886	144	1.94E-03	0	0.0159	0.0386
240	0.1784	0.015	0.5728	1.9927	240	0.014	7.79E-03	9.07E-03	0.1387
360	0.1603	4.33E-04	0.5648	1.9732	360	0.0153	1.73E-03	0.0188	0.1046
CCN	average concentration				CCN	standard error			
time (h)	Al (mg/L)	Fe (mg/L)	Mg (mg/L)	Si (mg/L)	time (h)	Al (mg/L)	Fe (mg/L)	Mg (mg/L)	Si (mg/L)
1.33	0.1413	1.00E-03	0.786	1.1311	1.33	0.0156	0	0.0356	0.155
24	0.5277	7.00E-04	1.3147	1.4471	24	0.0375	1.77E-03	0.0105	0.3153
72	0.9986	0.0182	1.9913	1.6713	72	0.0719	0.0173	0.1146	0.282
144	1.5272	0.0596	2.9193	2.0631	144	0.0643	0.0178	0.0907	0.1037
240	1.853	0.0557	3.5176	1.7173	240	0.0916	5.13E-03	0.1836	0.1809
360	2.0224	0.0533	3.8381	3.1766	360	0.0155	2.95E-03	4.20E-03	0.8822

Table A:2. Data corresponding to Figure 3.2

NNN	average concentration				NNN	standard error			
time (h)	Al (mg/L)	Fe (mg/L)	Mg (mg/L)	Si (mg/L)	time (h)	Al (mg/L)	Fe (mg/L)	Mg (mg/L)	Si (mg/L)
1.33	0.0669	1.00E-03	0.3038	1.5776	1.33	0.0618	0	8.37E-03	0.0567
24	5.53E-03	3.03E-03	0.3103	1.9465	24	4.53E-03	2.03E-03	2.31E-03	0.0991
72	2.53E-03	1.00E-03	0.327	2.0343	72	1.53E-03	0	7.25E-03	0.0276
144	3.67E-03	0.056	0.3116	2.4932	144	3.66E-03	0.055	0.0119	0.3102
240	0.0351	3.20E-03	0.3336	2.566	240	7.76E-03	2.20E-03	0.0136	0.3193
360	0.0616	0.1383	0.3543	3.2119	360	0.0316	0.1263	0.0198	0.5186
SNN	average concentration				SNN	standard error			
time (h)	Al (mg/L)	Fe (mg/L)	Mg (mg/L)	Si (mg/L)	time (h)	Al (mg/L)	Fe (mg/L)	Mg (mg/L)	Si (mg/L)
1.33	0.0108	0.0483	0.3041	0.9843	1.33	0.0106	0.0473	6.86E-03	0.0811
24	0.0306	0.1734	1.0683	1.5074	24	0.0155	0.1584	0.6924	0.2124
72	0.0365	1.00E-03	0.448	3.2591	72	0.0245	0	0.0168	0.3662
144	0.061	1.00E-03	0.4471	1.9318	144	0.0623	0	7.53E-03	0.2141
240	0.0214	1.00E-03	0.4615	2.2111	240	0.0204	0	0.0275	0.2071
360	0.0242	1.00E-03	0.4369	3.0996	360	0.0192	0	7.39E-03	0.3481
CNN	average concentration				CNN	standard error			
time (h)	Al (mg/L)	Fe (mg/L)	Mg (mg/L)	Si (mg/L)	time (h)	Al (mg/L)	Fe (mg/L)	Mg (mg/L)	Si (mg/L)
1.33	6.30E-03	1.00E-03	0.8506	1.152	1.33	6.23E-03	0	0.0111	0.1727
24	0.031	1.00E-03	0.8513	2.6139	24	3.84E-03	0	9.63E-03	0.5625
72	0.0964	1.00E-03	1.0047	2.8336	72	0.0954	0	0.0627	0.1605
144	8.93E-03	1.00E-03	0.9713	2.7199	144	7.93E-03	0	0.0194	0.3997
240	2.20E-03	1.00E-03	0.9192	2.961	240	1.89E-03	0	0.0588	0.2686
360	2.50E-03	1.00E-03	0.9864	3.558	360	1.50E-03	0	0.0668	0.0988

Table A:3. Data corresponding to Figure 3.3

NCN	average concentration				NCN	standard error			
time (h)	Al (mg/L)	Fe (mg/L)	Mg (mg/L)	Si (mg/L)	time (h)	Al (mg/L)	Fe (mg/L)	Mg (mg/L)	Si (mg/L)
1.33	0.1164	0.0301	0.3648	2.1313	1.33	4.45E-03	0.0297	0.0615	0.0464
24	0.1305	0.0344	0.3363	1.8437	24	0.0192	0.0168	0.0174	0.0922
72	0.1675	0.0778	0.4151	2.352	72	0.0104	0.0282	7.88E-04	0.1608
144	0.1984	0.1781	0.4653	2.2301	144	0.053	0.1349	0.0486	0.3775
240	0.2079	0.0568	0.4574	2.7922	240	8.20E-03	0.0294	0.0174	0.4268
360	0.1922	6.13E-03	0.3783	1.5391	360	0.0231	4.08E-03	7.48E-03	0.0524
NCC	average concentration				NCC	standard error			
time (h)	Al (mg/L)	Fe (mg/L)	Mg (mg/L)	Si (mg/L)	time (h)	Al (mg/L)	Fe (mg/L)	Mg (mg/L)	Si (mg/L)
1.33	0.5019	0.0391	1.5523	2.6557	1.33	0.131	0.0145	0.0991	0.3299
24	0.483	0.0623	1.7488	2.962	24	0.0197	4.81E-03	0.0227	0.199
72	0.6809	0.4066	1.46	3.1936	72	0.0205	0.2555	8.35E-03	0.4434
144	1.0113	0.719	1.7105	2.9386	144	0.4922	0.4423	0.0733	0.4977
240	0.471	0.1627	1.6168	2.9275	240	0.0238	0.0723	0.1016	0.7685
360	0.5227	0.059	1.497	1.7855	360	0.0443	0.0194	0.0226	0.415
NCS	average concentration				NCS	standard error			
time (h)	Al (mg/L)	Fe (mg/L)	Mg (mg/L)	Si (mg/L)	time (h)	Al (mg/L)	Fe (mg/L)	Mg (mg/L)	Si (mg/L)
1.33	0.072	4.37E-03	0.3964	1.2458	1.33	0.0257	3.37E-03	0.0166	0.183
24	0.131	0.1043	0.3963	1.6713	24	9.59E-03	0.0483	9.17E-03	0.1623
72	0.1255	0.0473	0.4427	1.6522	72	0.012	0.0131	0.0167	0.2293
144	0.131	0.152	0.5287	1.7678	144	0.0148	0.0862	0.0416	0.0772
240	0.1777	0.2101	0.5511	2.2475	240	9.03E-03	0.1271	0.0192	0.378
360	0.1856	0.0548	0.4726	2.3862	360	5.50E-03	3.30E-03	0.0121	0.2939

Table A:4. Data corresponding to Figure 3.4

NNN	average concentration				NNN	standard error			
time (h)	Al (mg/L)	Fe (mg/L)	Mg (mg/L)	Si (mg/L)	time (h)	Al (mg/L)	Fe (mg/L)	Mg (mg/L)	Si (mg/L)
1.33	0.0669	1.00E-03	0.3038	1.5776	1.33	0.0618	0	8.37E-03	0.0567
24	5.53E-03	3.03E-03	0.3103	1.9465	24	4.53E-03	2.03E-03	2.31E-03	0.0991
72	2.53E-03	1.00E-03	0.327	2.0343	72	1.53E-03	0	7.25E-03	0.0276
144	3.67E-03	0.056	0.3116	2.4932	144	3.66E-03	0.055	0.0119	0.3102
240	0.0351	3.20E-03	0.3336	2.566	240	7.76E-03	2.20E-03	0.0136	0.3193
360	0.0616	0.1383	0.3543	3.2119	360	0.0316	0.1263	0.0198	0.5186
NNC	average concentration				NNC	standard error			
time (h)	Al (mg/L)	Fe (mg/L)	Mg (mg/L)	Si (mg/L)	time (h)	Al (mg/L)	Fe (mg/L)	Mg (mg/L)	Si (mg/L)
1.33	0.3469	1.00E-03	1.3737	1.5269	1.33	0.0219	0	1.46E-02	0.1746
24	0.4566	1.00E-03	1.4032	1.6282	24	6.32E-03	0	0.0341	0.0482
72	0.4469	1.00E-03	1.4841	2.1735	72	0.0677	0	0.0722	0.1426
144	0.4458	1.57E-01	1.4566	2.6052	144	0.0194	0.1583	2.02E-02	0.1763
240	0.3705	1.00E-03	1.3645	2.3679	240	0.0365	0	0.0313	0.281
360	0.3986	1.93E-01	1.3644	2.8451	360	0.0436	0.1922	2.54E-02	0.1876
NNS	average concentration				NNS	standard error			
time (h)	Al (mg/L)	Fe (mg/L)	Mg (mg/L)	Si (mg/L)	time (h)	Al (mg/L)	Fe (mg/L)	Mg (mg/L)	Si (mg/L)
1.33	2.81E-02	2.17E-02	0.3648	1.5726	1.33	1.27E-02	0.0207	0.0225	0.0633
24	0.0132	1.00E-03	0.355	1.9612	24	1.28E-02	0	8.87E-03	0.0426
72	2.93E-03	5.60E-03	0.3543	2.1333	72	4.78E-03	6.92E-03	9.44E-03	0.1779
144	5.98E-01	2.03E-01	0.4164	2.3497	144	5.95E-01	0.1994	0.0374	0.1761
240	2.26E-02	1.00E-03	0.3873	2.8965	240	1.49E-02	0	4.51E-03	0.1205
360	2.34E-01	1.35E-01	0.3686	2.5477	360	2.04E-01	0.0846	0.0192	0.2534

Table A:5. Data corresponding to Figure 3.5

NNS	average concentration				NNS	standard error			
time (h)	Al (mg/L)	Fe (mg/L)	Mg (mg/L)	Si (mg/L)	time (h)	Al (mg/L)	Fe (mg/L)	Mg (mg/L)	Si (mg/L)
1.33	0.0281	0.0217	0.3648	1.5726	1.33	0.0127	0.0207	0.0225	0.0633
24	0.0132	1.00E-03	0.355	1.9612	24	0.0128	0	8.87E-03	0.0426
72	2.93E-03	5.60E-03	0.3543	2.1333	72	4.78E-03	6.92E-03	9.44E-03	0.1779
144	0.5979	0.203	0.4164	2.3497	144	0.5951	0.1994	0.0374	0.1761
240	0.0226	1.00E-03	0.3873	2.8965	240	0.0149	0	4.51E-03	0.1205
360	0.2344	0.1348	0.3686	2.5477	360	0.2035	0.0846	0.0192	0.2534
NCS	average concentration				NCS	standard error			
time (h)	Al (mg/L)	Fe (mg/L)	Mg (mg/L)	Si (mg/L)	time (h)	Al (mg/L)	Fe (mg/L)	Mg (mg/L)	Si (mg/L)
1.33	0.072	4.37E-03	0.3964	1.2458	1.33	0.0257	3.37E-03	0.0166	0.183
24	0.131	0.1043	0.3963	1.6713	24	9.59E-03	0.0483	9.17E-03	0.1623
72	0.1255	0.0473	0.4427	1.6522	72	0.012	0.0131	0.0167	0.2293
144	0.131	0.152	0.5287	1.7678	144	0.0148	0.0862	0.0416	0.0772
240	0.1777	0.2101	0.5511	2.2475	240	9.03E-03	0.1271	0.0192	0.378
360	0.1856	0.0548	0.4726	2.3862	360	5.50E-03	3.30E-03	0.0121	0.2939

Table A:5. Data corresponding to Figure 3.5 (continued)

RNS	average concentration				RNS	standard error			
time (h)	Al (mg/L)	Fe (mg/L)	Mg (mg/L)	Si (mg/L)	time (h)	Al (mg/L)	Fe (mg/L)	Mg (mg/L)	Si (mg/L)
1.33	9.80E-03	0.99	2.3069	2.9729	1.33	0.0118	0.0187	0.0137	0.0685
24	0.0148	1.0809	2.4533	3.9512	24	0.0138	0.033	0.0283	0.1697
72	0.0146	1.1185	2.4221	4.7085	72	0.0136	0.0865	0.0289	0.1283
144	1.00E-03	1.3647	2.5216	4.8814	144	0	0.2551	0.0408	0.2836
240	0.0138	2.4958	2.9021	4.6383	240	8.10E-03	0.9051	0.1622	0.2551
360	7.40E-03	4.354	2.9802	6.4405	360	6.40E-03	1.3074	0.1841	0.532
RCS	average concentration				RCS	standard error			
time (h)	Al (mg/L)	Fe (mg/L)	Mg (mg/L)	Si (mg/L)	time (h)	Al (mg/L)	Fe (mg/L)	Mg (mg/L)	Si (mg/L)
1.33	0.0927	12.1244	3.4823	3.5112	1.33	0.0171	0.1155	0.0281	0.1663
24	0.1468	24.9264	5.0421	5.1977	24	0.0124	0.1122	0.035	0.2296
72	0.1829	31.3126	5.6318	7.2634	72	2.40E-03	0.0698	8.25E-03	0.0266
144	0.152	35.8772	6.0575	9.7674	144	0.0181	0.1515	0.0292	0.1247
240	0.1824	40.6906	6.6482	13.3878	240	0.0555	1.3777	0.3196	0.3543
360	0.1383	42.7809	6.6087	16.6159	360	0.0144	1.4973	0.2328	0.4423

Table A:6. Data corresponding to Figure 3.7

0NS	average concentration				0NS	standard error			
time (h)	Al (mg/L)	Fe (mg/L)	Mg (mg/L)	Si (mg/L)	time (h)	Al (mg/L)	Fe (mg/L)	Mg (mg/L)	Si (mg/L)
1.33	0.0227	4.53E-03	0.2084	0.9448	1.33	0.0217	3.53E-03	0.011	0.2592
24	5.57E-03	0.0133	0.3206	1.6137	24	4.57E-03	0.0123	0.0989	0.247
72	3.97E-03	1.00E-03	0.2892	2.2248	72	2.17E-03	0	0.073	0.317
0CS	average concentration				0CS	standard error			
time (h)	Al (mg/L)	Fe (mg/L)	Mg (mg/L)	Si (mg/L)	time (h)	Al (mg/L)	Fe (mg/L)	Mg (mg/L)	Si (mg/L)
1.33	0.0743	1.00E-03	0.1721	1.7222	1.33	7.06E-04	0	0.0212	0.0594
24	0.0661	1.00E-03	0.2206	1.9102	24	7.67E-03	0	0.0366	0.3138
72	0.0525	1.00E-03	0.1977	1.9527	72	5.56E-03	0	0.0461	0.2795
0PS	average concentration				0PS	standard error			
time (h)	Al (mg/L)	Fe (mg/L)	Mg (mg/L)	Si (mg/L)	time (h)	Al (mg/L)	Fe (mg/L)	Mg (mg/L)	Si (mg/L)
1.33	0.0197	0.0478	0.1233	1.3354	1.33	5.63E-03	0.0136	0.0212	0.1487
24	0.0304	0.0834	0.1146	1.2207	24	0.0208	0.0134	0.0147	0.2801
72	0.0277	0.1308	0.1025	1.3105	72	8.34E-03	0.0191	8.69E-04	0.028
NNS	average concentration				NNS	standard error			
time (h)	Al (mg/L)	Fe (mg/L)	Mg (mg/L)	Si (mg/L)	time (h)	Al (mg/L)	Fe (mg/L)	Mg (mg/L)	Si (mg/L)
1.33	0.0281	0.0217	0.3648	1.5726	1.33	0.0127	0.0207	0.0225	0.0633
24	0.0132	1.00E-03	0.355	1.9612	24	0.0128	0	8.87E-03	0.0426
72	2.93E-03	5.60E-03	0.3543	2.1333	72	4.78E-03	6.92E-03	9.44E-03	0.1779
144	0.5979	0.203	0.4164	2.3497	144	0.5951	0.1994	0.0374	0.1761
240	0.0226	1.00E-03	0.3873	2.8965	240	0.0149	0	4.51E-03	0.1205
360	0.2344	0.1348	0.3686	2.5477	360	0.2035	0.0846	0.0192	0.2534

Table A:6. Data corresponding to Figure 3.7 (continued)

NCS	average concentration				NCS	standard error			
time (h)	Al (mg/L)	Fe (mg/L)	Mg (mg/L)	Si (mg/L)	time (h)	Al (mg/L)	Fe (mg/L)	Mg (mg/L)	Si (mg/L)
1.33	0.072	4.37E-03	0.3964	1.2458	1.33	0.0257	3.37E-03	0.0166	0.183
24	0.131	0.1043	0.3963	1.6713	24	9.59E-03	0.0483	9.17E-03	0.1623
72	0.1255	0.0473	0.4427	1.6522	72	0.012	0.0131	0.0167	0.2293
144	0.131	0.152	0.5287	1.7678	144	0.0148	0.0862	0.0416	0.0772
240	0.1777	0.2101	0.5511	2.2475	240	9.03E-03	0.1271	0.0192	0.378
360	0.1856	0.0548	0.4726	2.3862	360	5.50E-03	3.30E-03	0.0121	0.2939
NPS	average concentration				NPS	standard error			
time (h)	Al (mg/L)	Fe (mg/L)	Mg (mg/L)	Si (mg/L)	time (h)	Al (mg/L)	Fe (mg/L)	Mg (mg/L)	Si (mg/L)
0.5	0.4413	4.0096	0.6011	2.1072	0.5	0.0427	0.1144	0.0182	0.0693
1.1667	0.5768	5.1829	0.6599	2.7139	1.1667	0.0225	0.2923	0.0295	0.2205
1.33	0.5565	4.8695	0.5992	2.4578	1.33	0.0106	0.0539	4.31E-03	0.0682
2.3333	0.6694	5.8813	0.6688	3.2827	2.3333	5.60E-03	0.1064	9.90E-03	0.0306
3.3333	0.6917	6.342	0.6602	3.7231	3.3333	0.0346	0.0376	6.55E-03	0.0641
5.8333	0.8787	8.0076	0.7211	5.3823	5.8333	0.0143	0.4048	0.031	0.3669
24	1.5043	17.201	0.789	14.4169	24	0.0249	0.2343	7.25E-03	0.2227
72	2.2384	31.9046	0.851	30.4959	72	0.0393	0.383	6.81E-03	0.338

Table A:7. Data corresponding to Figure 3.8

0NS	average concentration				0NS	standard error			
time (h)	Al (mg/L)	Fe (mg/L)	Mg (mg/L)	Si (mg/L)	time (h)	Al (mg/L)	Fe (mg/L)	Mg (mg/L)	Si (mg/L)
1.33	0.0227	4.53E-03	0.2084	0.9448	1.33	0.0217	3.53E-03	0.011	0.2592
24	5.57E-03	0.0133	0.3206	1.6137	24	4.57E-03	0.0123	0.0989	0.247
72	3.97E-03	1.00E-03	0.2892	2.2248	72	2.17E-03	0	0.073	0.317
0CS	average concentration				0CS	standard error			
time (h)	Al (mg/L)	Fe (mg/L)	Mg (mg/L)	Si (mg/L)	time (h)	Al (mg/L)	Fe (mg/L)	Mg (mg/L)	Si (mg/L)
1.33	0.0743	1.00E-03	0.1721	1.7222	1.33	7.06E-04	0	0.0212	0.0594
24	0.0661	1.00E-03	0.2206	1.9102	24	7.67E-03	0	0.0366	0.3138
72	0.0525	1.00E-03	0.1977	1.9527	72	5.56E-03	0	0.0461	0.2795
0PS	average concentration				0PS	standard error			
time (h)	Al (mg/L)	Fe (mg/L)	Mg (mg/L)	Si (mg/L)	time (h)	Al (mg/L)	Fe (mg/L)	Mg (mg/L)	Si (mg/L)
1.33	0.0197	0.0478	0.1233	1.3354	1.33	5.63E-03	0.0136	0.0212	0.1487
24	0.0304	0.0834	0.1146	1.2207	24	0.0208	0.0134	0.0147	0.2801
72	0.0277	0.1308	0.1025	1.3105	72	8.34E-03	0.0191	8.69E-04	0.028
RNS	average concentration				RNS	standard error			
time (h)	Al (mg/L)	Fe (mg/L)	Mg (mg/L)	Si (mg/L)	time (h)	Al (mg/L)	Fe (mg/L)	Mg (mg/L)	Si (mg/L)
1.33	9.80E-03	0.99	2.3069	2.9729	1.33	0.0118	0.0187	0.0137	0.0685
24	0.0148	1.0809	2.4533	3.9512	24	0.0138	0.033	0.0283	0.1697
72	0.0146	1.1185	2.4221	4.7085	72	0.0136	0.0865	0.0289	0.1283
144	1.00E-03	1.3647	2.5216	4.8814	144	0	0.2551	0.0408	0.2836
240	0.0138	2.4958	2.9021	4.6383	240	8.10E-03	0.9051	0.1622	0.2551
360	7.40E-03	4.354	2.9802	6.4405	360	6.40E-03	1.3074	0.1841	0.532

Table A:7. Data corresponding to Figure 3.8continued

RCS	average concentration				RCS	standard error			
time (h)	Al (mg/L)	Fe (mg/L)	Mg (mg/L)	Si (mg/L)	time (h)	Al (mg/L)	Fe (mg/L)	Mg (mg/L)	Si (mg/L)
1.33	0.0927	12.1244	3.4823	3.5112	1.33	0.0171	0.1155	0.0281	0.1663
24	0.1468	24.9264	5.0421	5.1977	24	0.0124	0.1122	0.035	0.2296
72	0.1829	31.3126	5.6318	7.2634	72	2.40E-03	0.0698	8.25E-03	0.0266
144	0.152	35.8772	6.0575	9.7674	144	0.0181	0.1515	0.0292	0.1247
240	0.1824	40.6906	6.6482	13.3878	240	0.0555	1.3777	0.3196	0.3543
360	0.1383	42.7809	6.6087	16.6159	360	0.0144	1.4973	0.2328	0.4423
RPS	average concentration				RPS	standard error			
time (h)	Al (mg/L)	Fe (mg/L)	Mg (mg/L)	Si (mg/L)	time (h)	Al (mg/L)	Fe (mg/L)	Mg (mg/L)	Si (mg/L)
0.5	3.3232	68.153	7.0772	10.3003	0.5	0.0208	0.8299	0.0588	0.1209
1.1667	3.5063	76.7177	7.2944	13.0672	1.1667	0.1536	0.3963	0.1152	0.0481
1.33	3.7016	82.8873	7.615	14.7919	1.33	0.0773	1.2549	0.1033	0.4241
2.3333	3.9239	87.612	7.6597	17.8398	2.3333	0.0651	1.2486	0.1581	0.5308
3.3333	3.9733	89.5041	7.4813	20.8669	3.3333	0.0121	0.0138	8.00E-03	0.1192
5.8333	4.5281	107.5072	7.8935	28.8985	5.8333	0.0423	0.4623	0.0758	0.132
24	6.2026	154.6607	8.7823	49.006	24	0.1753	2.6137	0.223	1.0645
72	6.8082	160.9364	8.7964	48.952	72	0.1413	1.9057	0.0788	0.4533

Table A:8. Data corresponding to Figure 3.10

	Fe (mol/L) / Al (mol/L)					Fe (mol/L) / Si (mol/L)			
time (h)	NPS	RPS	time	theoretical	time (h)	NPS	RPS	time	theoretical
0.5	9.3971	20.5082	0.1	3.9904	0.5	5.1332	6.6166	0.1	0.5772
1.1667	9.2176	21.88	100	3.9904	1.1667	3.7251	5.871	100	0.5772
1.33	8.9823	22.3923			1.33	4.2959	5.6036		
2.3333	8.9788	22.3278			2.3333	2.9957	4.911		
3.3333	9.3664	22.5264			3.3333	2.6361	4.2893		
5.8333	9.2664	23.7422			5.8333	1.9669	3.7202		
24	11.6138	24.9348			24	1.2972	3.156		
72	14.3727	23.6386			72	1.0887	3.2876		
	Al (mol/L) / Si (mol/L)					Mg (mol/L) / Al (mol/L)			
time (h)	NPS	RPS	time	theoretical	time (h)	NPS	RPS	time	theoretical
0.5	0.5463	0.3226	0.1	0.1446	0.5	1.1333	2.1296	0.1	0.0962
1.1667	0.4041	0.2683	100	0.1446	1.1667	0.9632	2.0804	100	0.0962
1.33	0.4783	0.2502			1.33	0.8865	2.0572		
2.3333	0.3336	0.22			2.3333	0.8396	1.9521		
3.3333	0.2814	0.1904			3.3333	0.799	1.8829		
5.8333	0.2123	0.1567			5.8333	0.6959	1.7432		
24	0.1117	0.1266			24	0.4576	1.4159		
72	0.0757	0.1391			72	0.3386	1.292		

Table A:9. Data corresponding to Figure 3.11

NPS						
time (min)	Fe(II)/Fe in solid	standard error	dissolved Fe(II)/Fe	standard error	overall Fe(II)/Fe	standard error
10	0.0418	1.01E-03	0.1236	0	0.0573	0
25	0.0413	2.43E-03	0.1359	9.71E-03	0.0596	1.12E-04
50	0.0388	1.15E-03	0.0813	0	0.0492	0
75	0.0431	2.38E-03	0.1344	0.0186	0.0612	7.65E-03
120	0.0432	7.65E-04	0.0936	0.0149	0.0573	2.56E-03
180	0.0474	0	0.0913	7.92E-03	0.0603	1.20E-03
330	0.0452	1.52E-03	0.0788	0.0121	0.0562	1.92E-05
RPS						
time (min)	Fe(II)/Fe in solid	standard error	dissolved Fe(II)/Fe	standard error	overall Fe(II)/Fe	standard error
10	0.2984	1.47E-03	0.7926	0.0244	0.5283	5.06E-03
25	0.2571	1.54E-03	0.8066	5.74E-03	0.5382	6.03E-04
50	0.2411	1.19E-03	0.7991	2.93E-03	0.5634	8.13E-03
75	0.2106	1.63E-03	0.7886	8.05E-04	0.5639	2.63E-03
120	0.1995	4.85E-04	0.7533	0.0133	0.5686	0.0106
180	0.1943	3.16E-03	0.7421	7.03E-03	0.5726	6.41E-03
330	0.1872	3.93E-03	0.6385	9.63E-03	0.549	7.50E-03

Table A:10. Data corresponding to Figure 3.12

	average Fe(II)/Fe					standard error			
time (h)	UNNS	UNCS	URNS	URCS	time (h)	UNNS	UNCS	URNS	URCS
1.33	0.0618	0.0707	0.4942	0.5199	1.33	4.79E-03	1.05E-03	6.61E-03	6.08E-03
24	0.0691	0.1269	0.4982	0.5004	24	4.90E-03	1.84E-03	2.07E-03	2.54E-03
72	0.1	0.1439	0.4953	0.5008	72	0.017	4.36E-04	0.0113	3.59E-03
144	0.098	0.1548	0.4682	0.4955	144	6.17E-03	3.60E-03	7.90E-03	7.73E-03
240	0.0961	0.1776	0.4767	0.4432	240	3.24E-04	0	4.23E-03	0.0216
360	0.1048	0.1809	0.4775	0.4707	360	1.81E-03	2.71E-03	2.97E-03	0.0107
	average Fe(II)/Fe					standard error			
time (h)	NNS	NCS	RNS	RCS	time (h)	NNS	NCS	RNS	RCS
1.33	0.0285	0.0382	0.4663	0.4922	1.33	7.56E-04	9.91E-04	3.01E-03	2.58E-03
24	0.0379	0.0277	0.4678	0.4868	24	1.83E-03	2.18E-04	7.84E-03	5.52E-03
72	0.0274	0.0289	0.4666	0.4988	72	1.26E-03	1.70E-03	3.26E-03	0.0159
144	0.0396	0.0386	0.4643	0.4874	144	8.11E-04	6.12E-04	5.87E-03	9.91E-03
240	0.0384	0.0348	0.476	0.4763	240	9.19E-04	1.08E-03	4.11E-03	1.30E-03
360	0.0383	0.0294	0.4688	0.4672	360	1.28E-03	5.75E-04	4.03E-03	6.76E-03

Table A:10. Data corresponding to Figure 3.12 (continued)

	U(VI) average concentration (mmol/L)						standard error (mmol/L)					
	UNNS			UNCS			UNNS			UNCS		
time (h)	dissolved	acid-extracted	total	dissolved	acid-extracted	total	dissolved	acid-extracted	total	dissolved	acid-extracted	total
1.33	0.4213	9.86E-03	0.4312	0.4168	0.0129	0.4298	4.71E-03	2.23E-03	4.87E-03	2.33E-03	2.88E-03	1.19E-03
24	0.43	0.0118	0.4418	0.4178	0.0111	0.429	5.31E-04	1.29E-03	1.44E-03	1.97E-03	8.31E-04	2.63E-03
72	0.4129	8.59E-03	0.4215	0.4245	9.06E-03	0.4335	6.34E-04	5.21E-04	1.13E-04	5.60E-04	1.56E-04	4.03E-04
144	0.4262	8.75E-03	0.4349	0.4449	0.0138	0.4587	1.66E-03	1.22E-03	1.13E-05	8.99E-04	8.82E-04	5.13E-04
240	0.4354	0.0115	0.4468	0.4302	0.0166	0.4467	2.59E-03	1.32E-03	1.27E-03	1.33E-03	4.68E-03	6.01E-03
360	0.4207	0.0127	0.4334	0.4072	0.0156	0.4227	1.13E-03	5.12E-03	4.17E-03	3.19E-03	3.57E-03	2.62E-03
	U(VI) average concentration (mmol/L)						standard error (mmol/L)					
	URNS			URCS			URNS			URCS		
time (h)	dissolved	acid-extracted	total	dissolved	acid-extracted	total	dissolved	acid-extracted	total	dissolved	acid-extracted	total
1.33	0.4198	0.0212	0.441	0.4118	0.0317	0.4435	2.37E-03	6.93E-04	2.53E-03	3.10E-03	4.56E-03	7.51E-03
24	0.4295	0.0266	0.4561	0.4062	0.0278	0.4339	2.09E-03	1.04E-03	1.49E-03	6.72E-03	2.33E-03	0.016
72	0.4173	0.0241	0.4414	0.4158	0.0295	0.4452	7.06E-05	3.56E-03	3.63E-03	2.50E-03	2.81E-03	5.31E-03
144	0.4235	0.0239	0.4474	0.4317	0.0301	0.4618	3.22E-03	3.52E-03	5.85E-03	6.27E-03	7.97E-04	5.93E-03
240	0.431	0.0255	0.4565	0.4134	0.0229	0.4363	2.38E-03	5.26E-03	7.42E-03	5.83E-03	1.02E-03	4.81E-03
360	0.4171	0.0249	0.4421	0.3989	0.0325	0.4315	2.77E-03	1.30E-03	2.06E-03	4.42E-03	3.43E-03	7.81E-03

Table A:11. Data corresponding to Figure 3.13

	average Fe(II)/Fe								standard error							
	UNNS				UNCS				UNNS				UNCS			
time (h)	dissolved	acid-extracted	solid	overall	dissolved	acid-extracted	solid	overall	dissolved	acid-extracted	solid	overall	dissolved	acid-extracted	solid	overall
1.33	NA	0.4365	0.0439	0.0618	0.8514	0.5148	0.0455	0.0707	NA	8.27E-03	5.34E-03	4.79E-03	0.0243	0.0104	1.14E-03	1.05E-03
24	NA	0.5577	0.0464	0.0691	0.9199	0.7426	0.0736	0.1269	NA	4.02E-03	3.83E-03	4.90E-03	7.46E-03	5.17E-03	3.79E-03	1.84E-03
72	NA	0.5599	0.0761	0.1	0.8467	0.787	0.0787	0.1439	NA	8.16E-03	0.0179	0.017	0.0778	0.0167	1.34E-03	4.36E-04
144	NA	0.5931	0.0692	0.098	0.9211	0.8229	0.0771	0.1548	NA	0.0102	6.75E-03	6.17E-03	4.95E-03	0.0192	2.62E-03	3.60E-03
240	NA	0.5801	0.0639	0.0961	0.9229	0.9577	0.0796	0.1776	NA	0.0227	6.02E-04	3.24E-04	9.76E-04	0.0958	0	0
360	NA	0.6039	0.0702	0.1048	0.9117	0.7965	0.0852	0.1809	NA	0.0113	2.79E-03	1.81E-03	3.12E-03	0.0137	3.96E-03	2.71E-03
	average Fe(II)/Fe								standard error							
	URNS				URCS				URNS				URCS			
time (h)	dissolved	acid-extracted	solid	overall	dissolved	acid-extracted	solid	overall	dissolved	acid-extracted	solid	overall	dissolved	acid-extracted	solid	overall
1.33	NA	0.9186	0.2649	0.4942	0.953	0.9259	0.2569	0.5199	0.0662	6.41E-03	6.54E-03	6.61E-03	3.74E-03	7.05E-03	9.44E-03	6.08E-03
24	NA	0.895	0.245	0.4982	0.9531	0.9015	0.2542	0.5004	0.0251	0.0206	8.70E-03	2.07E-03	3.06E-03	9.42E-03	0.0109	2.54E-03
72	NA	0.9359	0.2697	0.4953	0.9556	0.8894	0.2512	0.5008	0.0303	0.0129	0.011	0.0113	4.17E-05	4.77E-03	4.46E-03	3.59E-03
144	NA	0.9096	0.2429	0.4682	0.9571	0.874	0.2601	0.4955	0.0946	0.0109	0.0116	7.90E-03	1.77E-03	7.51E-03	7.42E-04	7.73E-03
240	NA	0.9187	0.2464	0.4767	0.96	0.8961	0.2173	0.4432	0.0788	8.64E-03	8.66E-03	4.23E-03	2.20E-03	0.0312	0.0189	0.0216
360	NA	0.8755	0.2461	0.4775	0.9525	0.8625	0.2292	0.4707	0.0358	0.0249	0.0106	2.97E-03	3.08E-03	6.38E-03	3.45E-03	0.0107

Table A:12. Data corresponding to Figure 3.14

Fe concentration (mmol/L)	UNNS			UNCS		
time (h)	dissolved	acid-extracted	solid	dissolved	acid-extracted	solid
1.33	NA	0.1077	1.6766	NA	0.116	1.8746
24	NA	0.0765	1.679	NA	0.0858	1.9754
72	NA	0.09	1.8366	NA	0.0838	1.8559
144	NA	0.0806	1.7645	NA	0.0723	1.7598
240	NA	0.089	1.8887	NA	0.0869	2.0475
360	NA	0.0785	1.7786	NA	0.0879	1.9848
Fe concentration (mmol/L)	URNS			URCS		
time (h)	dissolved	acid-extracted	solid	dissolved	acid-extracted	solid
1.33	NA	1.0848	1.9777	0.1385	1.0567	1.8606
24	NA	1.1713	1.7868	0.2581	0.865	1.8899
72	NA	1.0369	2.0105	0.4162	0.765	1.9508
144	NA	0.9932	1.9508	0.5026	0.6213	2
240	NA	1.0723	2.0551	0.4956	0.4775	2.0826
360	NA	1.1755	2.0023	0.6072	0.5223	2.0644

Table A:13. Data corresponding to Figure 3.15

RCS	average concentration				RCS	standard error			
time (h)	Al (mg/L)	Fe (mg/L)	Mg (mg/L)	Si (mg/L)	time (h)	Al (mg/L)	Fe (mg/L)	Mg (mg/L)	Si (mg/L)
1.33	0.0927	12.1244	3.4823	3.5112	1.33	0.0171	0.1155	0.0281	0.1663
24	0.1468	24.9264	5.0421	5.1977	24	0.0124	0.1122	0.035	0.2296
72	0.1829	31.3126	5.6318	7.2634	72	2.40E-03	0.0698	8.25E-03	0.0266
144	0.152	35.8772	6.0575	9.7674	144	0.0181	0.1515	0.0292	0.1247
240	0.1824	40.6906	6.6482	13.3878	240	0.0555	1.3777	0.3196	0.3543
360	0.1383	42.7809	6.6087	16.6159	360	0.0144	1.4973	0.2328	0.4423
URCS	average concentration				URCS	standard error			
time (h)	Al (mg/L)	Fe (mg/L)	Mg (mg/L)	Si (mg/L)	time (h)	Al (mg/L)	Fe (mg/L)	Mg (mg/L)	Si (mg/L)
1.33	0.0161	6.8897	2.7902	6.8465	1.33	0.0108	0.0498	4.85E-03	0.1833
24	0.0197	12.763	3.4192	7.9012	24	0.012	0.3345	0.073	0.1536
72	9.48E-03	22.088	4.6182	11.2382	72	5.18E-03	0.3748	0.1058	0.1734
144	0.0137	23.4646	4.7047	12.3492	144	6.76E-03	1.5825	0.1783	1.0783
240	0.0123	26.3709	5.1032	14.9901	240	7.76E-03	1.5037	0.1447	0.3131
360	0.1226	31.0292	5.402	19.4435	360	0.1226	0.6299	0.042	0.219

Table A:14. Data corresponding to Figure 3.16

RNS	average concentration				RNS	standard error			
time	Al (mg/L)	Fe (mg/L)	Mg (mg/L)	Si (mg/L)	time	Al (mg/L)	Fe (mg/L)	Mg (mg/L)	Si (mg/L)
1.33	9.80E-03	0.99	2.3069	2.9729	1.33	0.0118	0.0187	0.0137	0.0685
24	0.0148	1.0809	2.4533	3.9512	24	0.0138	0.033	0.0283	0.1697
72	0.0146	1.1185	2.4221	4.7085	72	0.0136	0.0865	0.0289	0.1283
144	1.00E-03	1.3647	2.5216	4.8814	144	0	0.2551	0.0408	0.2836
240	0.0138	2.4958	2.9021	4.6383	240	8.10E-03	0.9051	0.1622	0.2551
360	7.40E-03	4.354	2.9802	6.4405	360	6.40E-03	1.3074	0.1841	0.532
URNS	average concentration				URNS	standard error			
time	Al (mg/L)	Fe (mg/L)	Mg (mg/L)	Si (mg/L)	time	Al (mg/L)	Fe (mg/L)	Mg (mg/L)	Si (mg/L)
1.33	2.37E-03	3.4856	2.8702	6.4752	1.33	1.37E-03	0.1228	0.1328	0.5496
24	0.038	2.6406	2.9059	6.9006	24	0.0204	0.082	0.1046	0.287
72	2.80E-03	0.8222	2.7117	6.584	72	3.14E-03	0.2796	0.0744	0.3997
144	0.0113	0.3084	2.6789	6.5652	144	5.17E-03	0.0695	0.0507	0.1584
240	0.0156	0.2311	2.7388	7.5215	240	0.011	0.0309	0.0839	0.409
360	0.0254	0.1464	2.6593	7.5738	360	0.0125	0.0202	1.23E-03	0.232

Table A:15. Data corresponding to Figure 3.17

U4NNS	Fe(II)/Fe				standard error			
time (h)	dissolved	acid-extracted	solid	overall	dissolved	acid-extracted	solid	overall
1.33	NA	0.4365	0.0439	0.0618	NA	8.27E-03	5.34E-03	4.79E-03
24	NA	0.5577	0.0464	0.0691	NA	4.02E-03	3.83E-03	4.90E-03
72	NA	0.5599	0.0761	0.1	NA	8.16E-03	0.0179	0.017
144	NA	0.5931	0.0692	0.098	NA	0.0102	6.75E-03	6.17E-03
240	NA	0.5801	0.0639	0.0961	NA	0.0227	6.02E-04	3.24E-04
360	NA	0.6039	0.0702	0.1048	NA	0.0113	2.79E-03	1.81E-03
U4NCS	Fe(II)/Fe				standard error			
time (h)	dissolved	acid-extracted	solid	overall	dissolved	acid-extracted	solid	overall
1.33	0.8514	0.5148	0.0455	0.0707	0.0243	0.0104	1.14E-03	1.05E-03
24	0.9199	0.7426	0.0736	0.1269	7.46E-03	5.17E-03	3.79E-03	1.84E-03
72	0.8467	0.787	0.0787	0.1439	0.0778	0.0167	1.34E-03	4.36E-04
144	0.9211	0.8229	0.0771	0.1548	4.95E-03	0.0192	2.62E-03	3.60E-03
240	0.9229	0.9577	0.0796	0.1776	9.76E-04	0.0958	0	0
360	0.9117	0.7965	0.0852	0.1809	3.12E-03	0.0137	3.96E-03	2.71E-03

Table A:16. Data corresponding to Figure 3.18

U4NNS	U (VI) average concentration (mmol/L)			standard error (mmol/L)		
time (h)	dissolved	acid-extracted	sum	dissolved	acid-extracted	sum
2	2.81E-03	0.2133	0.2161	3.18E-04	0.0166	0.0169
26	3.78E-03	0.2012	0.205	1.79E-04	9.86E-03	9.75E-03
72	5.16E-03	0.2244	0.2295	4.11E-04	0.0171	0.0175
144	7.18E-03	0.218	0.2251	4.29E-05	0.0114	0.0114
240	9.63E-03	0.2263	0.236	8.05E-04	0.0101	0.0109
360	0.0193	0.261	0.2803	2.70E-03	9.31E-03	0.012
U4NCS	U (VI) average concentration (mmol/L)			standard error (mmol/L)		
time (h)	dissolved	acid-extracted	sum	dissolved	acid-extracted	sum
2	0.0509	0.1916	0.2425	2.36E-03	0.0118	0.0114
26	0.1351	0.1342	0.2693	2.98E-03	6.35E-03	7.39E-03
72	0.169	0.109	0.278	2.47E-03	8.90E-03	0.0114
144	0.2166	0.1032	0.3198	5.15E-03	2.76E-04	5.43E-03
240	0.2456	0.0807	0.3263	4.75E-03	3.30E-03	1.45E-03
360	0.2835	0.0849	0.3684	5.65E-03	2.82E-03	5.88E-03
no clay control	U(VI) average concentration (mmol/L)			standard error (mmol/L)		
time (h)	N_2	CO_2		N_2	CO_2	
0	0.1399	0.1399		5.36E-03	5.36E-03	
168	0.1648	0.2106		0.0347	0.0512	
360	0.1966	0.2379		0.0419	0.0585	

Table A:17. Data corresponding to Figure 3.19

increase (mmol/L)	U4NNS		U4NCS	
time (h)	Fe(II)	U(VI)	Fe(II)	U(VI)
1.33	0.0608	0.0762	0.0803	0.1026
24	0.0768	0.0651	0.2031	0.1294
72	0.1443	0.0896	0.2402	0.1381
144	0.1399	0.0852	0.264	0.1799
240	0.1358	0.0961	0.3139	0.1864
360	0.1548	0.1404	0.3211	0.2285

Table A:18. Data corresponding to Figure 3.20

Fe (mmol/L)	U4NNS			U4NCS		
time (h)	dissolved	acid-extracted	solid	dissolved	acid-extracted	solid
2	NA	0.0994	2.0832	9.46E-03	0.1004	2.0586
26	NA	0.0963	2.0668	0.0346	0.1285	2.0023
72	NA	0.1072	2.0562	0.0647	0.1338	2.0105
144	NA	0.1197	2.058	0.0825	0.1338	1.9613
240	NA	0.1416	2.1178	0.101	0.1447	1.9859
360	NA	0.139	2.0047	0.1239	0.1567	1.9531

Table A:19. Data corresponding to Figure 3.21

NCS	average concentration				NCS	standard error			
time (h)	Al (mg/L)	Fe (mg/L)	Mg (mg/L)	Si (mg/L)	time (h)	Al (mg/L)	Fe (mg/L)	Mg (mg/L)	Si (mg/L)
1.33	0.072	4.37E-03	0.3964	1.2458	1.33	0.0257	3.37E-03	0.0166	0.183
24	0.131	0.1043	0.3963	1.6713	24	9.59E-03	0.0483	9.17E-03	0.1623
72	0.1255	0.0473	0.4427	1.6522	72	0.012	0.0131	0.0167	0.2293
144	0.131	0.152	0.5287	1.7678	144	0.0148	0.0862	0.0416	0.0772
240	0.1777	0.2101	0.5511	2.2475	240	9.03E-03	0.1271	0.0192	0.378
360	0.1856	0.0548	0.4726	2.3862	360	5.50E-03	3.30E-03	0.0121	0.2939
UNCS	average concentration				UNCS	standard error			
time (h)	Al (mg/L)	Fe (mg/L)	Mg (mg/L)	Si (mg/L)	time (h)	Al (mg/L)	Fe (mg/L)	Mg (mg/L)	Si (mg/L)
1.33	0.0188	1.00E-03	0.2674	1.4857	1.33	5.19E-03	0	3.78E-03	0.134
24	0.0531	1.00E-03	0.3944	1.8459	24	0.0154	0	9.49E-03	0.1283
72	0.0222	1.00E-03	0.3521	1.7846	72	0.0128	0	0.0168	0.1458
144	0.0126	1.00E-03	0.361	2.0193	144	5.86E-03	0	6.12E-03	0.0407
240	0.04	1.00E-03	0.3703	1.5865	240	0.0113	0	0.0114	0.2638
360	0.0134	1.00E-03	0.3562	1.9397	360	6.82E-03	0	0.0125	0.6336
U4NCS	average concentration				U4NCS	standard error			
time (h)	Al (mg/L)	Fe (mg/L)	Mg (mg/L)	Si (mg/L)	time (h)	Al (mg/L)	Fe (mg/L)	Mg (mg/L)	Si (mg/L)
2	0.0315	0.3012	0.3011	1.3442	2	0.0176	0.0296	0.0125	0.1149
26	0.0652	1.7653	0.3433	1.3795	26	0.0186	0.1008	0.0185	0.1112
72	0.0887	3.1329	0.3691	1.7347	72	4.13E-03	0.0846	0.0111	6.22E-03
144	0.1207	4.577	0.3925	2.2961	144	1.00E-04	0.386	0.0236	0.1071
240	0.0967	5.1975	0.3891	2.1944	240	0.018	0.1505	0.0141	0.3428
360	0.1017	6.8418	0.4456	2.8509	360	9.46E-03	0.6364	0.0326	0.526

Table A:20. Data corresponding to Figure 3.22

NNS	average concentration				NNS	standard error			
time (h)	Al (mg/L)	Fe (mg/L)	Mg (mg/L)	Si (mg/L)	time (h)	Al (mg/L)	Fe (mg/L)	Mg (mg/L)	Si (mg/L)
1.33	0.0281	0.0217	0.3648	1.5726	1.33	0.0127	0.0207	0.0225	0.0633
24	0.0132	1.00E-03	0.355	1.9612	24	0.0128	0	8.87E-03	0.0426
72	2.93E-03	5.60E-03	0.3543	2.1333	72	4.78E-03	6.92E-03	9.44E-03	0.1779
144	0.5979	0.203	0.4164	2.3497	144	0.5951	0.1994	0.0374	0.1761
240	0.0226	1.00E-03	0.3873	2.8965	240	0.0149	0	4.51E-03	0.1205
360	0.2344	0.1348	0.3686	2.5477	360	0.2035	0.0846	0.0192	0.2534
UNNS	average concentration				UNNS	standard error			
time (h)	Al (mg/L)	Fe (mg/L)	Mg (mg/L)	Si (mg/L)	time (h)	Al (mg/L)	Fe (mg/L)	Mg (mg/L)	Si (mg/L)
1.33	0.0105	1.00E-03	0.2958	1.3846	1.33	0.0114	0	5.54E-03	0.4205
24	6.60E-03	1.00E-03	0.3066	2.2333	24	5.60E-03	0	3.39E-03	0.2241
72	0.0617	0.0412	0.2962	3.6293	72	0.0434	0.0402	0.0153	0.6809
144	0.0968	1.00E-03	0.2688	4.3463	144	0.0189	0	0.0115	0.782
240	0.0344	1.00E-03	0.2659	4.173	240	0.0186	0	2.77E-03	0.255
360	0.0118	1.00E-03	0.261	4.1679	360	5.47E-03	0	0.0106	0.3005
U4NNS	average concentration				U4NNS	standard error			
time (h)	Al (mg/L)	Fe (mg/L)	Mg (mg/L)	Si (mg/L)	time (h)	Al (mg/L)	Fe (mg/L)	Mg (mg/L)	Si (mg/L)
2	1.00E-03	3.80E-03	0.2766	0.8624	2	0	2.80E-03	2.90E-03	0.1961
26	1.00E-03	0.0289	0.2886	1.0775	26	0	0.0192	7.94E-03	0.0601
72	1.00E-03	0.1749	0.3207	1.2702	72	0	0.0121	3.69E-04	0.0721
144	1.00E-03	0.1873	0.3326	1.8381	144	0	0.0246	9.20E-03	0.145
240	1.00E-03	0.185	0.3353	2.2359	240	0	7.00E-04	0.014	0.42
360	1.00E-03	0.2008	0.3383	2.049	360	0	0.0135	1.17E-03	0.3702

Table A:21. Data corresponding to Figure 3.23

U (mmol/L)	U4NNS		U4NCS	
time (h)	dissolved	acid-extracted	dissolved	acid-extracted
2	6.28E-04	0.2894	0.0505	0.2819
26	1.52E-03	0.3006	0.1276	0.1758
144	5.32E-03	0.3077	0.2249	0.1265
360	0.0191	0.337	0.3014	0.0985

Table A:22. Data corresponding to Figure 3.24

U4NCS	U(VI)/U		standard error	
time (h)	dissolved	acid-extracted	dissolved	acid-extracted
2	1.0104	0.6787	0.0579	0.0113
26	1.0586	0.7641	0.0212	0.0355
144	0.9631	0.8159	0.0197	3.97E-03
360	0.9404	0.8634	7.67E-03	0.031

Appendix B - SEM images of clay minerals

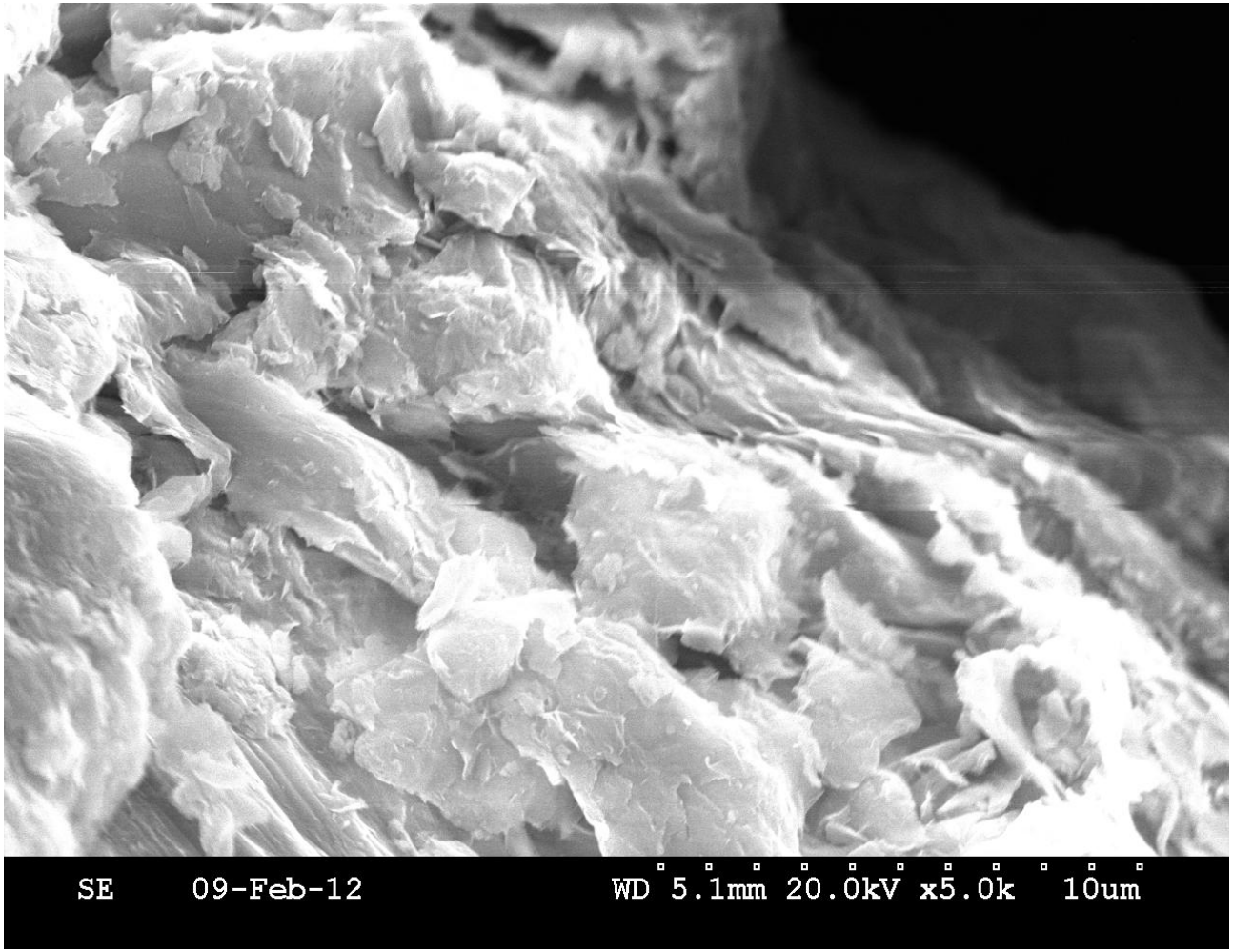

Figure B:1. SEM image of size-fractionated nontronite NAu-2

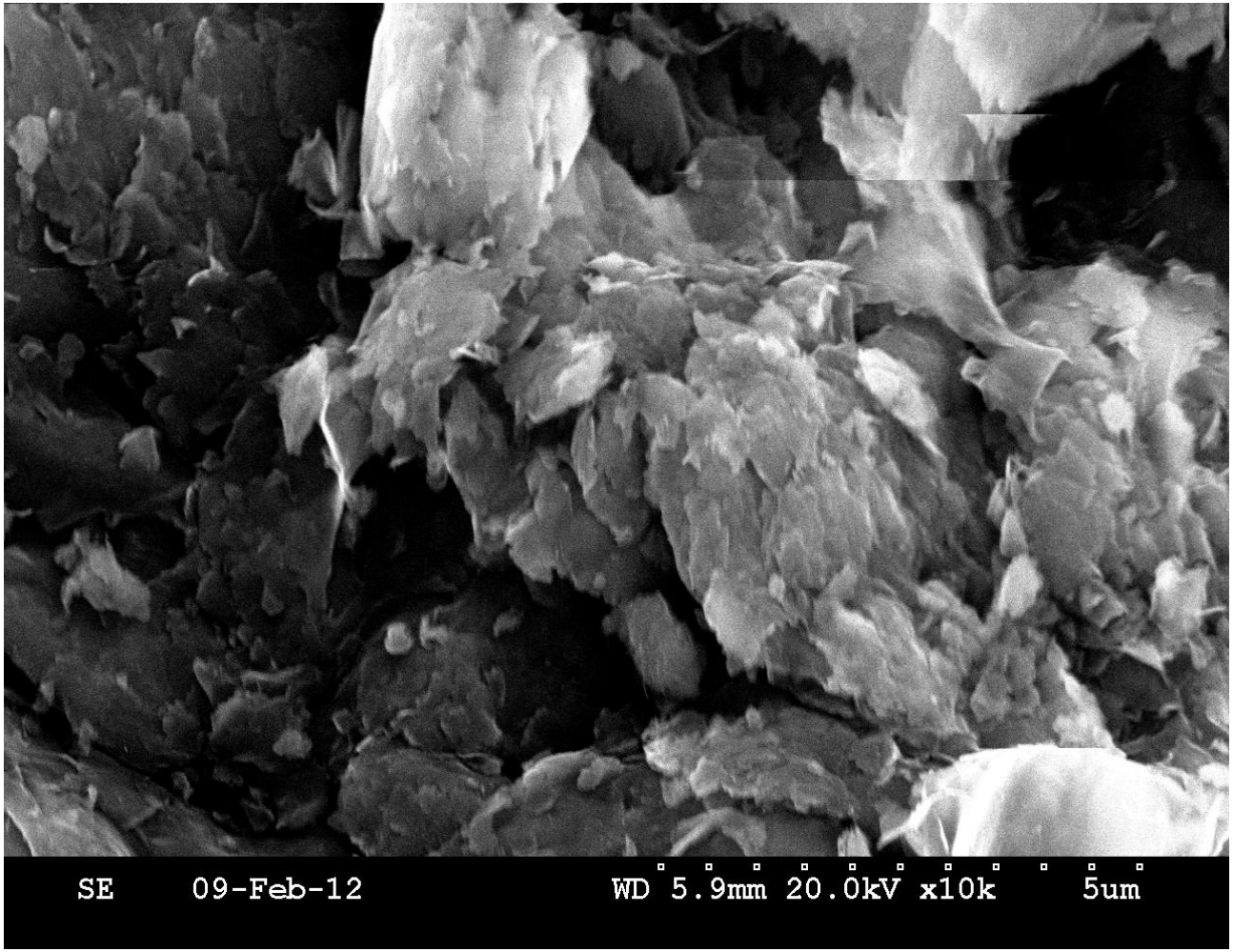

Figure B:2. SEM image of size-fractionated nontronite NAu-2

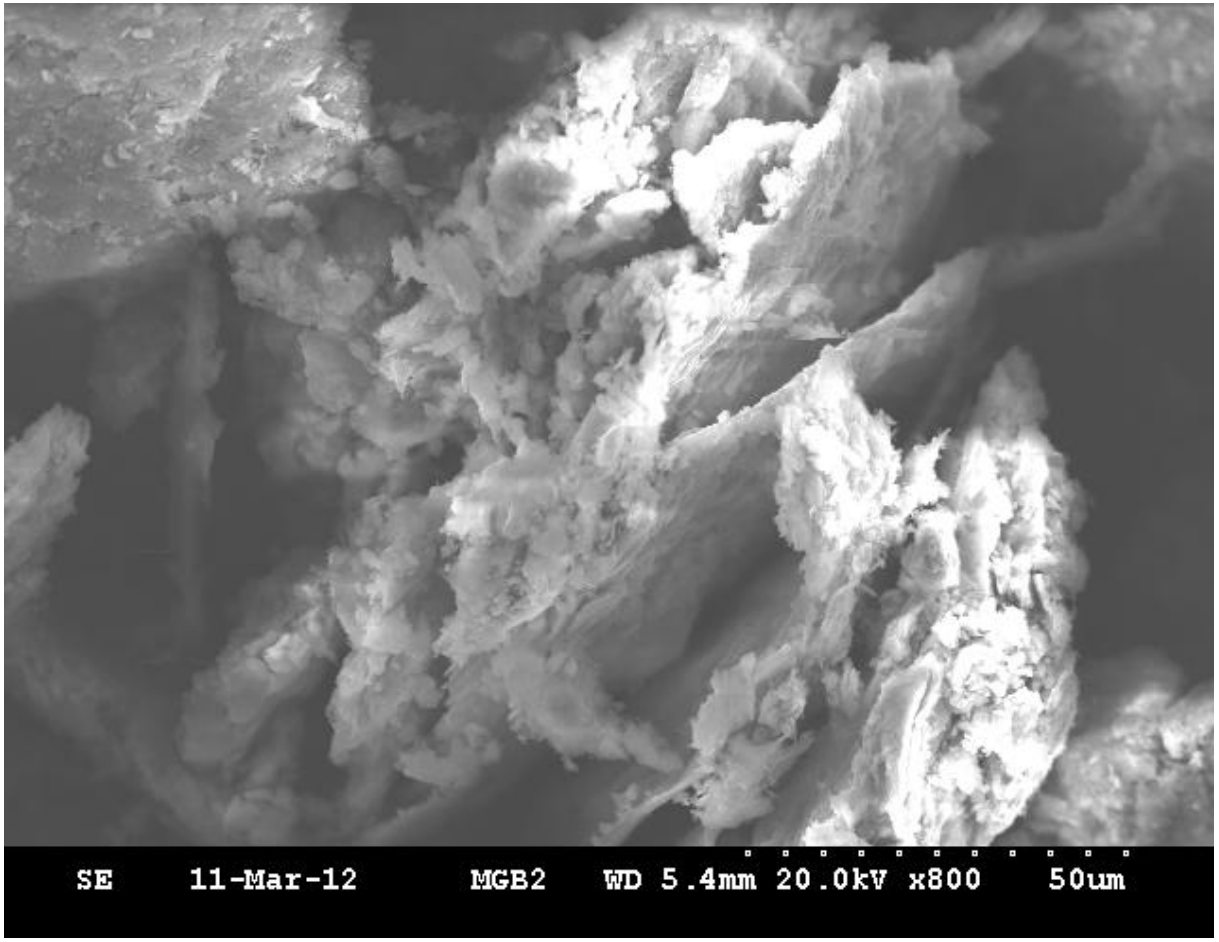

Figure B:3. SEM image of nontronite NAu-2, after reaction of 10 g/L NAu-2 in 2M NaCl under high pressure CO_2 conditions (P_T = 9.66 bar, $P_{CO2} \geq$ 8.66 bar CO_2). Clay mineral samples were washed, dried and grinded before SEM imaging.

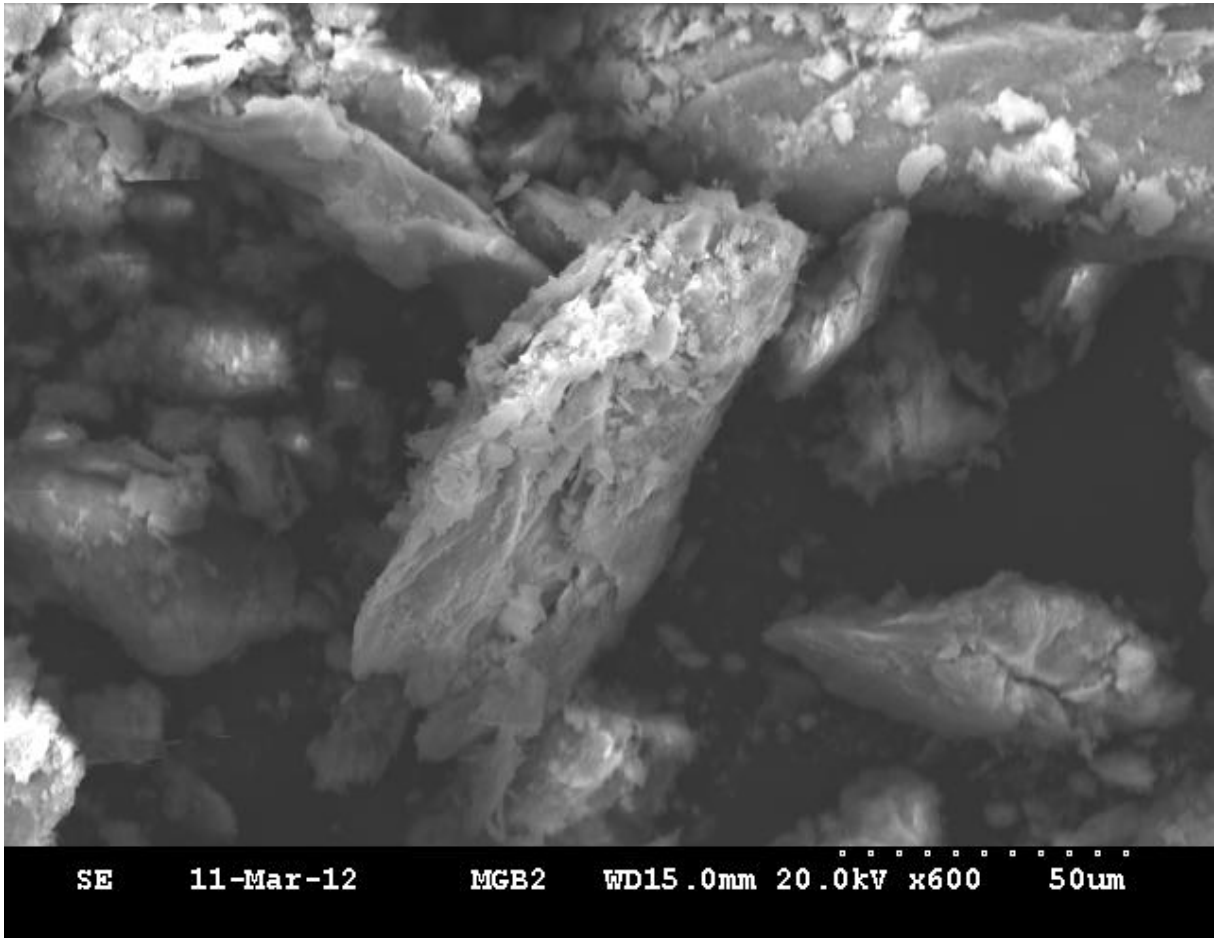

Figure B:4. SEM image of nontronite NAu-2, after reaction of 10 g/L NAu-2 in 2M NaCl under high pressure CO_2 conditions (P_T = 9.66 bar, $P_{CO2} \geq$ 8.66 bar CO_2). Clay mineral samples were washed, dried and grinded before SEM imaging.

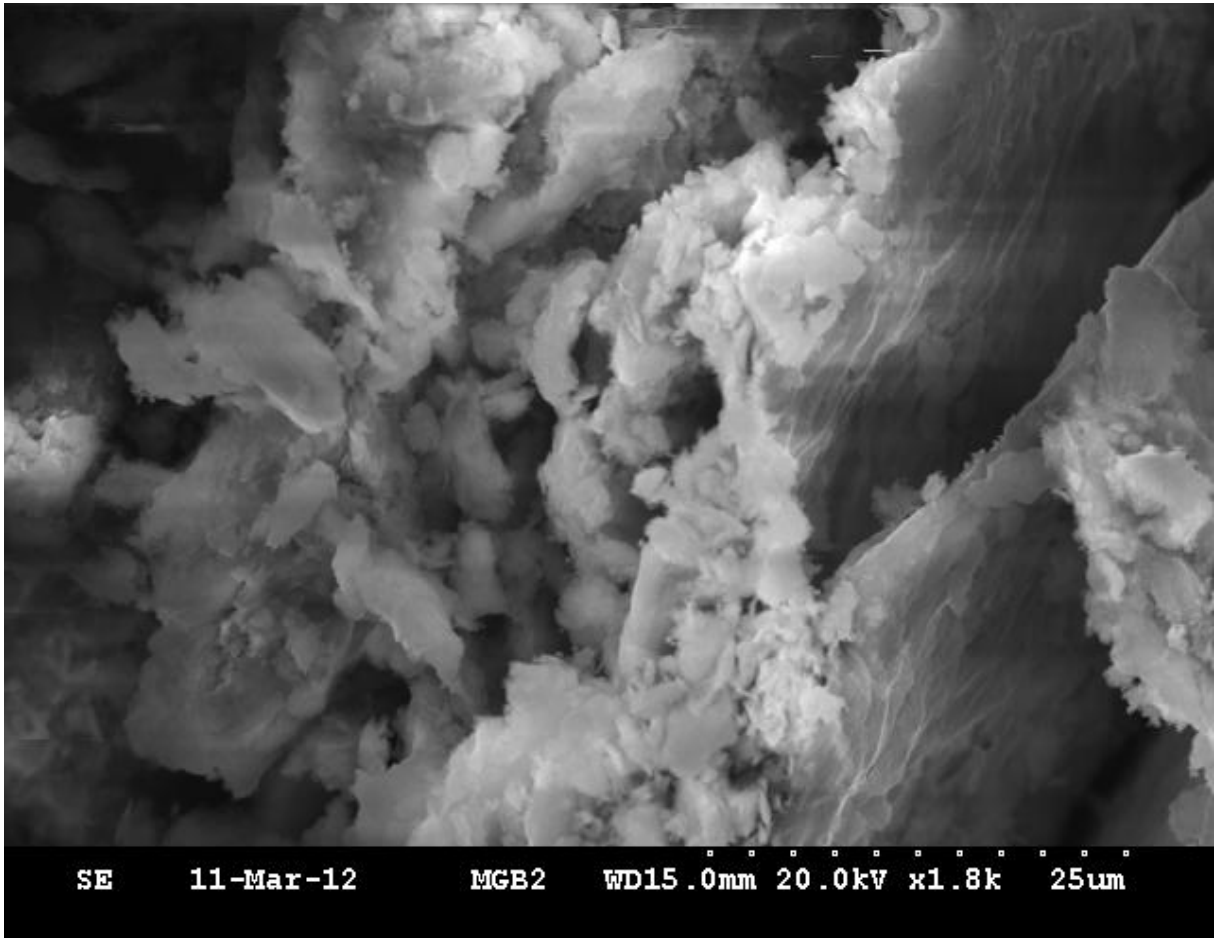

Figure B:5. SEM image of nontronite NAu-2, after reaction of 10 g/L NAu-2 in 2M NaCl under high pressure CO_2 conditions (P_T = 9.66 bar, $P_{CO2} \geq$ 8.66 bar CO_2). Clay mineral samples were washed, dried and grinded before SEM picturing.

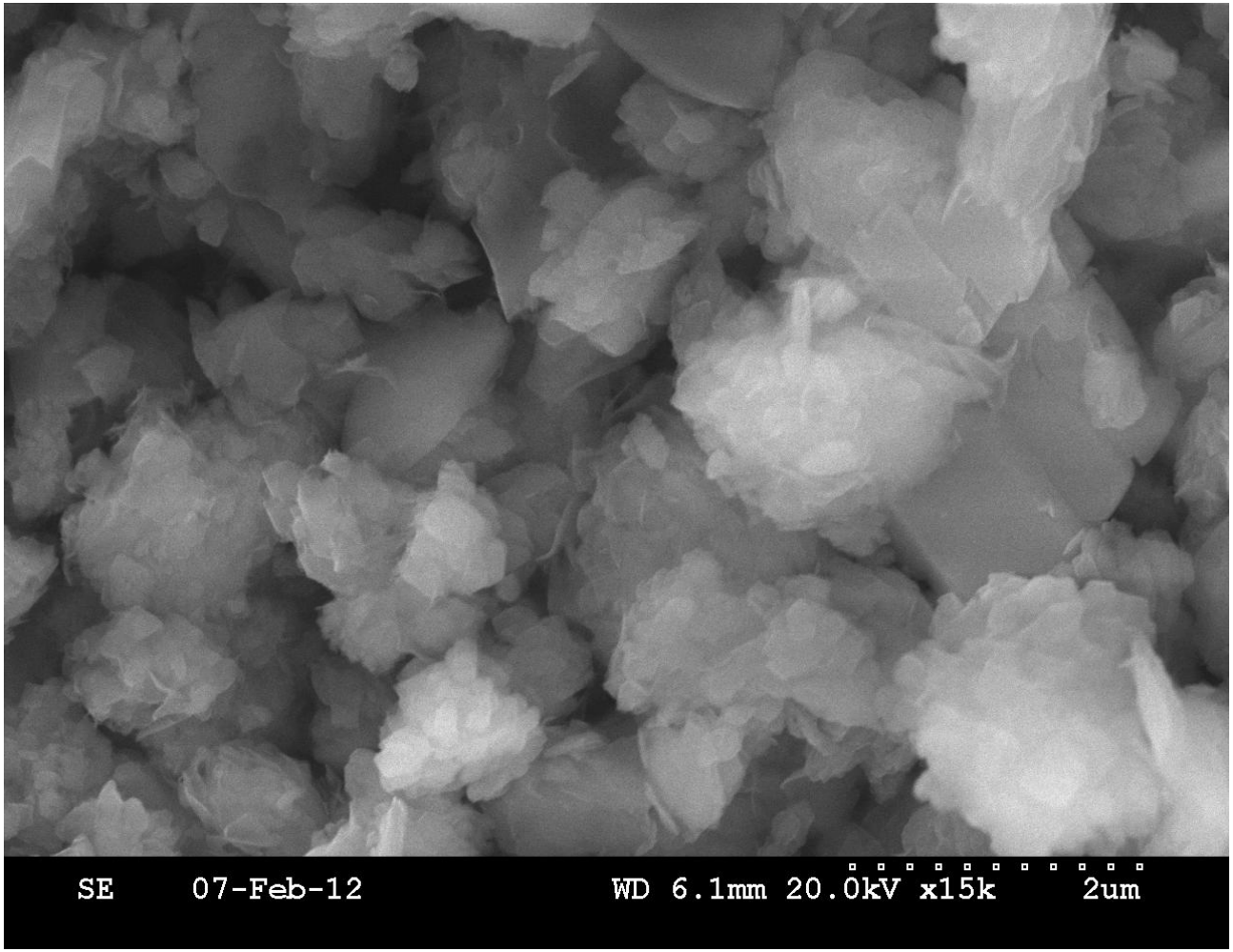

Figure B:6. SEM image of size-fractionated montmorillonite SWy-2

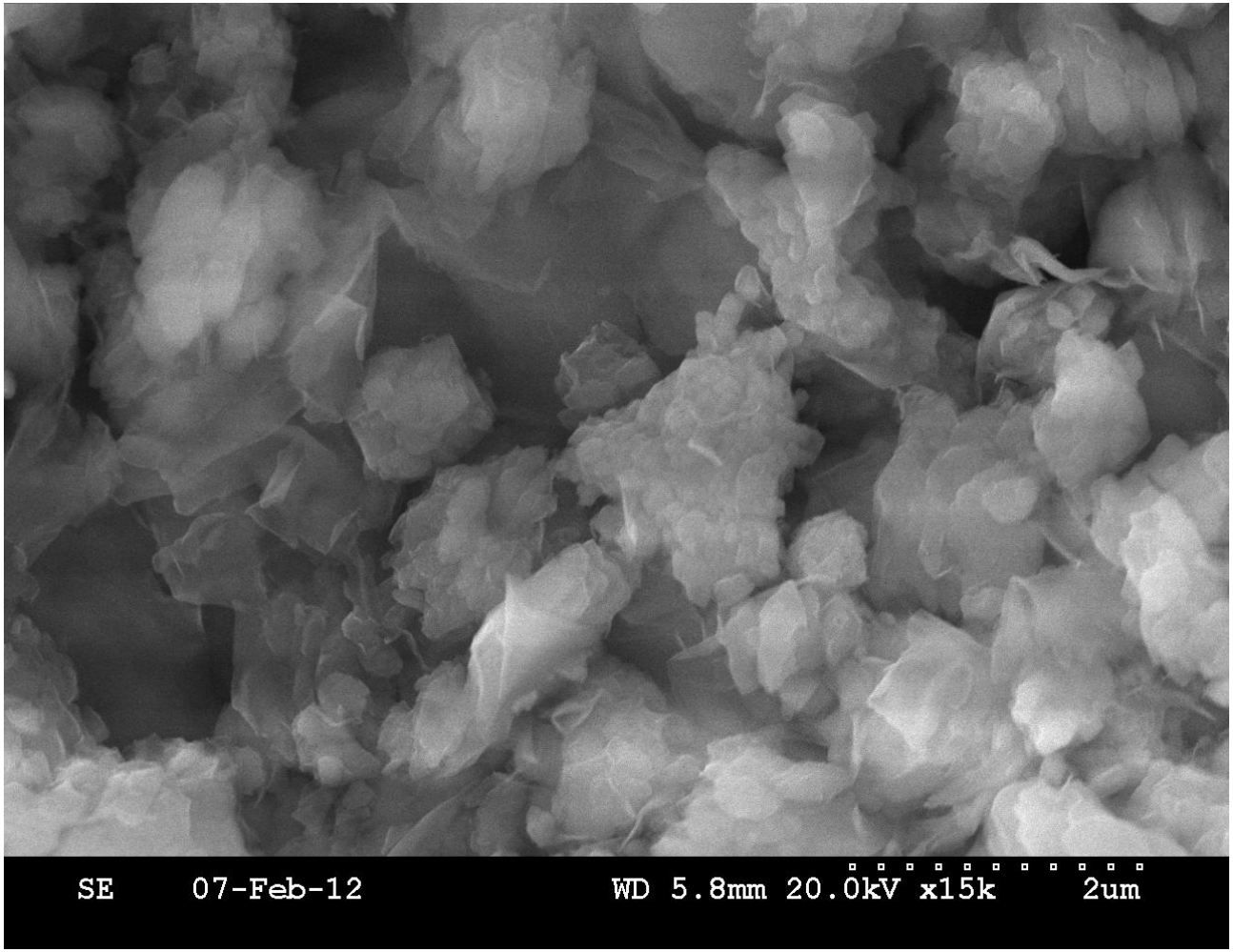

Figure B:7. SEM image of size-fractionated montmorillonite SWy-2

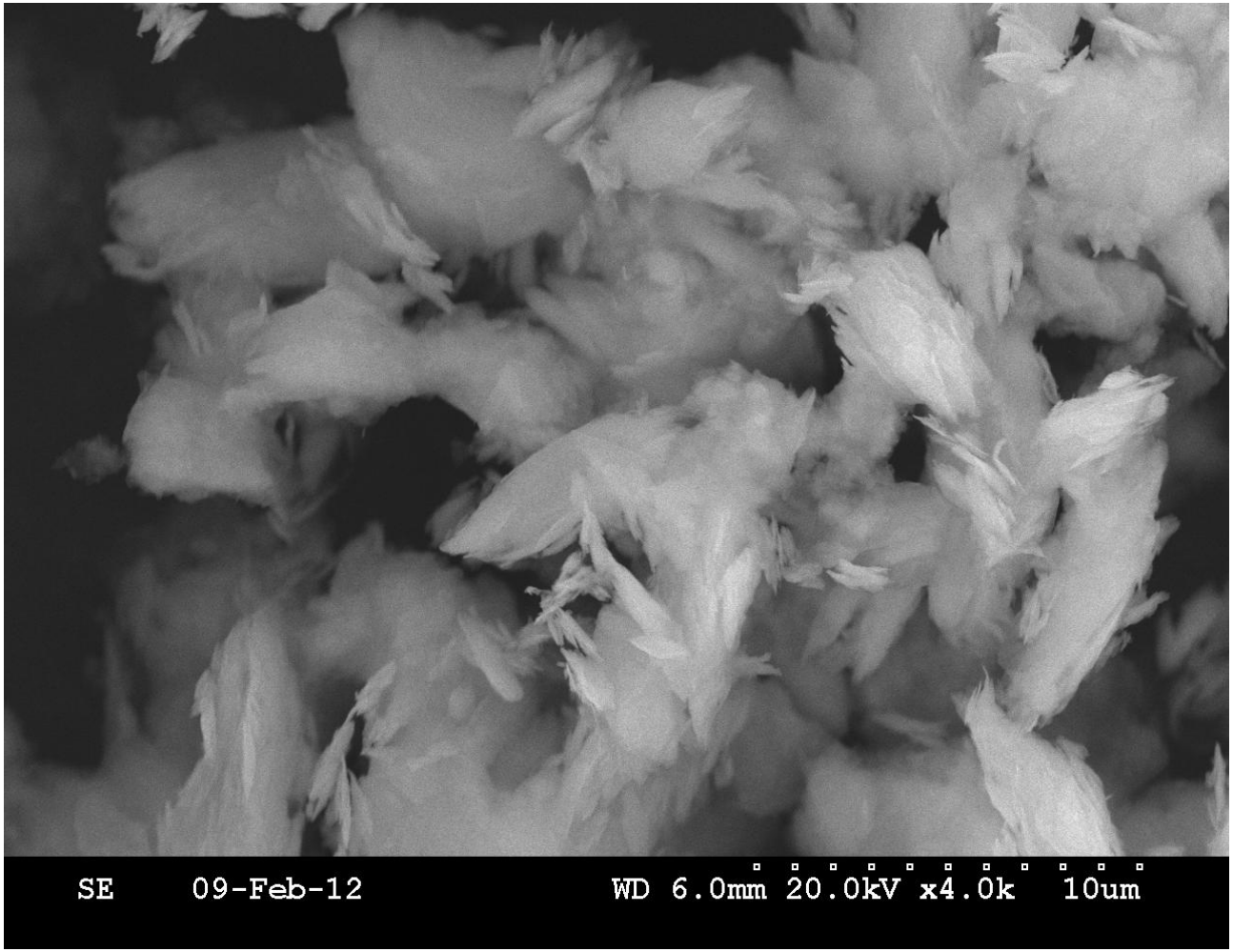

Figure B:8. SEM image of size-fractionated chlorite CCa-2

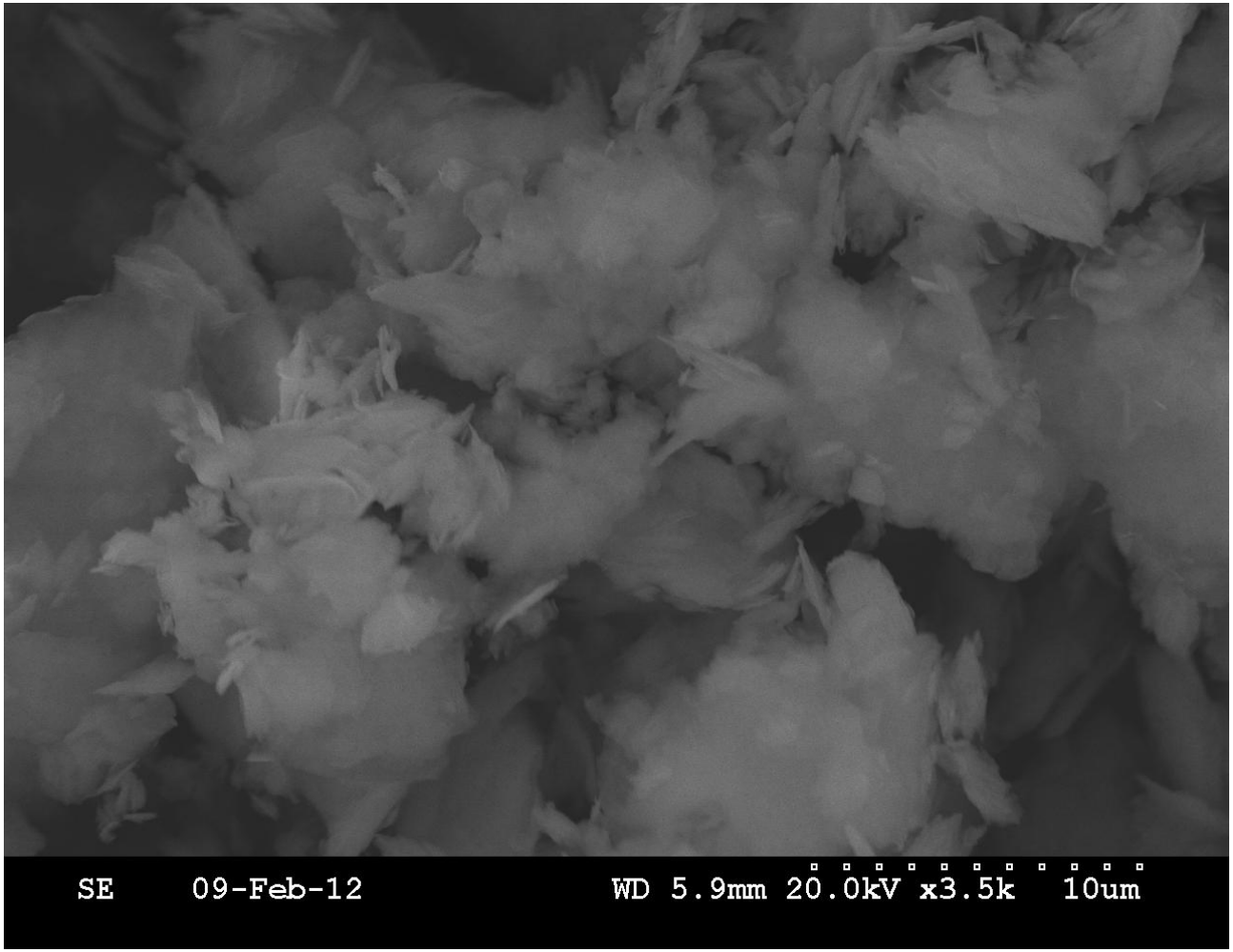

Figure B:9. SEM image of size-fractionated chlorite CCa-2

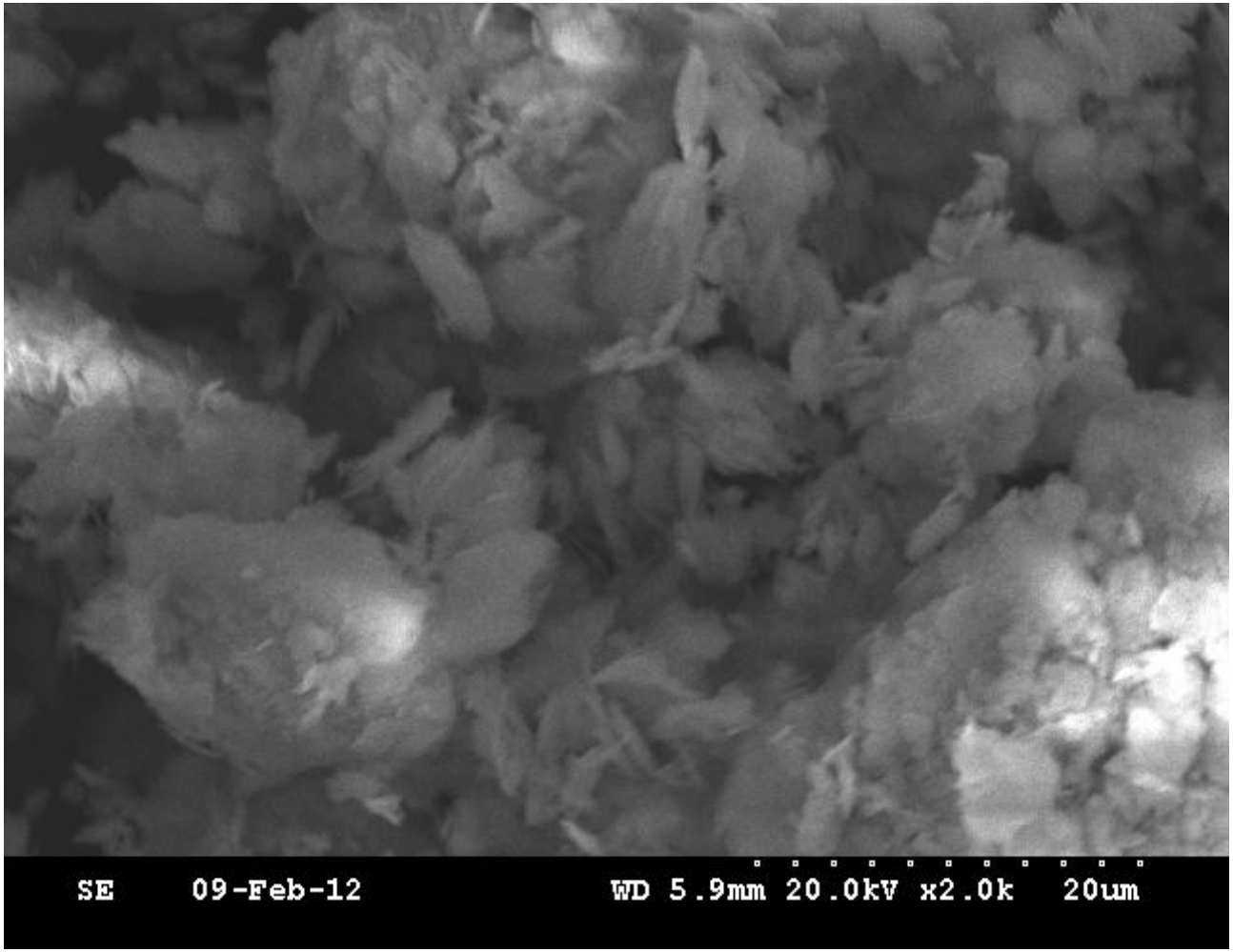

Figure B:10. SEM image of size-fractionated chlorite CCa-2

Appendix C - XRD patterns of clay minerals

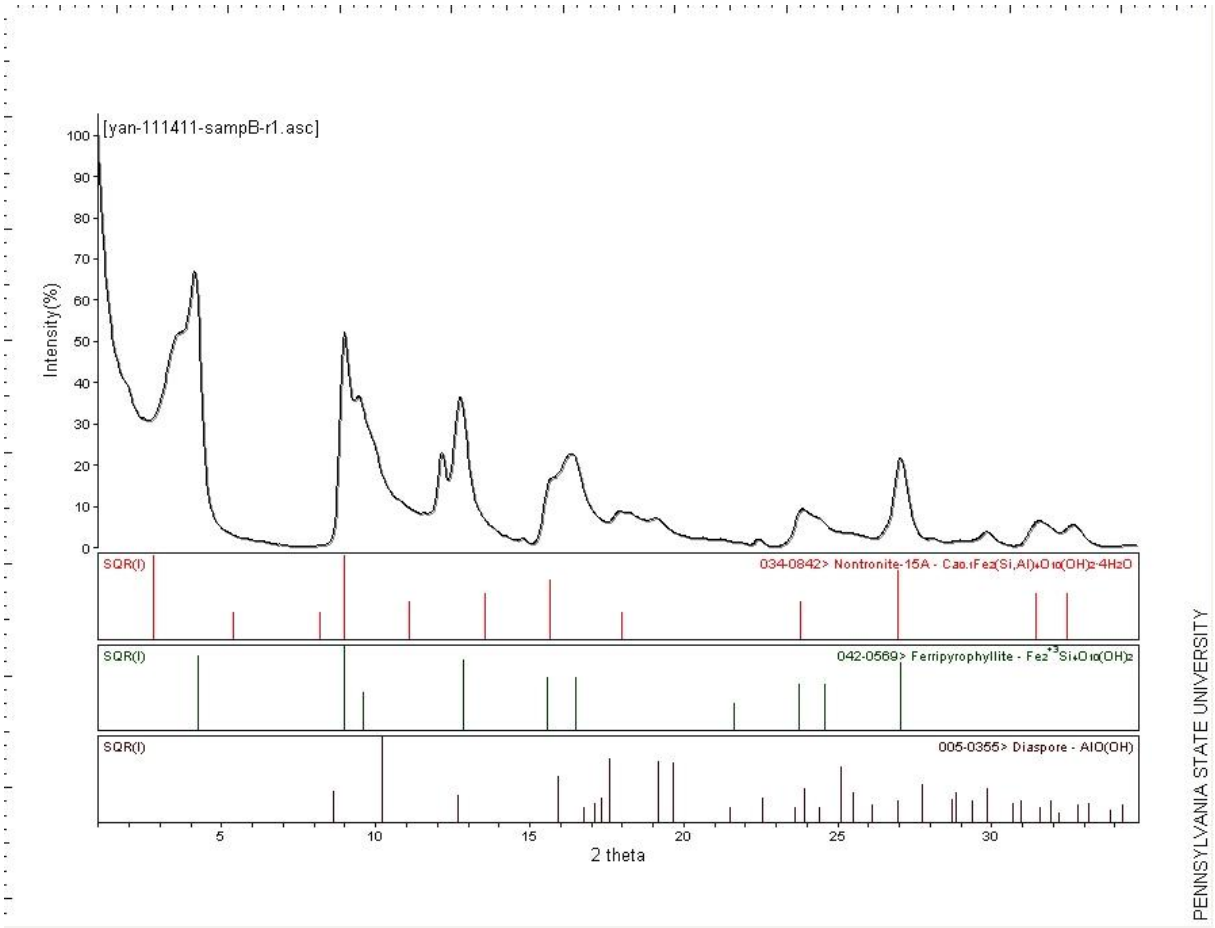

Figure C:1. XRD pattern of size-fractionated nontronite NAu-2

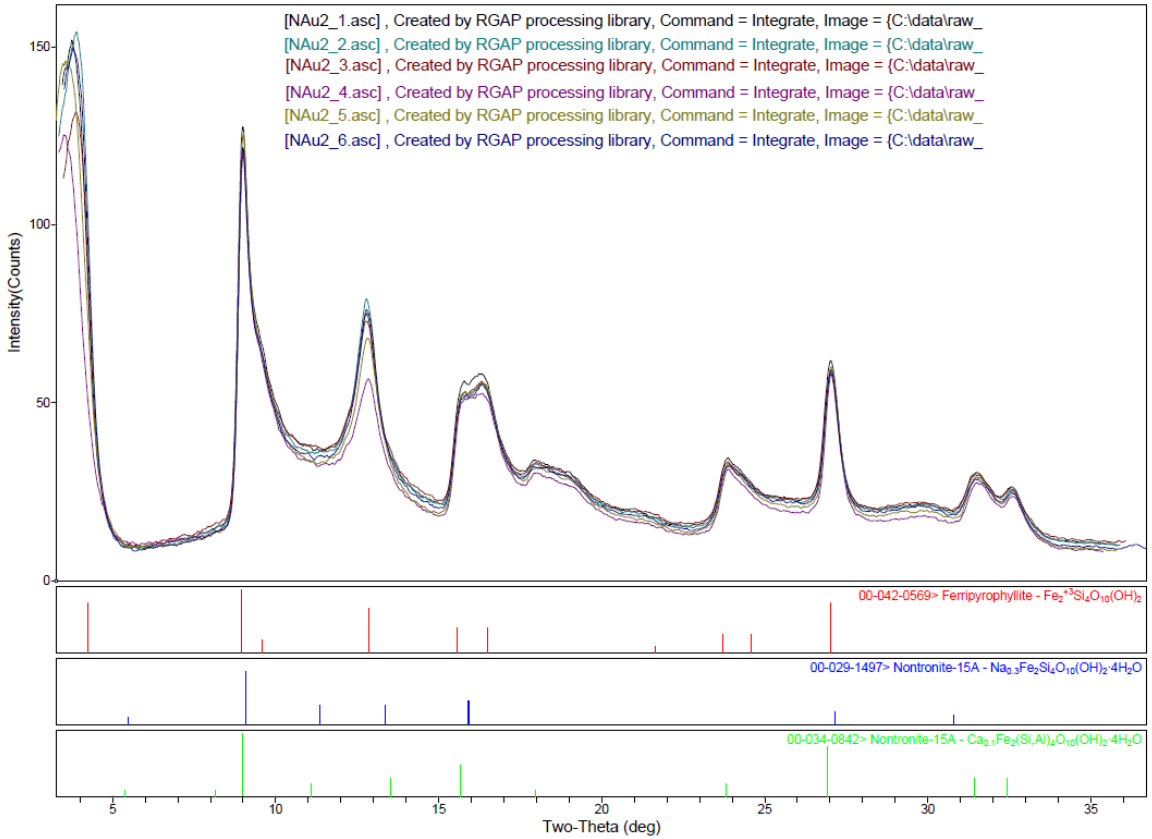

Figure C:2. XRD patterns of NAu-2. Experiments conducted with 10 g/L NAu-2 in 2 M NaCl. Clay mineral samples were washed, dried, grinded and sieved before XRD analysis.

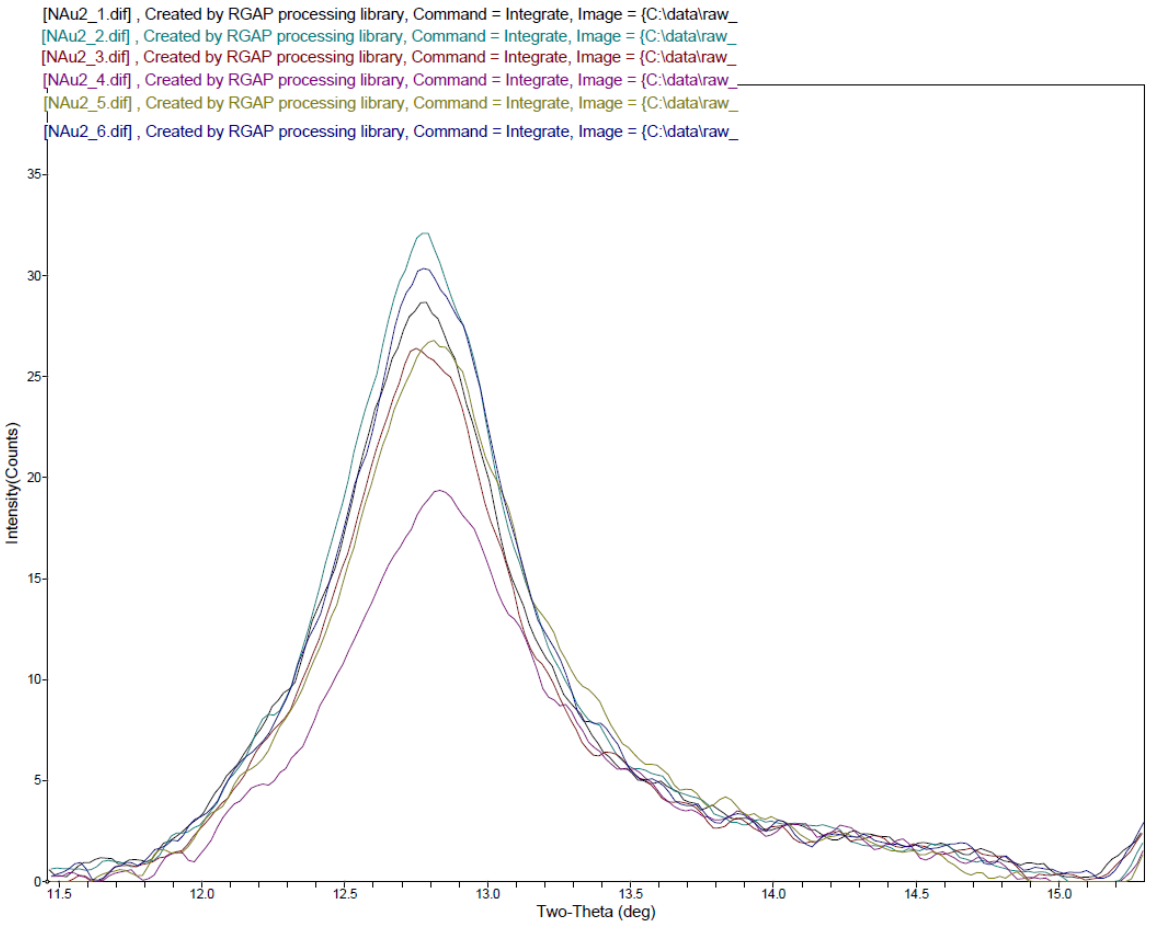

Figure C:3. Magnification of Figure C:2. Peaks at ~12.6 deg of Two Theta. From top to bottom: ambient for 15d, high pressure CO_2 for 6d, initial NAu-2, high pressure CO_2 for 3d, high pressure CO_2 for 15d, high pressure CO_2 for 1d. Experiments conducted with 10 g/L NAu-2 in 2 M NaCl. Clay mineral samples were washed, dried, grinded and sieved before XRD analysis.

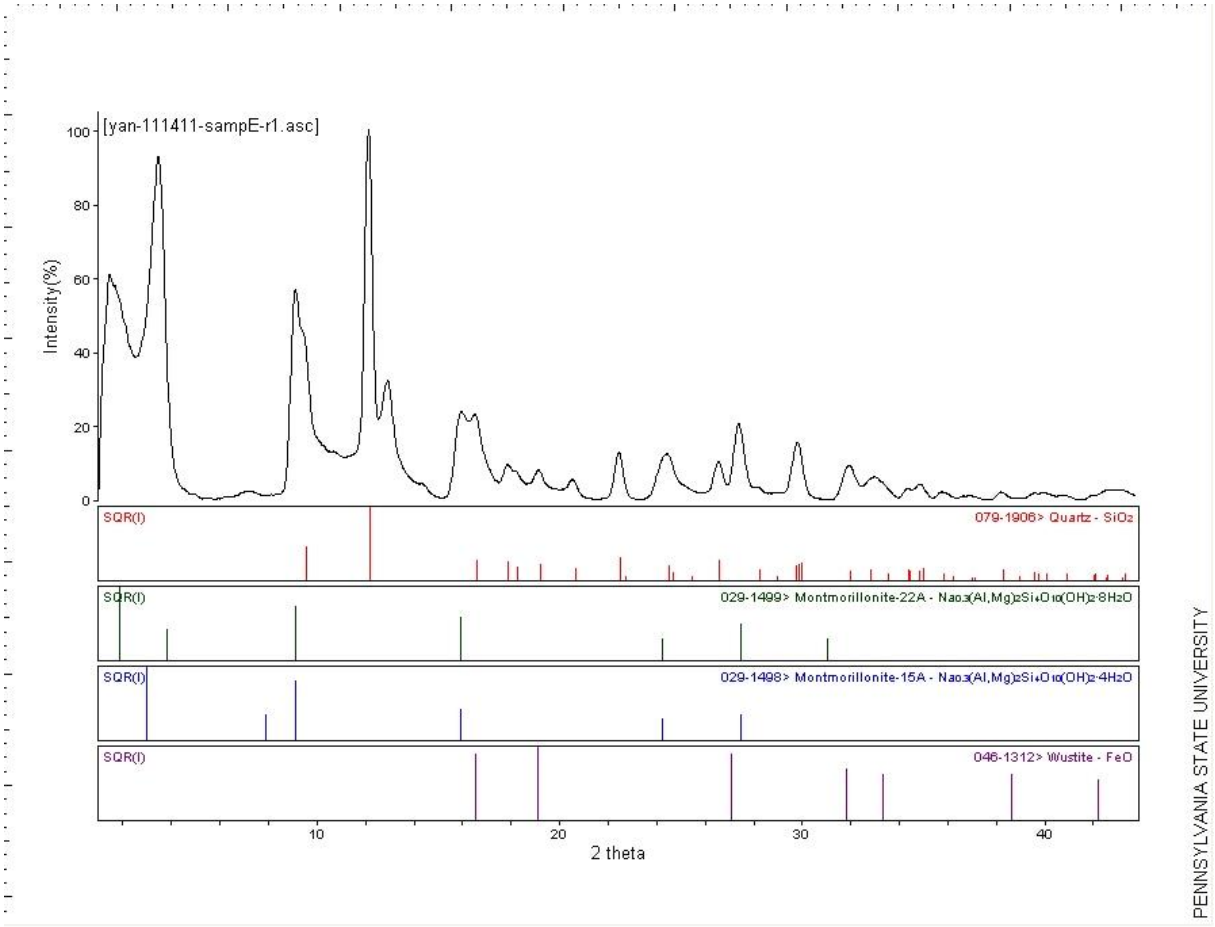

Figure C:3. XRD patterns of size-fractionated montmorillonite SWy-2